SILICA DISSOLUTION AT LOW pH IN THE PRESENCE AND ABSENCE OF FLUORIDE

Arijit Mitra

Dissertation submitted to the faculty of the Virginia Polytechnic Institute and State University in partial fulfillment of the requirements for the degree of

DOCTOR OF PHILOSOPHY
In
GEOSCIENCES

J. Donald Rimstidt, *Chair*
Patricia M. Dove
John A. Chermak
Madeline E. Schreiber

April 29, 2008
Blacksburg, Virginia

Keywords: silica, quartz, dissolution rate, hydrofluoric acid, dissolution kinetics, low pH

SILICA DISSOLUTION AT LOW pH IN THE PRESENCE AND ABSENCE OF FLUORIDE

Arijit Mitra

ABSTRACT

SiO_2 is the most abundant oxide in the earth and its properties, behaviors and interactions are of immense scientific and technological importance. Of particular importance are the interactions of silica with aqueous fluids because these fluids are present in nearly every natural setting. The dissolution of silica and glass by HF plays a very important role in technology and is widely used for the etching of silica and silicate glasses in the glass industry, in the flint industry, in surface micromachining, in etching of glass fibers for near-field optical probes, in the creation of frosted surfaces for decorative applications like frosted glass and cosmetic vials.

I performed 57 batch reactor experiments in acidic fluoride solutions to measure the dissolution rate of quartz. Quartz dissolution rate data from other published studies were combined with the rate data from my experiments and these 75 data were analyzed using multiple linear regression to produce an empirical rate law for quartz

$$r_{qz} = 10^{-4.53}\left(e^{\frac{-18932}{RT}}\right)a_{HF}^{1.18}a_{H^+}^{-0.39}$$

where -5.13 < a_{HF} < 1.60, -0.28 < pH < 7.18, and 25 < T < 100 °C.

Similarly, 97 amorphous silica dissolution rate data from published studies were analyzed using multiple linear regression to develop an empirical rate law for amorphous silica

$$r_{as} = 10^{0.48}\left(e^{\frac{-34243}{RT}}\right)a_{HF}^{1.50}a_{H^+}^{-0.46}$$

where -5.13 < a_{HF} < 1.60, -0.28 < pH < 7.18 and 25 < T < 70 °C.

An examination of the empirical rate laws suggests that the rate-determining step in the reaction mechanism involves a coordinated attack of HF and H^+ on the Si-O bond where the H^+ ion, acting as a Lewis acid, attacks the bridging O atom, while the F end of

a HF molecule, acting as a Lewis base, attacks the Si atom. This allows a redistribution of electrons from the Si-O bond to form a O-H and a Si-FH bond, thus "breaking" the Si-O bond.

In order to quantify the effect of fluoride on the dissolution of silica, I also performed a series of 81 quartz dissolution and 20 amorphous silica dissolution experiments in batch reactors over a pH range of 0 to 7 to investigate the effect of H^+ on silica dissolution rates. Between pH 3.5 and 7 silica dissolution rates are independent of pH, but they increase significantly below pH 3.5, so that the dissolution rate of both quartz and amorphous silica at pH 0 is more than an order magnitude faster than the dissolution rate at pH 3.5. I found that the empirical rate law for the dissolution of the "disturbed surface" of quartz in the pH range of 0 to 3.5 is

$$r_{qz,pH} = 10^{-0.23}\left(e^{\frac{-59392}{RT}}\right)a_{H^+}^{0.28}$$

where 0 < pH < 3.5 and 25 < T < 55°C. The empirical rate law for amorphous silica dissolution in the pH range 0 to 3.5 is

$$r_{as,pH} = 10^{0.56}\left(e^{\frac{-64754}{RT}}\right)a_{H^+}^{0.40}$$

where 0 < pH < 3.5 and 25 < T < 55°C.

Based on the empirical rate laws I suggest that the rate-determining step in the reaction mechanism involves a coordinated attack of H_3O^+, acting as a Lewis acid reacts, on a bridging O atom and the O end of a H_2O, acting as a Lewis base, on the Si atom. This results in a redistribution of electrons from the Si-O bridging bond to form two Si-OH surface species.

ACKNOWLEDGEMENTS

A lot of people have been instrumental in the successful completion of this dissertation. First and foremost, I would like to thank my advisor, Don Rimstidt, whose constant encouragement, guidance, help and support made working on this dissertation a real pleasure. I would also like to thank my committee members, Trish Dove, John Chermak and Maddy Schreiber for helpful suggestions and advice. This work was supported by the U.S. Department of Energy Basic Energy Sciences Grant DE-FG02-03ER14751. I would like to thank the U.S. Silica Company, Berkeley Springs, West Virginia for furnishing the SIL-CO-SIL 250 quartz sample and Nizhou Han for furnishing the amorphous silica sample. I thank the faculty, staff and fellow graduate students for making my time here at Virginia Tech a very enjoyable and gratifying experience. I have made many friends for life. A special word of thanks to Clayton Loehn, Amanda Olsen, Jon Trujillo and Jon Roller.

This work most certainly would not have been possible without the constant support and encouragement of my family. Firstly I want to thank my loving wife Jenn, who has been a constant source of support and strength. Thank you for being there every time I needed you and for everything else honey! Next I want to thank my daughter, Simran, who reinforced my patience skills. I would also like thank my sister, Arpita "Piyu" Mitra for being a great sis and for all her support. Finally and above all, I want to thank my parents, Dwijendra Nath Mitra and Manju Mitra, for EVERYTHING. Thank you. I would not be here today without all your sacrifices, efforts, blessings and love. Ma and Baba, I dedicate this dissertation to you.

TABLE OF CONTENTS

TABLE OF FIGURES

TABLE OF TABLES

CHAPTER 1. INTRODUCTION

Silicon is the second most abundant element and oxygen is the most abundant element in the earth's crust. So it is not surprising that 88% of all named minerals are silicates and silicate minerals make up approximately 88 weight percent of the earth's crust. Nearly 70% of all oxygen bonds in the earth's crust involve silicon and almost all silicon bonds involve oxygen, so that, reactions involving the Si-O bond are geochemically very important. Silica, the most abundant free oxide in the earth, exists as a number of polymorphs, but quartz is by far the most common accounting for about 12% of all the minerals of the earth's crust. This makes silica, its properties, behaviors and interactions of immense scientific and technological importance.

Fluorine is the thirteenth most abundant element in the earth's crust (MASON, 1966) and is the most abundant halogen, nearly five times more abundant than chlorine. Although more abundant than chlorine, the concentration of fluoride in natural waters is generally much lower than chloride because fluorine is more reactive and remains strongly associated with cations in rocks during weathering.

The dissolution of silica and glass by HF plays a very important role in technology (BARBOUX et al., 2004). HF is widely used for the etching of silica and silicate glasses in the glass industry, in the flint industry, in surface micromachining, in etching of glass fibers for near-field optical probes, in the creation of frosted surfaces for decorative applications like frosted glass and cosmetic vials. Frosted glass is made by etching the glass surface in the presence of cations like ammonium or potassium, which forms a fluorosilicate precipitate on the surface and controls the etching pattern (BARBOUX et al., 2004).

Hydrogen fluoride-hydrogen chloride (HF-HCl) mixtures have been used since the 1940's in the petroleum industry for matrix acidization of sandstone oil field reservoirs to increase oil production rates by enhancing permeability. This is achieved by pumping the acid mixture into the formation where it dissolves formation damage produced by drilling activities (CROWE et al., 1992; FORSANS et al., 1993). A HF-HCl mixture, called mud acid, was first used for this purpose by the Dowell Co. in the Gulf Coast of the USA. Prior to this only HCl was used to increase production, but the

precipitation of reaction products clogged up the formation and as a result its use was discontinued. Matrix acidization in sandstone formations is carried out by first preflushing the formation with HCl to dissolve the most soluble components like carbonate material, then followed by the injection of a limited quantity of the HF-HCl mud acid and finally finished up with overflushing the formation with weak HCl. The mud acid dissolves the fine particles blocking the pores in the formation and also increases the pore diameter (FORSANS et al., 1993). Good field results depend upon an optimum acid composition and contact time between the mud acid and the oil formation. This composition is based on laboratory studies which are used to develop acid models for that given oil reservoir (FORSANS et al., 1993).

One of the most important applications of HF solutions is in the semiconductor industry in the manufacture of integrated circuits, where it is used in silicon wafer cleaning and pattern delineation by silicon dioxide etching (OSSEO-ASARE, 1996). HF solutions are also used to chemically clean silicon semiconductor surfaces for selective growth of silicon and metallization, and this is achieved by rinsing the surface in a HF solution or by exposing the surface to a HF/H_2O vapor that condenses on the surface (KANG and MUSGRAVE, 2002). HF solutions are used to chemically clean silicon surfaces in order to remove surface contaminants and native oxides and in processing silicon dioxide patterns on silicon substrates of less that 3 mm thick and 70-100 mm wide. Hence, precision etch control for these processes is extremely crucial and can be achieved by understanding the relationship between the HF concentration, the ionic composition of the solution, and the etch rate (KNOTTER, 2000).

Aqueous fluoride concentrations in natural systems can range from 0 to more than 20 ppm (GACIRI and DAVIES, 1993; LAHERMO et al., 1991; MAHON, 1964; REIMANN et al., 2003). EDMUNDS and SMEDLEY (2005) constructed a hydrogeochemical cycle of fluorine and reported the range of fluoride concentrations in different natural settings. "The cycle involves transfer of fluorine to the atmosphere by volcanic emissions, evaporation, marine aerosols, and industrial pollution. Wet and dry deposition transfer fluorine to the biosphere and geosphere. In the geosphere, uptake and release of fluorine are controlled by various water-rock interactions and by the inputs from anthropogenic sources" (EDMUNDS and SMEDLEY, 2005). The reported values for fluoride

concentrations in rainfall range from 0 to 0.08 mg/L. Surface waters in different parts of the world, on the other hand have been reported to have fluoride concentrations ranging from 0.03 to 0.154 mg/L, while surface waters in high fluoride regions have fluoride concentrations ranging from 0.1 to as high as 1980 mg/L in Lake Magadi, Tanzania. The fluoride concentrations in geothermal springs where near neutral pH conditions exist are typically in the range of 1 to 10 mg/L (ELLIS and MAHON, 1977), but can reach as high as 330 mg/L (EDMUNDS and SMEDLEY, 2005). But under acidic conditions, fluoride concentrations in geothermal sources can be more than 1000 mg/L (ELLIS, 1973). Fluoride concentrations in groundwater can range from 0.01 to nearly 30 mg/L and can be as high as 250 mg/L in groundwater in volcanic rocks.

Osseo-Asare (OSSEO-ASARE, 1996) summed it up nicely, "It is a remarkable fact that, in spite of the tremendous technological importance of silicon chips, and the numerous publications already available on various aspects of aqueous chemical processing, the physicochemical details of the SiO_2–H_2O–HF reaction are still waiting to be unraveled." This need to understand the physicochemical aspects of the effect of fluoride ions and HF on the dissolution rate of silica was the motivation for this project. The second chapter of this dissertation reports empirical rate laws for the reaction between HF solutions and both quartz and silica glass. It also describes the chemistry of the HF – SiO_2 – H_2O system needed to understand those rate laws. This information will not only enhance our understanding of the SiO_2 – HF interactions in nature but will also allow improved technological applications of the reaction.

But in order to quantify the effect of fluoride on the dissolution of silica I first needed to investigate the effect of pH on the dissolution of silica. A study to quantify the effect of H^+ ions was necessary in order to determine if pH alone has an effect on dissolution rates, and if it does, whether that effect is important in the dissolution of silica in acidic fluoride solutions.

The effect of pH on the dissolution of silica at high pH has been widely investigated. At high pH, the dissolution rate appears to be controlled by the nucleophilic attack of OH^- ligands on Si atoms and the rate increases with increasing pH. On the other hand, the dissolution behavior and reaction mechanism of silica at low pH is not well understood. Studies of the dissolution rate of silica at low pH are limited and there

appears to be a lack of consensus regarding the reaction mechanism. These studies report different silica dissolution behaviors at low pH. For example, BRADY and WALTHER (1990); KNAUSS and WOLERY (1988); and WOLLAST and CHOU (1988) have reported that the dissolution rates of quartz are independent of pH below pH 8. HOUSE and HICKINBOTHAM (1992) and HOUSE and ORR (1992) report that dissolution rate increases from low to high pH. On the other hand, KNAUSS and WOLERY (1988); POKROVSKY et al. (2006); WOLLAST and CHOU (1988) and WORLEY et al. (1996) document to various degrees fast dissolution rates below pH 3 at temperatures ranging from 25°C to 200°C. But with the exception of POKROVSKY et al. (2006), these studies did not identify or discuss this behavior. In order to clarify the role of low pH in the dissolution of silica I performed a series of dissolution rate experiments using quartz and amorphous silica and the results of this study are summarized in the third chapter of this dissertation. This study produced empirical rate laws for the dissolution rate of the disturbed surface layer on quartz grains and for amorphous silica for pH < 3.5. Additionally, I proposed an explanation for the rate versus pH trends in terms of a reaction mechanism.

1.1 REFERENCES

Barboux, P., Laghzizil, A., Bessoles, Y., Deroulhac, H., and Trouve, G., 2004. Paradoxical crystalline morphology of frosted glass. *Journal of Non-Crystalline Solids* **345-346**, 137-141.

Brady, P. V. and Walther, J. V., 1990. Kinetics of quartz dissolution at low temperatures. *Chemical Geology* **82**, 253-264.

Crowe, C., Masmonteil, J., and Thomas, R., 1992. Trends in Matrix Acidizing. *Oilfield Review* **4**, 24-40.

Edmunds, M. and Smedley, P., 2005. *Essentials of medical geology : impacts of the natural environment on public health*. Elsevier, Amsterdam ; Boston.

Ellis, A. J., 1973. Chemical Processes in Hydrothermal Systems - A Review. In: Ingerson, E. (Ed.), *Proceedings of a Symposium on Hydrogeochemistry and Biogeochemistry*. Clarke Co., Washington, D.C.

Ellis, A. J. and Mahon, W. A. J., 1977. *Chemistry and Geothermal Systems*. Academic Press, San Diego, CA.

Forsans, T., Zundel, J.-P., and Lichanot, A., 1993. Composition of acidification effluents of sandstones through geochemical calculation: validation of fluorosilicate equilibria by potentiometric assay of F. *Applied Geochemistry* **8**, 383-389.

Gaciri, S. J. and Davies, T. C., 1993. The occurrence and geochemistry of fluoride in some natural waters of Kenya. *Journal of Hydrology* **143**, 395-412.

House, W. A. and Hickinbotham, L. A., 1992. Dissolution kinetics of silica between 5 and 30°C. Application of a titrimetric method. *Jounal of the Chemical Society, Faraday Transactions* **88**, 2021-2026.

House, W. A. and Orr, D. R., 1992. Investigation of the pH dependence of the kinetics of Quartz dissolution at 25°C. *Jounal of the Chemical Society, Faraday Transactions* **88**, 233-241.

Kang, J. K. and Musgrave, C. B., 2002. The mechanism of HF/H_2O chemical etching of SiO_2. *The Journal of Chemical Physics* **116**, 275-280.

Knauss, K. G. and Wolery, T. J., 1988. The dissolution kinetics of quartz as a function of pH and time at 70°C. *Geochimica et Cosmochimica Acta* **52**, 43-53.

Knotter, D. M., 2000. Etching Mechanism of Vitreous Silicon Dioxide in HF-Based Solutions. *J. Am. Chem. Soc.* **122**, 4345-4351.

Lahermo, P., Sandstrom, H., and Malisa, E., 1991. The occurrence and geochemistry of fluorides in natural waters in Finland and East Africa with reference to their geomedical implications. *Journal of Geochemical Exploration* **41**, 65-79.

Mahon, W. A. J., 1964. Fluorine in the Natural Thermal Waters of New Zealand. *New Zealand Journal of Science* **7**, 3-28.

Mason, B. H., 1966. *Principles of geochemistry*. Wiley, New York.

Osseo-Asare, K., 1996. Etching Kinetics of Silicon Dioxide in Aqueous Fluoride Solutions: A Surface Complexation Model. *Journal of The Electrochemical Society* **143**, 1339-1347.

Pokrovsky, O. S., Golubev, S. V., and Mielczarski, J. A., 2006. Kinetic evidences of the existence of positively charged species at the quartz-aqueous solution interface. *Journal of Colloid and Interface Science* **296**, 189-194.

Reimann, C., Bjorvatn, K., Frengstad, B., Melaku, Z., Tekle-Haimanot, R., and Siewers, U., 2003. Drinking water quality in the Ethiopian section of the East African Rift Valley I--data and health aspects. *The Science of The Total Environment* **311**, 65-80.

Wollast, R. and Chou, L., 1988. Rate control of weathering of silicate minerals at room temperature and pressure. In: Lerman, A. and Meybeck, M. Eds.), *Physical and Chemical Weathering in Geochemical Cycles*. Kluwer Academic Publishers.

Worley, W. G., Tester, J. W., and Grigsby, C. O., 1996. Quartz dissolution kinetics from 100-200°C as a function of pH and ionic strength. *AIChE Journal* **42**, 3442-3457.

CHAPTER 2. SOLUBILITY AND DISSOLUTION RATE OF SILICA IN ACID FLUORIDE SOLUTIONS

2.1 ABSTRACT

I performed 57 batch reactor experiments in acidic fluoride solutions to measure the dissolution rate of quartz. Quartz dissolution rate data from other published studies were combined with the rate data from our experiments and these 75 data were analyzed using multiple linear regression to produce an empirical rate law for quartz

$$r_{qz} = 10^{-4.53}\left(e^{\frac{-18932}{RT}}\right)a_{HF}^{1.18}a_{H^+}^{-0.39}$$

where -5.13 < a_{HF} < 1.60, -0.28 < pH < 7.18, and 25 < T < 100 °C.

Similarly, 97 amorphous silica dissolution rate data from published studies were analyzed using multiple linear regression to develop an empirical rate law for amorphous silica

$$r_{as} = 10^{0.48}\left(e^{\frac{-34243}{RT}}\right)a_{HF}^{1.50}a_{H^+}^{-0.46}$$

where -5.13 < a_{HF} < 1.60, -0.28 < pH < 7.18 and 25 < T < 70 °C.

An examination of the empirical rate laws suggests that the rate-determining step in the reaction mechanism involves a coordinated attack of HF and H^+ on the Si-O bond where the H^+ ion, acting as a Lewis acid, attacks the bridging O atom, while the F end of a HF molecule, acting as a Lewis base, attacks the Si atom. This allows a redistribution of electrons from the Si-O bond to form a O-H and a Si-FH bond, thus "breaking" the Si-O bond.

2.2 INTRODUCTION

Fluorine is the thirteenth most abundant element in the earth's crust (MASON, 1966) and is the most abundant halogen, nearly five times more abundant than chlorine. Although more abundant than chlorine, the concentration of fluoride in natural waters is

generally much lower than chloride because fluorine is more reactive and remains strongly associated with cations in rocks during weathering. Silicon, on the other hand is the second most abundant element and oxygen is the most abundant element so it is not surprising that 88% of all named minerals are silicates. In the earth's crust, nearly 70% of all oxygen bonds involve silicon and almost all silicon bonds involve oxygen, so that, reactions involving the Si-O bond are geochemically the most important. Silica, the most abundant free oxide in the earth, exists as a number of polymorphs but quartz is by far the most common accounting for about 12% of all the minerals of the earth's crust. This makes silica, its properties, behaviors and interactions of immense scientific and technological importance.

The dissolution of silica and glass by HF plays a very important role in technology (BARBOUX et al., 2004). HF is widely used for the etching of silica and silicate glasses in the glass industry, in the flint industry, in surface micromachining, in etching of glass fibers for near-field optical probes, in the creation of frosted surfaces for decorative applications like frosted glass and cosmetic vials. Frosted glass is made by etching the glass surface in the presence of cations like ammonium or potassium, which forms a fluorosilicate precipitate on the surface and controls the etching pattern (BARBOUX et al., 2004).

Hydrogen fluoride-hydrogen chloride (HF-HCl) mixtures have been used since the 1940's in the petroleum industry for matrix acidization of sandstone oil field reservoirs to increase oil production rates by enhancing permeability. This is achieved by pumping the acid mixture into the formation where it dissolves formation damage produced by drilling activities (CROWE et al., 1992; FORSANS et al., 1993). Matrix acidization in sandstone formations is carried out by first preflushing the formation with HCl to dissolve the most soluble components like carbonate material, then followed by the injection of a limited quantity of the HF-HCl mud acid and finally finished up with overflushing the formation with weak HCl. The mud acid dissolves the fine particles blocking the pores in the formation and also increases the pore diameter (FORSANS et al., 1993). Good field results depend upon an optimum acid composition and contact time between the mud acid and the oil formation. This composition is based on laboratory

studies which are used to develop acid models for that given oil reservoir (FORSANS et al., 1993).

One of the most important applications of HF solutions is in the semiconductor industry in the manufacture of integrated circuits, where it is used in silicon wafer cleaning and pattern delineation by silicon dioxide etching (OSSEO-ASARE, 1996). HF solutions are also used to chemically clean silicon semiconductor surfaces for selective growth of silicon and metallization, and this is achieved by rinsing the surface in a HF solution or by exposing the surface to a HF/H_2O vapor that condenses on the surface (KANG and MUSGRAVE, 2002). HF solutions are used to chemically clean silicon surfaces in order to remove surface contaminants and native oxides and in processing silicon dioxide patterns on silicon substrates of less that 3 mm thick and 70-100 mm wide. Hence, precision etch control for these processes is extremely crucial and can be achieved by understanding the relationship between the HF concentration, the ionic composition of the solution, and the etch rate (KNOTTER, 2000).

Aqueous fluoride concentrations in natural systems can range from 0 to at least 20 ppm (GACIRI and DAVIES, 1993; LAHERMO et al., 1991; MAHON, 1964; REIMANN et al., 2003). EDMUNDS and SMEDLEY (2005) constructed a hydrogeochemical cycle of fluorine and reported range of fluoride concentrations in different natural settings. "The cycle involves transfer of fluorine to the atmosphere by volcanic emissions, evaporation, marine aerosols, and industrial pollution. Wet and dry deposition transfer fluorine to the biosphere and geosphere. In the geosphere, uptake and release of fluorine are controlled by various water-rock interactions and by the inputs from anthropogenic sources" (EDMUNDS and SMEDLEY, 2005). The fluoride concentrations in geothermal springs where near neutral pH conditions exist are typically in the range of 1 to 10 mg/L (ELLIS and MAHON, 1977), but can reach as high as 330 mg/L (EDMUNDS and SMEDLEY, 2005). But under acidic conditions, fluoride concentrations in geothermal sources can be more than 1000 mg/L (ELLIS, 1973) and in these settings the interaction of fluoride with silica could be of importance

This chapter reports empirical rate laws for the reaction between HF solutions and both quartz and silica glass. It also describes the chemistry of the $HF - SiO_2 - H_2O$ system needed to understand those rate laws. This information will not only enhance our

understanding of the SiO_2 – HF interactions in nature but will also allow improved technological applications of the reaction.

2.3 HF – SiO_2 – H_2O SYSTEM

The HF – SiO_2 – H_2O system is relatively complex and non-intuitive. Because of the importance of this chemistry for industrial applications there are several studies of limited parts of the system, but they have not been synthesized into a comprehensive form. In order to provide a framework for understanding the dissolution rate of silica in fluoride solutions we first review the equilibrium chemistry of this system.

2.3.1 HF – H_2O System

HF is a weak acid and dissociates in water by the reaction

$$HF = H^+ + F^- \qquad (2.1)$$

The pK_{HF} for the dissociation of HF in aqueous solutions has been determined both conductometrically (DAVIES and HUDLESTON, 1924; ELLIS, 1963; ROTH, 1939; WOOSTER, 1938) and potentiometrically (BAUMANN, 1969; BROENE and VRIES, 1947; HEFTER, 1984; KLEBOTH, 1970; KRESGE and CHIANG, 1973; PATEL et al., 1971; VANDERBORGH, 1968; WYNNE-JONES and HUDLESTON, 1924). The reported values for the pK_{HF} range from 2.82 to 3.33 at 25 °C. This range in reported values is partly due to the existence of an additional aqueous fluoride species (HF_2^-), the use of glass apparatus, the volatility of HF at room temperatures, and the contamination of fluoride salts with SiF_6^{2-} (HEFTER, 1984). We used pK_{HF} = 3.164 (IUPAC, 1979-1982; KRESGE and CHIANG, 1973; PERRIN, 1982) for all our calculations. Other significant studies (KNOTTER, 2000; MCTIGUE et al., 1985) also used this value. HEFTER (1984) performed a critical study of all reported acidity constants for HF and suggested a pK_{HF} value of 3.18 ± 0.02, which is similar to the value used in this study within error.

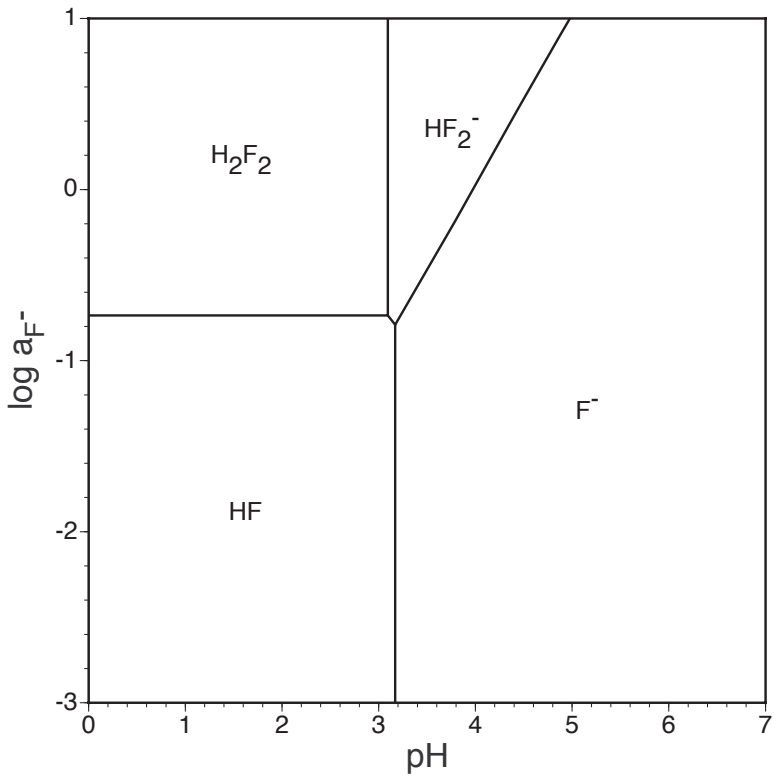

Figure 2.1. The distribution of aqueous fluoride species as a function of pH and log a_{F^-}. Calculated using the Geochemist's Workbench software.

Fig. 2.1 shows the distribution of the fluoride species as a function of pH and log a_{F^-}. MCTIGUE et al. (1985), suggest that the apparent acidity of HF – H_2O mixtures increases with increasing HF concentration such that, "from being a weak acid in dilute aqueous solutions, pure liquid HF is a super-acid". They attribute this to the formation of polymeric HF aqueous species ($H_nF_{n+1}^-$) resulting from the solvation of F^- by molecular HF by the reaction

$$nHF + F^- = H_nF_{n+1}^- \qquad (2.2)$$

where $1 \leq n \leq 4$. (BELL et al., 1956) argue that this solvation could qualitatively account for the increase in acidity in HF – H_2O solutions up to concentrations of 15 M HF. The first polymeric species (HF_2^-) is formed by the reaction

$$HF + F^- = HF_2^- \qquad \log K = 0.598 \qquad (2.33)$$

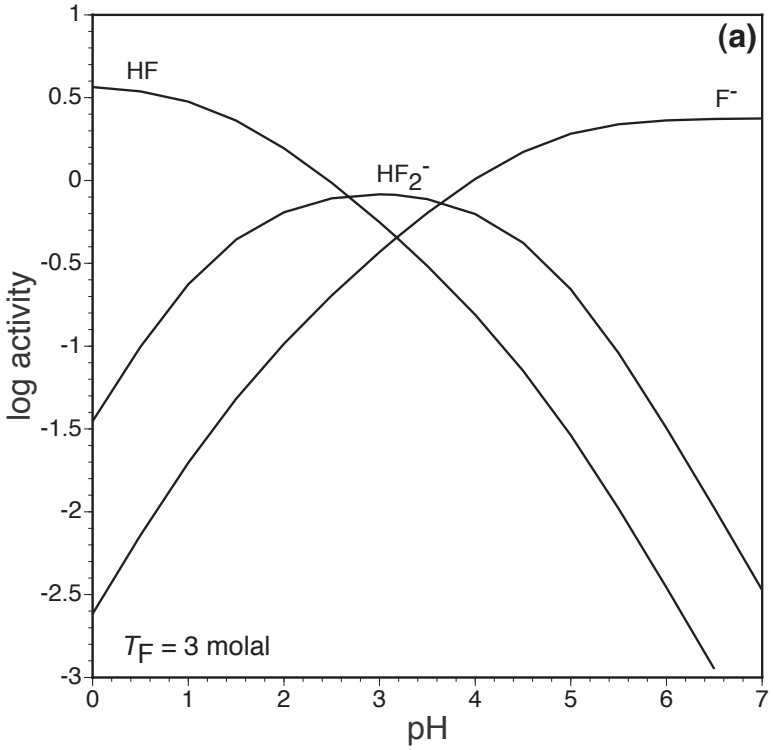
(a)
HF
F-
HF2-
log activity
TF = 3 molal
pH

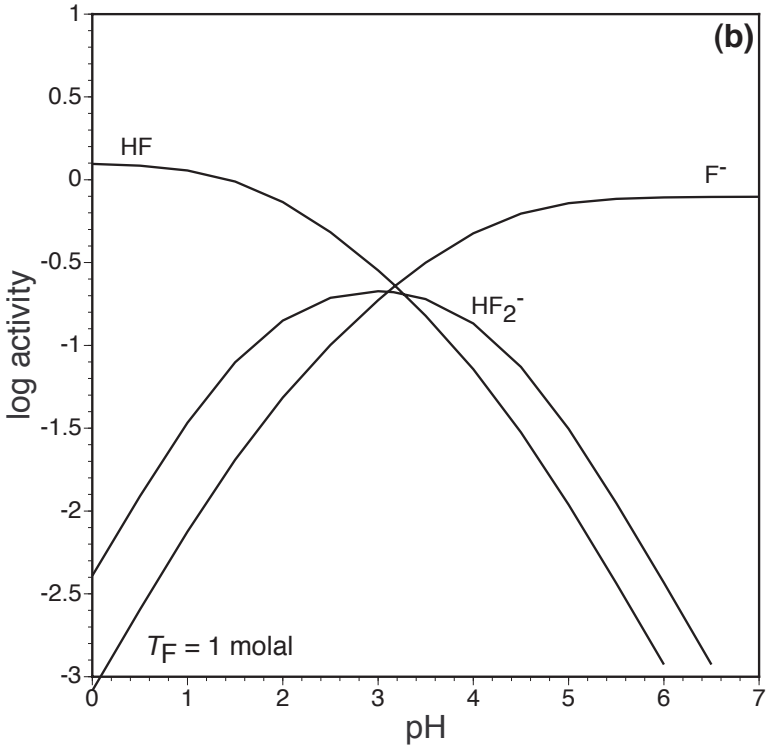
(b)
HF
F-
HF2-
log activity
TF = 1 molal
pH

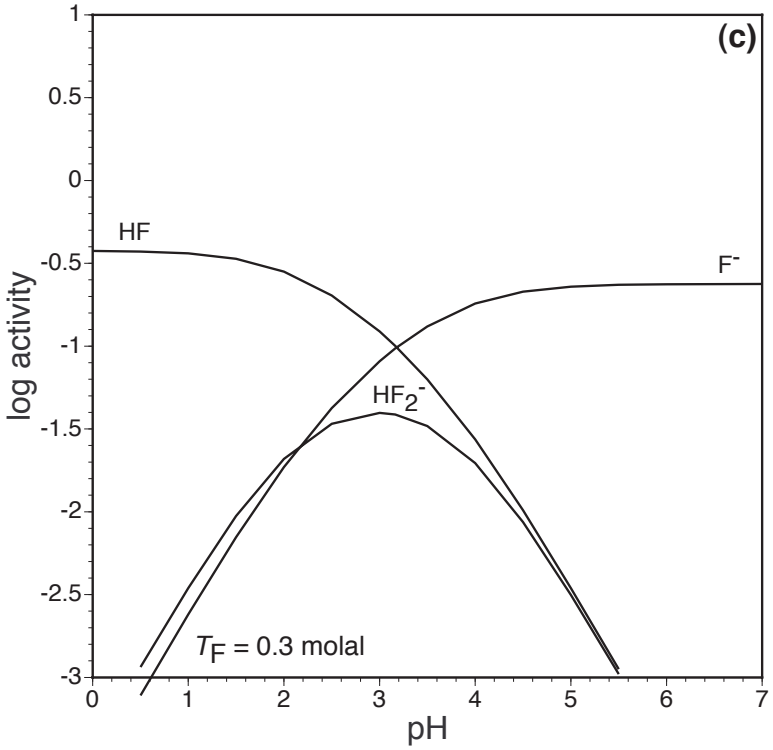

Figure 2.2. The distribution of the three fluoride species, HF, F^- and HF_2^- for fixed total fluoride (T_F) concentrations of (a) 3.0 m, (b) 1.0 m and (c) 0.3 m and a fixed ionic strength of 1.0. Calculated using the Visual MINTEQ software.

Fig. 2.2 shows the activity of HF, F^- and HF_2^- as a function of pH for total fluoride concentrations of 3.0, 1.0 and 0.3 molal and an ionic strength of 1.0. HF_2^- becomes a predominant species near pH 3 when total fluoride concentration exceeds 1 molal. The species HF_2^- exists in salts like KHF_2. The HF_2^- ion has been identified in aqueous solution using infrared spectroscopy with v_3 and v_2 vibration modes of 1364 cm^{-1} and 1217 cm^{-1} respectively (AULT, 1978).

Other HF polymeric species that exist in solution at higher total fluoride concentrations (above 1M) are $H_2F_3^-$, $H_3F_4^-$ and $H_4F_5^-$. None of these species are important in HF solutions containing less than 1 m HF (FARRER and ROSSOTTI, 1964). They form by the reactions (MCTIGUE et al., 1985)

$$2HF + F^- = H_2F_3^- \qquad \log K = -0.602 \qquad (2.4)$$

$$3HF + F^- = H_3F_4^- \qquad \log K = -0.602 \qquad (2.5)$$

$$4HF + F^- = H_4F_5^- \qquad \log K = 0.699 \qquad (2.6)$$

GENNICK et al. (1977) suggests the existence of all the above polymeric species in the solid state along with x-ray diffraction studies (COYLE et al., 1970; FORRESTER et al., 1963; IBERS, 1964) that confirm the structures of all the polymers except $H_3F_4^-$. MCTIGUE et al. (1985) argue that these species also exist in aqueous solutions. They further report that infrared and NMR spectroscopic studies support the existence of these species in aqueous solutions, where water molecules complete a tetrahedral arrangement of solvating species around a central fluoride ion when n = 2 or 3. They also suggest that there is no evidence for $H_nF_{n+1}^-$ polymeric aqueous species where n > 4. The polymers $H_2F_3^-$, $H_3F_4^-$ and $H_4F_5^-$ that form at higher total fluoride concentrations (> 1 molal) are not shown on Fig. 2.1 because their fields of predominance occur at much higher total fluoride concentrations.

WARREN (1971) suggested the existence of an HF dimer, H_2F_2, in aqueous solution, which is formed at very low pH (<3) by the reaction

$$2HF = H_2F_2 \qquad \log K = 0.431 \qquad (2.7)$$

Even though our calculations based on the equilibrium constant for the formation of this dimer suggests a large stability field, we are not aware of any reports that show spectroscopic evidence for its existence in solution. However, DYKE et al. (1972) identified this species in HF gas.

In our subsequent discussions we will only consider the species HF, F^- and HF_2^-. VERHAVERBEKE et al. (1994) have suggested that for understanding the etching process of silica by HF, the concentration range up to 1 m is the most important. HF, F^- and HF_2^- are the most important species in the pH range of 0 to 6, at $a_{F^-} < 1$ (Fig. 2.1). Although HF_2^- is never predominant at $T_F < 1.0$, it reaches a maximum concentration near pH 3 (Fig. 2.2). Because HF_2^- has been suggested as a reactant in the HF – SiO_2 reaction (JUDGE, 1971; SPIERINGS, 1993), the distribution of this species is important for interpreting reaction rate data.

2.3.2 SiO_2 – H_2O system

Quartz dissolves in pure water by the reaction

$$SiO_2(qz) + 2H_2O = H_4SiO_4 \qquad \log K = -3.96 \qquad (2.8)$$

In this paper we also consider the dissolution of amorphous silica

$$SiO_2(am) + 2H_2O = H_4SiO_4 \qquad \log K = -2.95 \qquad (2.9)$$

Both quartz and amorphous silica dissolve very slowly in pure water (RIMSTIDT and BARNES, 1980). According to the equilibrium constants in Eqs. (2.8) and (2.9), the solubility of quartz in pure water (~6.6 ppm) is about seventeen times lower than that of amorphous silica (~116 ppm). The Geochemist's Workbench and the Visual MINTEQ software use these values of solubility, but RIMSTIDT (1997) suggests a higher value for quartz solubility (~11 ppm). Since the dissolution rate constants vary directly with equilibrium constant for the dissolution reaction it follows that the dissolution rate of quartz (4.2×10^{-14} mol/m^{2}sec) is approximately 21 times slower than amorphous silica (9.0×10^{-13} mol/m^{2}sec). These slow dissolution rates along with the very low solubilities makes water a very poor solvent for industrial applications for these phases where faster dissolution and higher solubility is needed to allow for significant silica dissolution to occur in a short time.

2.3.3 HF – SiO_2 – H_2O

For pH > 3.16 (pK_{HF}), quartz dissolution in fluoride solutions is best described by the reaction

$$SiO_2(qz) + 4H^+ + 6F^- = SiF_6^{2-} + 2H_2O \qquad \log K = 26.26 \qquad (2.10)$$

For pH < 3.16 (pK_{HF}), quartz dissolution in fluoride solutions is described by

$$SiO_2(qz) + 6HF = SiF_6^{2-} + 2H^+ + 2H_2O \qquad \log K = 7.28 \qquad (2.11)$$

SiF_6^{2-} is responsible for the enhanced solubility of silica in fluoride solutions. In order to explain silica solubility as a function of pH both reactions must be considered. Fig. 2.3a shows that SiF_6^{2-} is a predominant fluoride species only when a_{F^-} exceeds ~10^{-4}. Because the fluoride is distributed between SiF_6^{2-}, HF and F^- (Figs. 2.3b and 2.3c) this requires a total fluoride concentration that exceeds 0.01 molal. When T_F exceeds 1 molal SiF_6^{2-} dominates fluoride speciation at pH < 5.

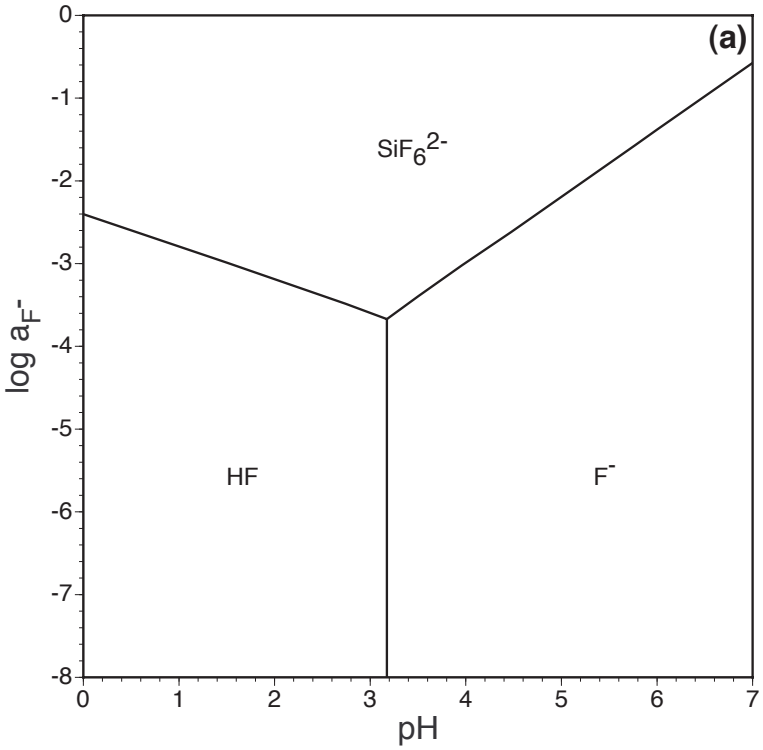
(a)
SiF_6^{2-}
HF
F^-
log a_{F^-}
pH

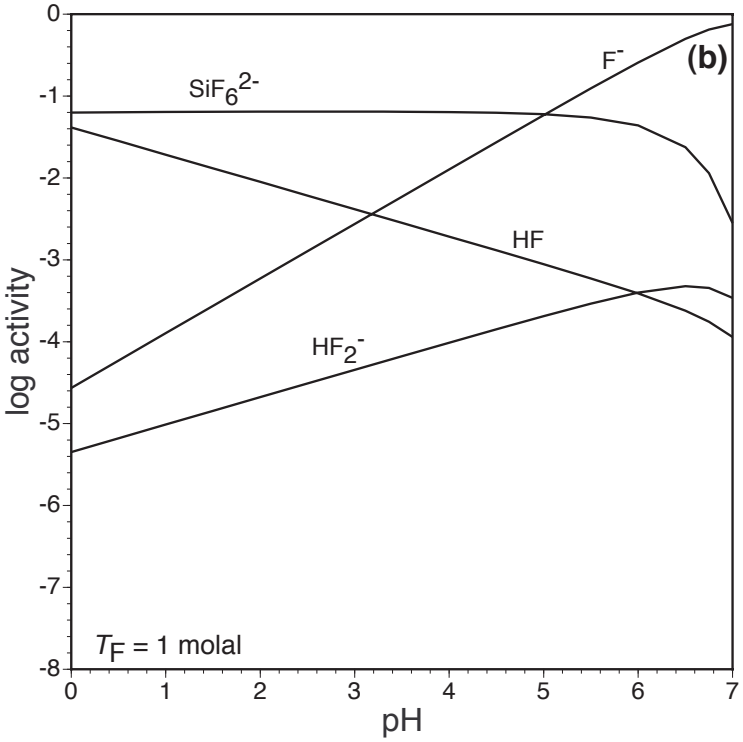
(b)
SiF_6^{2-}
F^-
HF
HF_2^-
T_F = 1 molal
log activity
pH

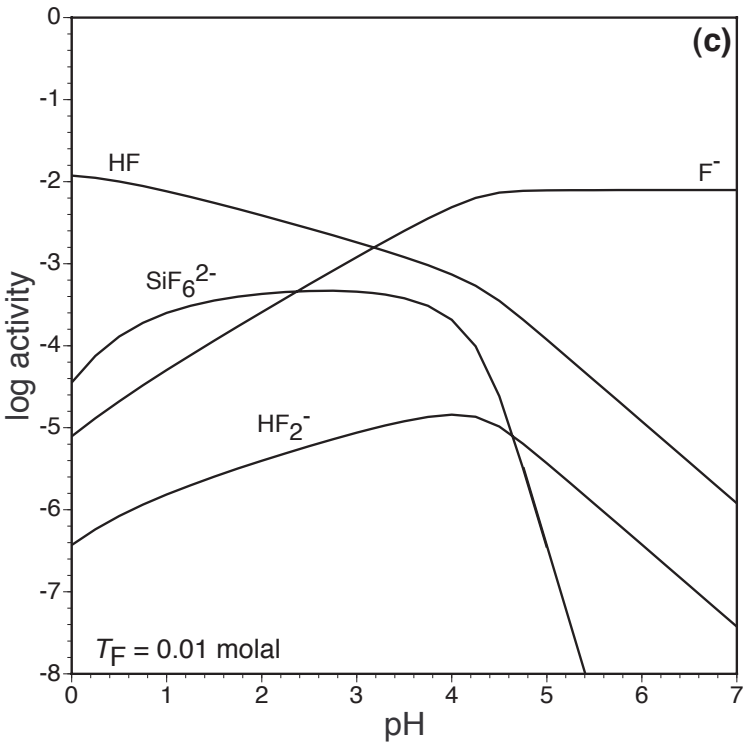

Figure 2.3. (a) Activity diagram showing the distribution of aqueous fluoride species in equilibrium with quartz as a function of pH and log a_{F^-}. Calculated using the Geochemist's Workbench software. (b) Species distribution diagram showing the activity of fluoride species in a solution with a total fluoride concentration of 1.0 m and I = 1.0. (c) Species distribution diagram showing the activity of fluoride species in a solution with a total fluoride concentration of 0.01 m and I = 1.0. Figs. (b) and (c) based on calculations from Visual MINTEQ .

There is consensus in the literature that H_2SiF_6 is a very strong acid similar to H_2SO_4 (URBANSKY, 2002) and is present in its dissociated form SiF_6^{2-} at pH > 0.65

$$H_2SiF_6 = SiF_6^{2-} + 2H^+ \qquad (2.12)$$

CIAVATTA et al. (1988) and SUDAKOVA et al. (1978) have argued that H_2SiF_6 exhibits two deprotonation reactions.

$$H_2SiF_6 = HSiF_6^- + H^+ \qquad (2.13)$$

$$HSiF_6^- = SiF_6^{2-} + H^+ \qquad (2.14)$$

The equilibrium constant (K) for the first deprotonation reaction is unknown and there are two existing values for K for the second deprotonation reaction, $10^{-0.65}$ (CIAVATTA et

al., 1988) and $10^{-1.83}$ (SUDAKOVA et al., 1978). BUSEY et al. (1980) cite Raman and NMR spectroscopic studies (DEAN and EVANS, 1967) that have identified aqueous SiF_6^{2-} as an octahedral ion in solution. BUSEY et al. (1980) also report that SiF_6^{2-} is the only fluorosilicate species that has been identified in solution using spectroscopic methods. CIAVATTA et al. (1988) report the formation of aqueous SiF_4 by the reaction

$$SiF_6^{2-} + 2H^+ = SiF_4 + 2HF \qquad (2.15)$$

KLEBOTH (1969) proposed SiF_6^{2-} (aq), SiF_5^- (aq) and SiF_4 (aq) as the principal aqueous species for the fluorosilicate system. The existence of SiF_5^- has been verified by both NMR spectroscopic (KLANBERG and MUETTERTIES, 1968) and x-ray crystallographic studies (CLARK et al., 1967; SCHOMBURG and KREBS, 1984) and SiF_4 has been identified in the vapor phase by its infrared spectrum (HEICKLEN and KNIGHT, 1964). URBANSKY (2002) argues that SiF_5^- (aq) and SiF_4 (aq) may exist only as an aquated species such as $SiF_5(H_2O)^-$ and $SiF_4(H_2O)_2$. But he also raises the question about the extent of occurrence of these species in aqueous solutions and also whether SiF_4 could ever be a predominant aqueous species.

Fig. 2.4a shows that the predominant silica species in solution is SiF_6^{2-} when a_{F^-} = 0.01. At high T_F concentration, SiF_6^{2-} is the dominant silica species that is responsible for significantly enhanced solubility of silica phases up to pH 7. For T_F concentrations below 0.01 molal the SiF_6^{2-} concentration is less than the H_4SiO_4 concentration, so SiF_6^{2-} makes a negligible contribution to the solubility of silica phases. The species distribution diagram (Fig. 2.4b) shows that SiF_6^{2-} is important at pH > 6 only when T_F is larger than 0.1 m. Because SiF_6^{2-} is produced by reaction (2.10), the solubility of silica phases increases with decreasing pH until pH 3. But below this pH, decreasing pH causes silica solubility to decline because the free F^- ions in solution used to produce SiF_6^{2-} by the first reaction are consumed to produce HF by reaction (2.1). This results in a decrease in SiF_6^{2-} concentration in solution and consequently a decrease in silica solubility.

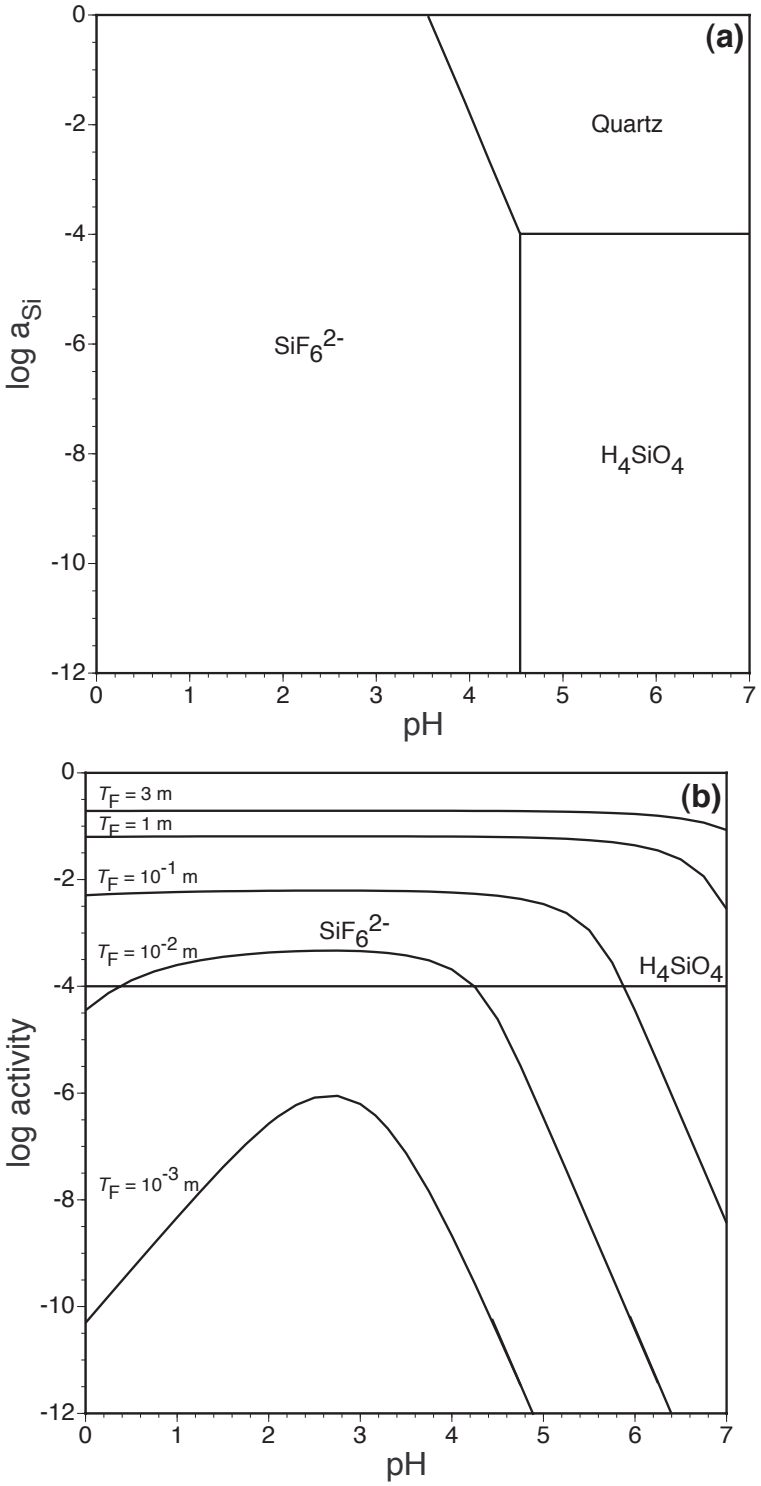

Figure 2.4. (a) Activity diagram showing the distribution of aqueous silica species for a fixed total fluoride activity of 0.01 molal as a function of pH and log a_{F^-}. Calculated using the Geochemist's Workbench software. (b) Species distribution diagram calculated using Visual MINTEQ showing the distribution of the different aqueous silica species in

terms of their activity for different total fluoride concentrations and an ionic strength of 1.0.

Fig. 2.5 shows the molal solubility of quartz in fluoride solutions as a function of pH contoured in total fluoride concentration. Fig. 2.5 reflects patterns that are consistent with Fig. 2.4b, but for constructing this diagram, the concentrations of SiF_6^{2-} for an ionic strength of 1.0 were calculated using Visual MINTEQ. When the total fluoride concentration is greater than about $10^{-2.5}$ molal, the solubility of quartz is enhanced above pure water at $T_F = 10^{-2}$. There is a maximum solubility around pH 3 that is related to the distribution of fluoride between SiF_6^{2-}, HF, HF_2^- and F^- as is illustrated in Figs. 2.3 and 2.4. At higher T_F values, quartz solubility increases and the fluoride enhanced solubility extends to higher pH because of the increased stability of SiF_6^{2-} as shown in Fig. 2.4b.

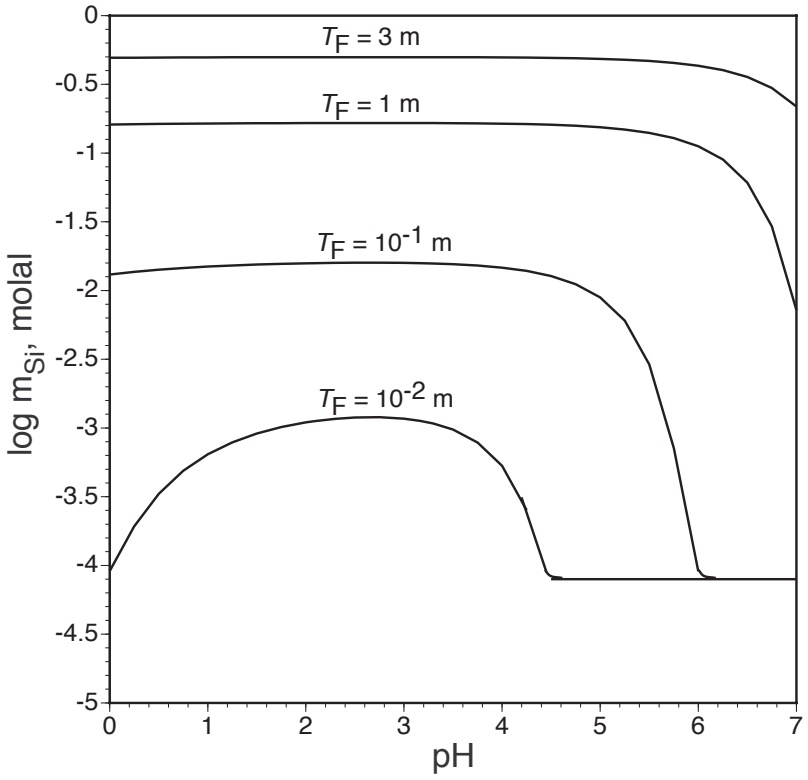

Figure 2.5. Solubility of quartz as a function pH contoured in total fluoride concentration.

A similar set of activity and species distribution diagrams could be constructed for amorphous silica. But because amorphous silica solubility in pure water is an order of magnitude higher than that of quartz solubility, more fluoride will be in SiF_6^{2-}.

2.4 METHODS

2.4.1 Experimental Methods

2.4.1.1 Materials and Experimental Design

Quartz sand from Corning Glass Works, State College, Pennsylvania (grain size 125-1000 μm) was used for this study. This sand has a specific surface area of 0.092 m^2/gm, as determined by Ar-BET (RIMSTIDT and BARNES, 1980).

Both hydrofluoric acid (HF) and sodium fluoride (NaF) was used as a source of fluoride for these experiments. We used a factorial series of experiments to simultaneously test the effect of fluoride, pH and temperature on the dissolution rate of quartz. No amorphous silica dissolution experiments were performed because there is a sufficient amount of rate data already available in the literature. For different fixed concentrations of HF and NaF, the pH was varied by adding HNO_3 to the solutions. These experiments were performed in water baths at temperatures of 25 ±1 °C, 35 ±1 °C and 55 ±1 °C. Reagent grade chemicals were used to prepare all solutions. We prepared HF solutions ranging in initial concentration from 0.03 m to 3 m and NaF solutions of initial concentrations ranging from 0.01 m to 1.0 m. The HNO_3 solutions ranged in concentration from 0.00001 m to 1 m. These individual solutions were then mixed in different combinations to obtain fifty-fifty solution mixtures by volume of HF-HNO_3 and NaF–HNO_3 that were then used for the experiments. The experimental conditions are tabulated in Appendix 2.1.

Fifty-seven batch reactor (RIMSTIDT and NEWCOMB, 1993) experiments were performed. The reactors were either Teflon bottles or polyethylene bottles (30-60 mL). A quartz sample ranging in mass from 1 to 3 grams was used for each experiment. To this sample, a known mass of solution (25-35 grams) was added. The reactors were then sealed and immersed in a constant temperature water bath set at the desired temperature for the duration (2-10 hours) of the experiments.

A sample of approximately 0.5 mL of solution was periodically withdrawn over the duration of each experiment. Each sample was filtered through a 0.22 μm nylon filter to remove any suspended quartz particles and then weighed and stored in polyethylene bottles for later analysis. The dissolved silica concentration was determined by the silicomolybdate blue colorimetric method (GOVETT, 1961) using standards prepared by dilution of a 1000 ppm commercial silica standard solution. The colorimetric analyses were done using plastic volumetric flasks to avoid contamination of the solution with dissolved silica released by etching of glass containers. Fluoride did not affect the colorimetric measurements as shown by tests using standard silica solutions dosed with hydrofluoric acid.

2.4.1.2 Correction for sample withdrawal

Because each experiment was sampled multiple times over the course of the experiment, a correction for the changing surface area to mass ratio was performed in order to analyze the data as an ideal batch reactor experiment. This was done by first summing the change in concentration over each time interval and multiplying that by the mass of solution present at the time of sampling. Then this product was divided by the mass of solution present at the beginning of the experiment to obtain the corrected concentration, m_c (molal).

$$m_c = \frac{\sum_{1}^{n} \Delta m \cdot M}{M_0} \qquad (2.16)$$

where Δm is the change in Si concentration (molal), M is the mass (g) of the solution at sample time and M_0 is the initial mass (g) of the solution. This adjusted the sample concentration downward by 2 to 25 percent. This correction method is discussed in detail by OLSEN and RIMSTIDT (2008) and also used in MITRA (2008).

2.4.1.3 Initial Rate Method

The concentration versus time data were analyzed using the initial rate method (RIMSTIDT and NEWCOMB, 1993) where the data were fit to a second order polynomial and the apparent rate (r', molal/sec) was obtained from the derivative of this fit at $t = 0$

(RIMSTIDT and NEWCOMB, 1993). The apparent rate was converted to the rate of quartz dissolution (r, mol/m^{2}sec) using the relationship:

$$r = \frac{r' M}{A} \quad (2.17)$$

where M is the mass (g) of the solution at sample time and A is surface area (m^2) of the quartz sample.

The activities of the aqueous fluoride species in solution and the solution pH were calculated using the Visual MINTEQ software version 2.52. The solution chemistry for each experiment is tabulated in Appendix 2.1.

The rate data obtained from our experiments and from the literature data set were analyzed using the JMP statistical software version 7.0. A p-value of less than 0.05 was chosen as the cut off for deciding that a regression coefficient is not statistically significant (OTT and LONGNECKER, 2001). JMP uses partial regression plots to illustrate the results of the multiple linear regression models. Partial regression plots provide a better representation of the effect of each individual independent variable on the dependent variable as opposed to using scatter plots of the dependent variables versus the independent variable (e.g., log r versus pH), which do not account for the other independent variables used in the regression model. See MONTGOMERY et al. (2001) for a discussion of partial regression plots.

2.4.2 Literature Data Set

Quartz dissolution rate data were complied from two published dissolution studies (HAROUIYA and OELKERS, 2004; LIANG and READEY, 1987) to create a quartz literature data set. All the data, including sources and solution chemistry are compiled in Appendix 2.2.

Rate data complied from four published amorphous silica dissolution studies (JUDGE, 1971; KNOTTER, 2000; LIANG and READEY, 1987; SPIERINGS, 1993) made up the amorphous silica literature data set. One of the amorphous silica data sources (SPIERINGS, 1993) includes a compilation of published rates from 10 different studies and these are reported here as a single data set. All the data, including sources and solution chemistry are compiled in Appendix 2.3.

The Graph Click digitizing software was used to capture data from graphs in the published document when the data were not tabulated. All dissolution rates were converted to units of mol/m^{2}sec. The solution chemistry including activities of the aqueous fluoride species and the pH were recalculated using the Visual MINTEQ software. These reference datasets cover a calculated pH range of -0.32 to 4.46 and a total fluoride concentration range of 0.3 to 28 molal.

2.5 RESULTS

2.5.1 Empirical rate law for quartz

The results from all our experiments along with the experimental conditions and solution chemistry are tabulated in Appendix 2.1. These data were pooled with the quartz literature data set from Appendix 2.2 and this combined dataset of 75 values was used to derive an empirical rate law.

We first investigated the choice of regression variables regressing the rates versus log a_{HF}, log $a_{HF_2^-}$, log a_{F^-}, pH and $1/T$ individually to develop a regression model of the form

$$\log r = \log A + \log a_i + \log a_{H^+} + \frac{E_a}{2.303\mathrm{R}}(1/T) \qquad (2.18)$$

where i = HF, F^- or HF_2^-, R is the gas constant (8.314 kJK^{-1}mol^{-1}), E_a is the activation energy (kJ/mol), and A is a constant (the pre-exponential factor). Some previous studies (OSSEO-ASARE, 1996) suggested that both a_{HF} and pH affect dissolution rate. On the other hand JUDGE (1971) and SPIERINGS (1993) related dissolution rate to a_{HF} and $a_{HF_2^-}$. KNOTTER (2000) suggests that the dissolution rate is a function of pH, $a_{HF_2^-}$ and $a_{H_2F_2}$ respectively. HAROUIYA and OELKERS (2004) developed a rate law as a function of pH and log a_{F^-}.

A challenge in developing a simple empirical rate law is caused by relationships (Eqs. (2.1) and (2.3)) between a_{HF}, $a_{HF_2^-}$, a_{F^-} and a_{H^+} that cause the activities of the fluoride species to be correlated with each other, as illustrated in Figs. 2.1 and 2.2. Three of these four variables will be correlated by equilibrium reactions in a regression model

that includes all four variables. Therefore, we considered only combinations of any two of the above variables at a time in our regression models (Table 2.1). In the subsequent discussion we will focus on the empirical rate law developed from the regression model that uses log a_{HF}, pH and $1/T$ as regression variables. This form of the rate law appears to be the most useful for practical purposes since the three variables i.e., a_{HF}, pH and $1/T$ are determined by direct measurement or by design. Fig. 2.6 shows the partial regression plots for this regression model. Log a_{HF}, pH and $1/T$ are all significant predictors of log r, so that

$$\log r_{qz} = -4.53(1.04) + 1.18(0.06)\log a_{HF} + 0.39(0.05)pH - 988.78(327.81)/T \qquad (2.19)$$

where the numbers in parentheses are one standard error of the regression coefficient (R^2 = 0.91; n = 75). Eq. (2.19) can be transformed to the rate law

$$r_{qz} = 10^{-4.53}\left(\mathrm{e}^{\frac{-18932}{\mathrm{R}T}}\right)a_{HF}^{1.18}a_{H^+}^{-0.39} \qquad (2.20)$$

where -5.13 < a_{HF} < 1.60, -0.28 < pH < 7.18, and 25 < T < 100 °C.

Table 2.1. Results of the regression models for the quartz rate data (n = 75) using different combinations of the variables. Bold font represents *p*-values more than 0.05 and are not statistically significant.

Regression model variables	**R^2**	**Regression coefficient (std. error)**	***p*-value**
log a_{HF}	0.910	1.18(0.06)	<0.0001
pH		0.39(0.05)	<0.0001
1/*T*		-988.78(327.80)	0.0035
Intercept		-4.53(1.04)	<0.0001
log $a_{\mathrm{HF_2^-}}$	0.907	0.59(0.03)	<0.0001
pH		-0.19(0.03)	<0.0001
1/*T*		-1194.15(338.03)	0.0007
Intercept		-2.31(1.11)	0.0408
log $a_{\mathrm{F^-}}$	0.907	1.18(0.06)	<0.0001
pH		-0.79(0.03)	<0.0001
1/*T*		-1641.78(355.18)	<0.0001
Intercept		1.44(1.23)	**0.2463**
log a_{HF}	0.907	0.39(0.07)	<0.0001
log $a_{\mathrm{HF_2^-}}$		0.39(0.06)	<0.0001
1/*T*		-1112.64(341.18)	0.0017

Intercept		-3.09(1.16)	0.0093
log a_{HF}	0.907	0.79(0.03)	<0.0001
log a_{F^-}		0.39(0.06)	<0.0001
1/*T*		-1192.84(347.09)	0.0010
Intercept		-2.59(1.20)	0.0342
log $a_{HF_2^-}$	0.907	0.79(0.03)	<0.0001
log a_{F^-}		-0.39(0.07)	<0.0001
1/*T*		-1030.83(347.42)	0.0041
Intercept		-3.60(1.20)	0.0037

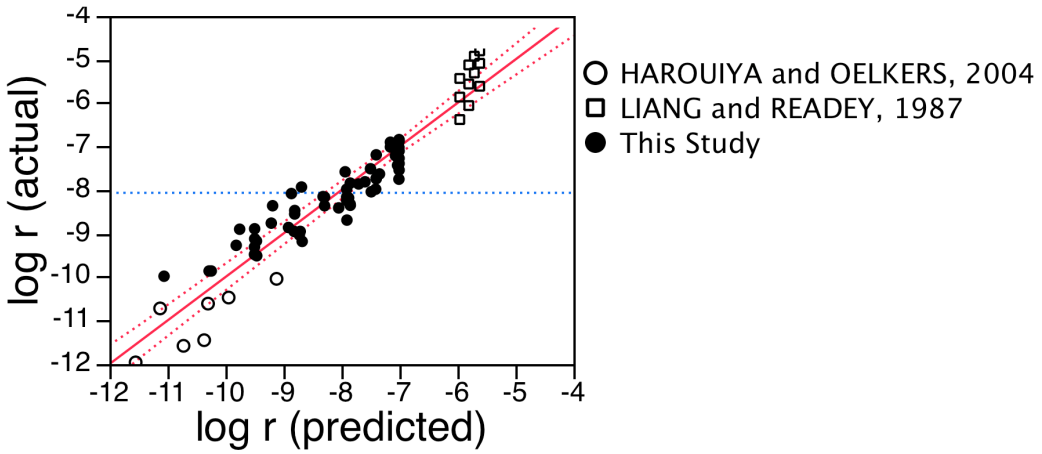

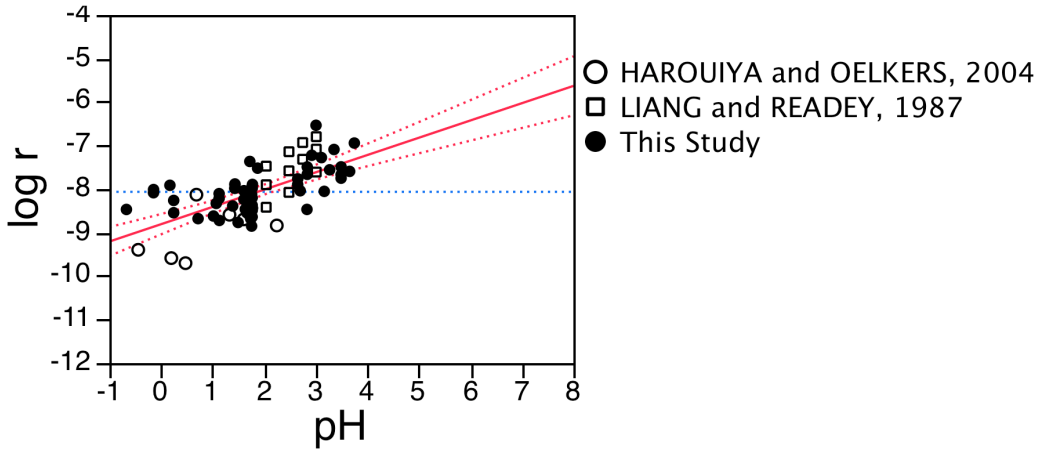

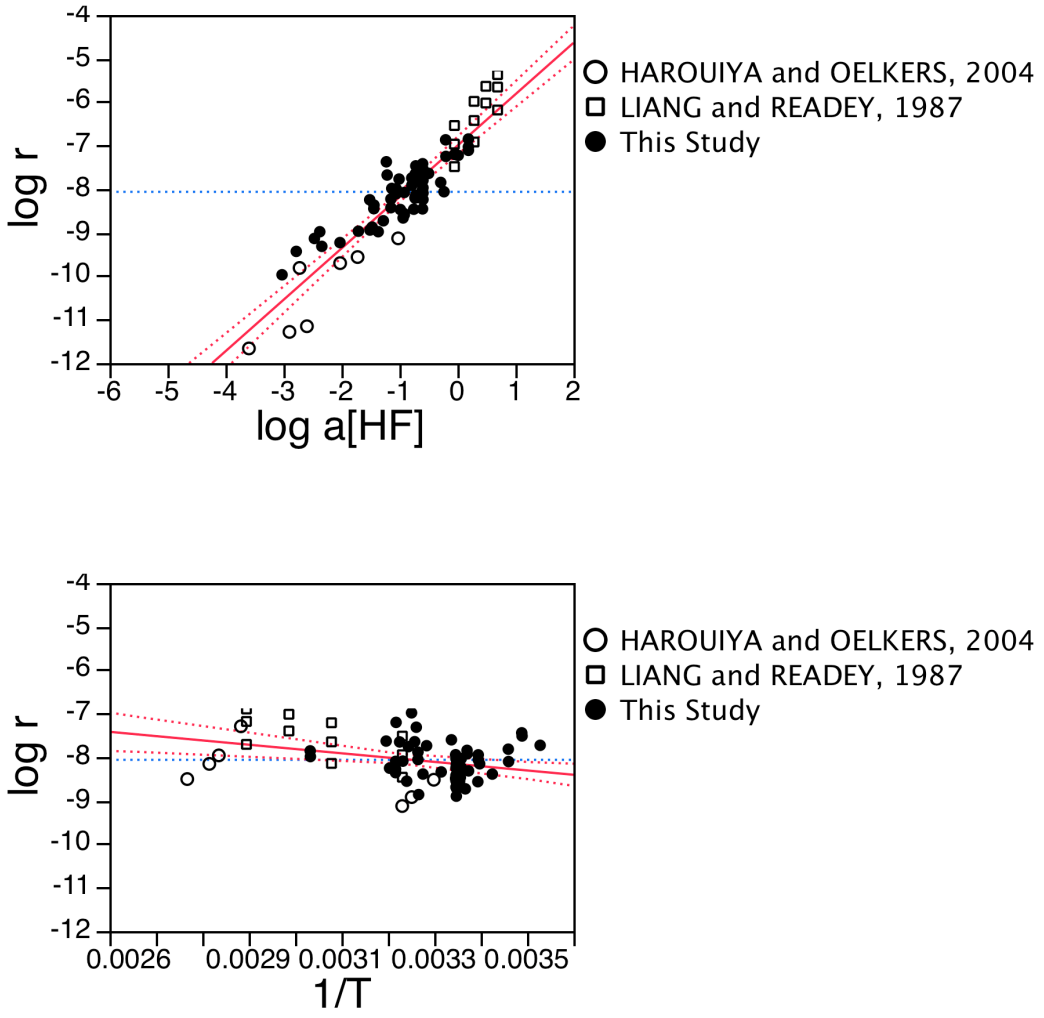

Figure 2.6. Partial regression plots for the multiple linear regression model of quartz dissolution rates as a function of log a_{HF}, pH and $1/T$. The first graph shows predicted log r versus observed log r. The next three graphs show the effect of pH, log a_{HF} and $1/T$ respectively on log r. R^2 and p-values are listed in Table 2.1.

2.5.2 Empirical rate law for amorphous silica

The amorphous silica literature data set was similarly analyzed. Log a_{HF}, pH and $1/T$ were all found to be significant predictors of log r, so that

$$\log r_{as} = 0.48(0.40) + 1.50(0.02)\log a_{HF} + 0.46(0.02)pH - 1788.39(120.59)/T \qquad (2.21)$$

where the numbers in parentheses are one standard error of the regression coefficient (R^2 = 0.91; n = 97). Fig. 2.7 shows the partial regression plots for this regression model. Eq. (2.21) can be transformed to the empirical rate law

$$r_{as} = 10^{0.48}\left(e^{\frac{-34243}{RT}}\right)a_{HF}^{1.50}a_{H^+}^{-0.46} \qquad (2.22)$$

where -5.13 < a_{HF} < 1.60, -0.28 < pH < 7.18 and 25 < T < 70 °C.

Results from all the regression models that were developed using multiple linear regression and different combinations of the regression variables are listed in Table 2.2.

Table 2.2. Results of the regression models for the amorphous silica literature data set (n = 97) using different combinations of the variables. Bold font represents *p*-values more than 0.05 and are not statistically significant

Regression model variables	R^2	Regression coefficient (std. error)	*p*-value
log a_{HF}	0.98	1.50(0.02)	<0.0001
pH		0.46(0.02)	<0.0001
1/*T*		-1788.39(120.59)	<0.0001
Intercept		0.48(0.40)	**0.2410**
log $a_{HF_2^-}$	0.98	0.75(0.01)	<0.0001
pH		-0.29(0.02)	<0.0001
1/*T*		-2146.98(120.41)	<0.0001
Intercept		3.61(0.40)	<0.0001
log a_{F^-}	0.98	1.50(0.02)	<0.0001
pH		-1.04(0.02)	<0.0001
1/*T*		-2824.44(120.61)	<0.0001
Intercept		8.71(0.41)	<0.0001
log a_{HF}	0.98	0.59(0.03)	<0.0001
log $a_{HF_2^-}$		0.46(0.02)	<0.0001
1/*T*		-2006.76(118.67)	<0.0001
Intercept		2.38(0.39)	<0.0001
log a_{HF}	0.98	1.04(0.02)	<0.0001
log a_{F^-}		0.46(0.02)	<0.0001
1/*T*		-2103.99(118.02)	<0.0001
Intercept		2.98(0.38)	<0.0001
log $a_{HF_2^-}$	0.98	1.04(0.02)	<0.0001
log a_{F^-}		-0.59(0.03)	<0.0001
1/*T*		-1881.72(117.52)	<0.0001
Intercept		1.61(0.38)	<0.0001

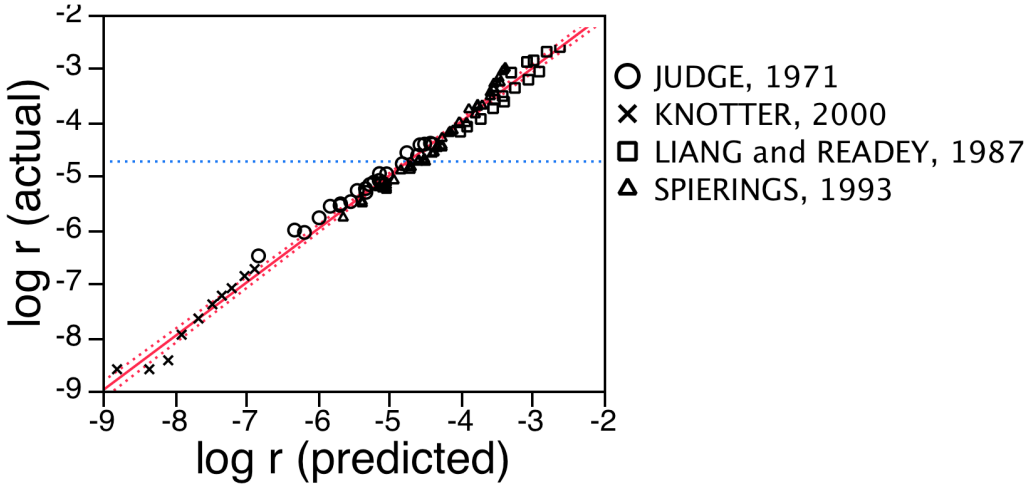
log r (actual)
log r (predicted)
-2
-3
-4
-5
-6
-7
-8
-9
JUDGE, 1971
KNOTTER, 2000
LIANG and READEY, 1987
SPIERINGS, 1993

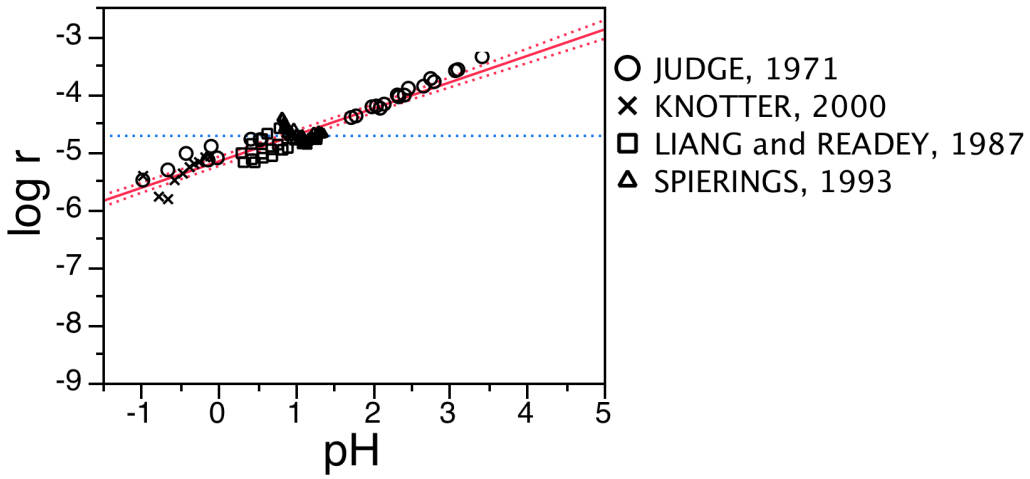
log r
pH
-3
-4
-5
-6
-7
-8
-9
-1
0
1
2
3
4
5
JUDGE, 1971
KNOTTER, 2000
LIANG and READEY, 1987
SPIERINGS, 1993

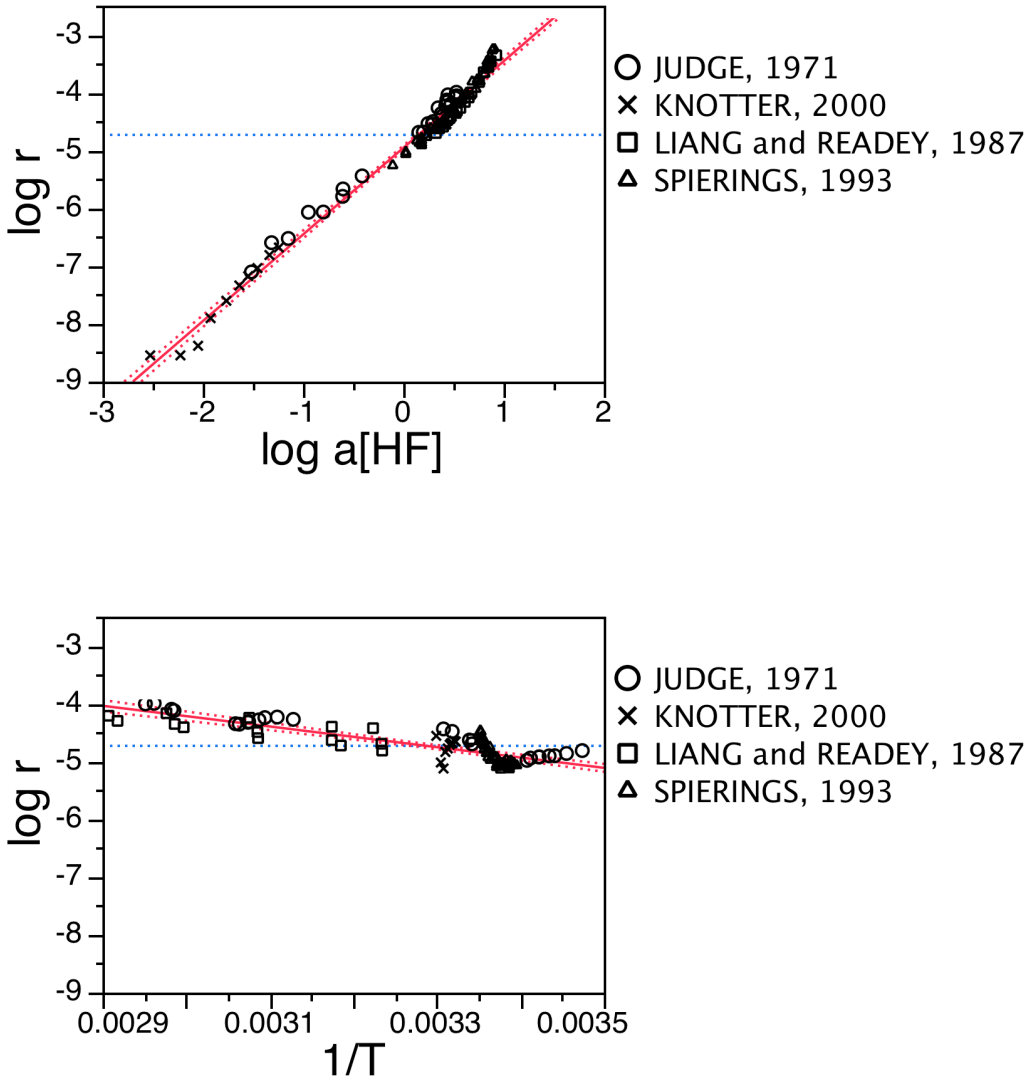

Figure 2.7. Partial regression plots for the multiple linear regression model for amorphous silica dissolution rates as a function of log a_{HF}, pH and $1/T$. The first graph shows predicted log r versus observed log r. The next three graphs show the effect of pH, log a_{HF} and $1/T$ respectively on log r. R^2 and p-values are listed in Table 2.2.

2.6 DISCUSSION

2.6.1 Dissolution kinetics and solution speciation

Analysis of the dissolution rate data for both quartz and amorphous silica reveals that their dissolution rates can be expressed equally well by rate laws that combine an a_{H^+} term with an a_{HF}, $a_{HF_2^-}$ or a_{F^-} term or by combinations of fluoride species terms. This is because the activities of the fluoride species are correlated with each other by the reactions in Eqs. (2.1) and (2.3), as illustrated in Figs. 2.1 and 2.2. Therefore, it is not possible to create a unique rate law that identifies one or another of these fluoride species as the primary reactant.

As a first approximation, for relatively low total fluoride concentrations (< 1 molal), using the rate laws that express the dissolution rates as a function of a_{HF}, a_{H^+} and $1/T$ provides a convenient approximation of the dissolution rates for pH < 3.164. The rate laws used to calculate the rates for quartz and amorphous silica are:

$$r_{qz} = 10^{-4.53}\left(e^{\frac{-18932}{RT}}\right)a_{HF}^{1.18}a_{H^+}^{-0.39} \qquad (2.20)$$

$$r_{as} = 10^{0.48}\left(e^{\frac{-34243}{RT}}\right)a_{HF}^{1.50}a_{H^+}^{-0.46} \qquad (2.22)$$

For low total fluoride concentrations and for pH > 3.16, the dissolution rates of quartz and amorphous silica can be estimated by these rate laws:

$$r_{qz} = 10^{1.44}\left(e^{\frac{-31435}{RT}}\right)a_{F^-}^{1.18}a_{H^+}^{0.79} \qquad (2.23)$$

$$r_{as} = 10^{8.71}\left(e^{\frac{-54080}{RT}}\right)a_{F^-}^{1.50}a_{H^+}^{1.04} \qquad (2.24)$$

This approach assumes that below pH 3.16, $a_{HF} \approx T_F$ and above pH 3.16, $a_{F^-} \approx T_F$ and thereby avoids a speciation calculation. Dissolution rates calculated using this approach are illustrated in Figs. 2.8a and 2.8b. The use of this approach is fairly accurate for $T_F < 1$ molal because of simple fluoride speciation as discussed in Section 2.3.1 and as illustrated in Figs. 2.1 and 2.2. At these concentrations when pH < 3.16 (pK_{HF}), HF is the predominant species and the form of the rate law that express the dissolution rate as a

function of a_{HF}, a_{H^+} and $1/T$ (Eqs. (2.20) and (2.22)) is used. And for pH > 3.16 (pK_{HF}), F^- is the predominant species and the form of the rate law that express the dissolution rate as a function of a_{F^-}, a_{H^+} and $1/T$ (Equations (2.23) and (2.24)) is used. A combination of both rate laws gives fairly accurate estimates of dissolution over the pH range of 0 to 7 as shown in Figs. 2.8a and 2.8b.

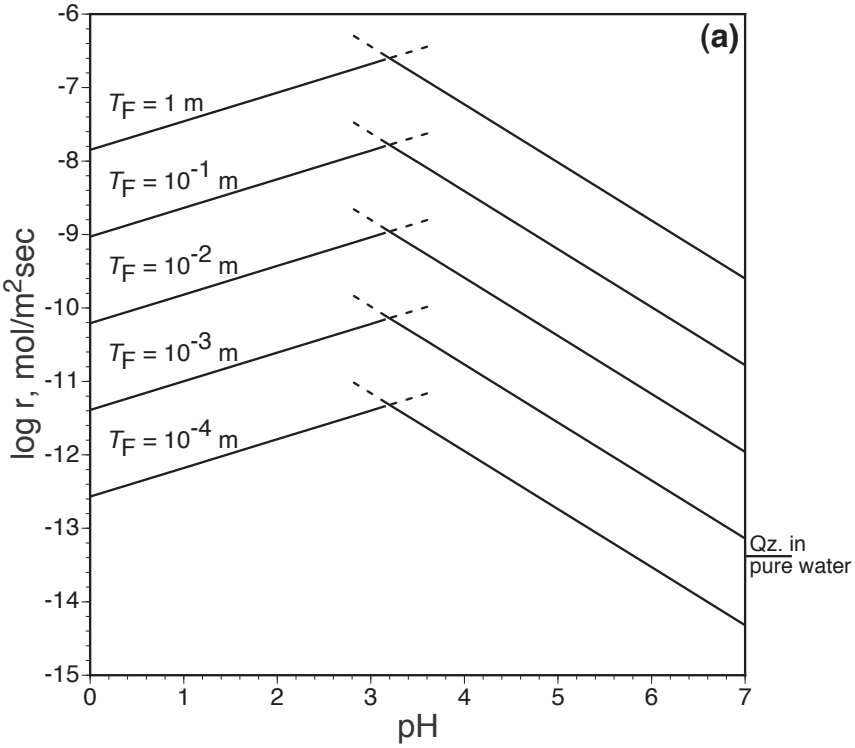

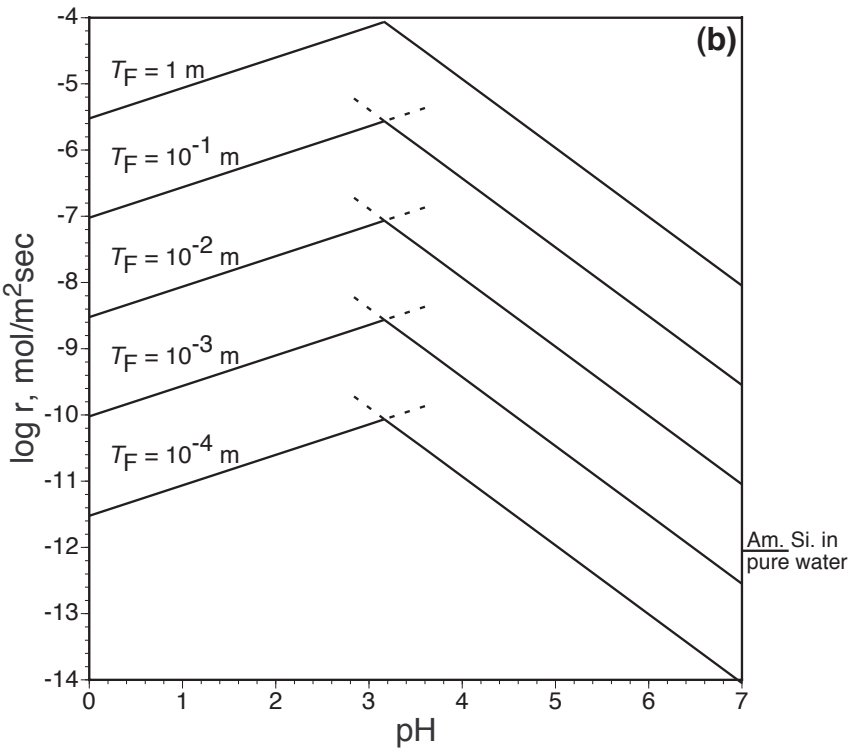

Figure 2.8. (a) Quartz dissolution rates calculated using Eqs. (2.20) and (2.23), contoured in total fluoride concentration. (b) Amorphous silica dissolution rates calculated using Eqs. (2.22) and (2.24) and contoured in total fluoride concentration. Dissolution rates in pure water predicted by RIMSTIDT and BARNES (1980) are shown by the tic marks on the right axis.

Using these two rate laws allows for a quick approximation (± 2x) of the dissolution rate, only for systems with relatively low total fluoride concentrations (< 1 molal). For higher fluoride concentrations (> 1 molal) the occurrence of HF_2^- in solution must be taken into account (Fig. 2.2).

Improved accuracy, especially for higher T_F, requires consideration of the distribution of aqueous fluoride species. Fig. 2.9 shows quartz dissolution rates calculated from Eq. (2.20) where the a_{HF} is taken from the Visual MINTEQ speciation model (see Fig. 2.2). Because the solution speciation model takes into account the occurrence of HF_2^- this approach can be used for much higher total fluoride concentrations (> 1 molal). Using the rate laws based on regression models that combine a a_{H^+} term with a $a_{HF_2^-}$ or a_{F^-}

term (Table 2.1) produces essentially the same predicted rates. This means that any of the rate laws can be used along with a solution speciation model to calculate rates.

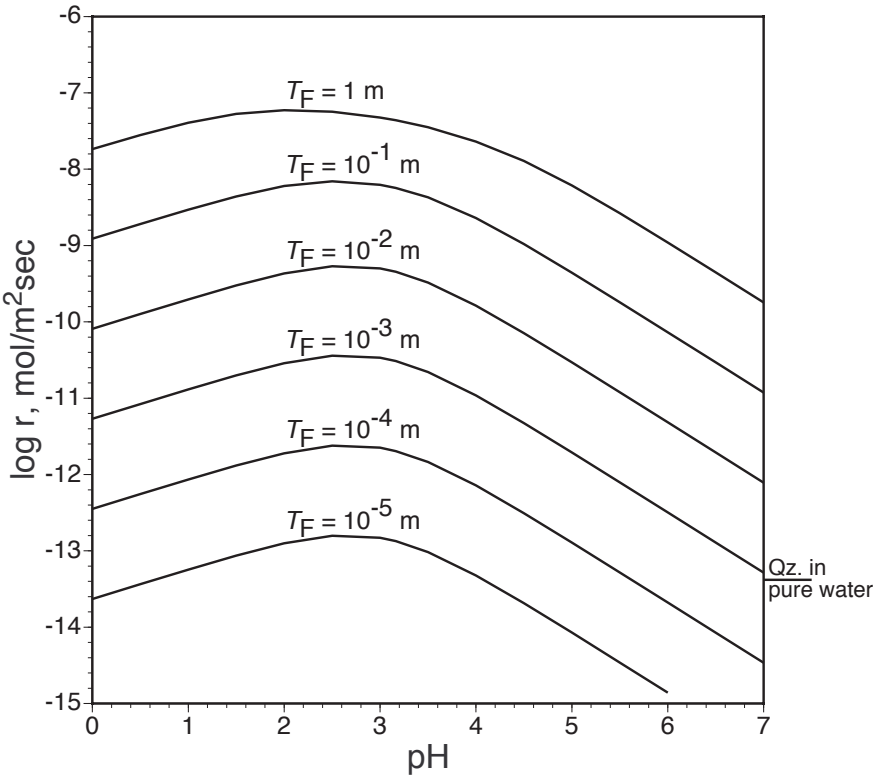

Figure 2.9. Calculated quartz dissolution rates using the rate law for quartz (Eq. (2.20)) and the speciation model approach, contoured in total fluoride concentration. Dissolution rates in pure water predicted by RIMSTIDT and BARNES (1980) are shown by the tic marks on the right axis.

The rate of quartz dissolution is highest near pK_{HF} and decreases with both decreasing and increasing pH. Note that for $T_F < 10^{-5.5}$ the maximum rate is lower than the dissolution rate in pure water. The maximum rate near pH 3 is caused by the interaction of the a_{H^+} and a_{HF} terms in the rate law. Decreasing pH causes a_{HF} to increase, which in turn causes the rate to increase. At the same time a_{H^+} increases, which causes the rate to decrease. These two counteracting terms result in a maximum rate near pH 3.

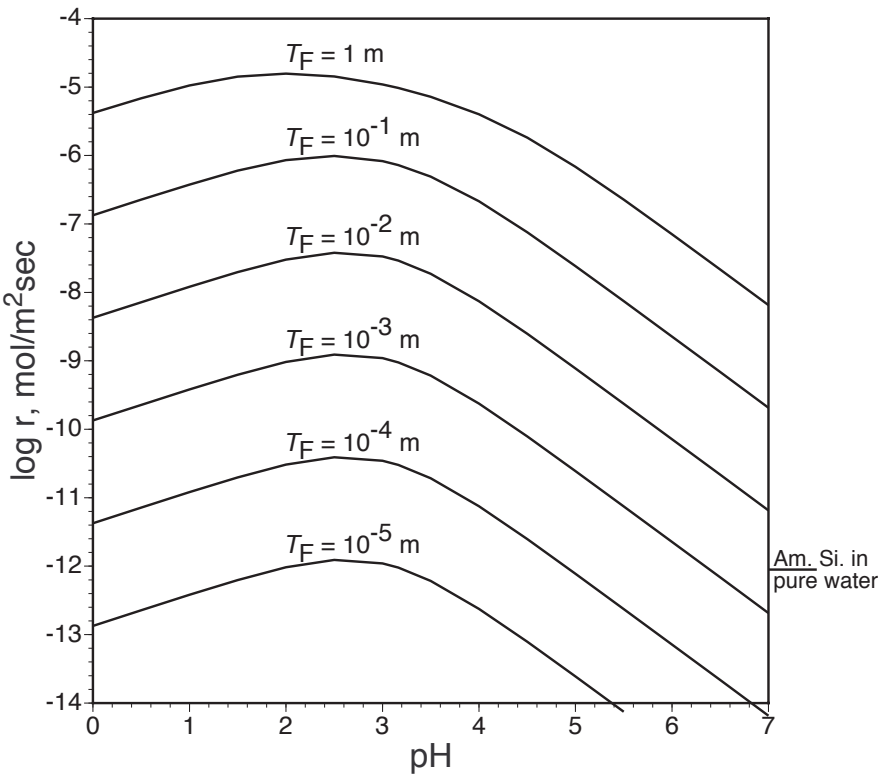

Figure 2.10. Calculated amorphous silica dissolution rates using the rate law for amorphous silica (Eq. (2.22)) and the speciation model approach, contoured in total fluoride concentration. Dissolution rates in pure water predicted by RIMSTIDT and BARNES (1980) are shown by the tic marks on the right axis.

Fig. 2.10 shows the rate of dissolution of amorphous silica in fluoride solutions for a pH range of 0 to 7, contoured in total fluoride concentration. These rates were calculated using Eq. (2.22) using the same approach used for calculating the quartz dissolution rates. The trends of the dissolution rates for amorphous silica are similar to that of quartz with a maximum dissolution near pH 3. When $T_F < 10^{-4.5}$ the maximum fluoride rate is lower than the rate of amorphous silica dissolution in pure water.

A comparison of Figs. 2.8a, 2.8b, 2.9 and 2.10 show very similar patterns though the slopes exhibited by the lines are slightly different due to the reaction orders in the rate laws. This is because the second approach for calculating the dissolution rates using the solution speciation model takes into account the occurrence of HF_2^- in solution and its increasing abundance with increasing total fluoride concentrations (Fig. 2.2).

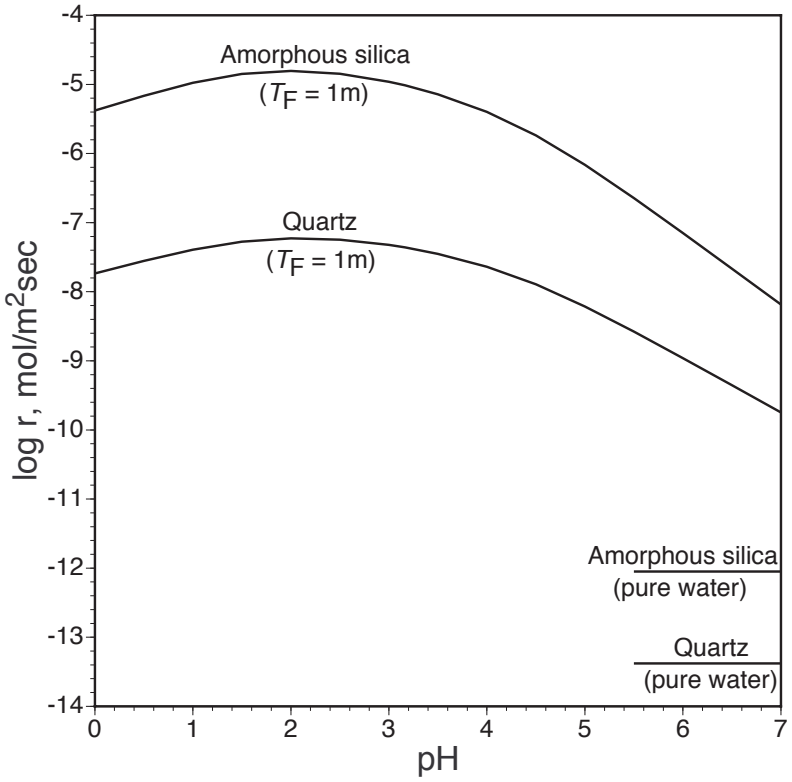

Figure 2.11. A comparison of dissolution rates of quartz and amorphous silica at 25°C, in solutions with total fluoride concentration of 1 m (T_F = 1 m) and pure water.

Fig. 2.11 compares quartz and amorphous silica dissolution rates in pure water predicted by RIMSTIDT and BARNES (1980) and in a 1 molal T_F solution calculated from Eqs. (2.20) and (2.22), at 25°C. The dissolution rate of quartz at pH 3 in a 1 molal T_F solution is nearly six orders of magnitude faster than its dissolution rate in pure water. On the other hand, at pH 3 the dissolution rate of amorphous silica in a 1 molal T_F solution is nearly seven orders of magnitude higher than its dissolution rate in pure water. Near pH 3, the maximum amorphous silica dissolution rate is about 250 times faster than the maximum quartz dissolution rate. This difference declines with increasing pH to only about 32 times faster at pH 7. In pure water, amorphous silica dissolution rate is approximately 18 times faster than quartz, a factor that is proportional to the solubility.

2.6.2 Comparison of solubility and rate diagrams

It is informative to compare the solubility and rate diagrams for quartz dissolution (Figs. 2.5 and 2.9). Both the solubility and the rate diagram exhibit similarly shaped trends. But this is not surprising because both the solubility and the dissolution rates are strongly controlled by the fluoride speciation. At lower total fluoride concentrations (< 10^{-2} molal) both diagrams have a peak near pH 3 (pK_{HF}). But for higher total fluoride concentrations (> 10^{-1} molal), quartz solubility is nearly constant over the pH range of 0 to 7, so that at higher T_F, pH has little effect on the solubility. This is not the case for quartz dissolution rates, which continue to show a rate maximum near pH 3 at higher T_F similar to that exhibited at lower total fluoride concentrations. This means that for higher total fluoride concentrations (> 10^{-1} molal) and higher pH's (>3.5), even though quartz solubility is high, the rate of dissolution decreases with increasing pH. This is because at high pH there are insufficient H^+ ions available to maintain a fast dissolution rate.

2.6.3 Reaction Mechanism

Several studies have proposed various reaction mechanisms for the dissolution of silica in hydrofluoric acid solutions based on either experimental observations (JUDGE, 1971; KIKUYAMA et al., 1992; KLINE and FOGLER, 1981; KNOTTER, 2000; OSSEO-ASARE, 1996; PROKOPOWICZ-PRIGOGINE, 1989; PROKSCHE et al., 1992; SPIERINGS, 1993; SPIERINGS and VAN DIJK, 1987; VERHAVERBEKE et al., 1994) or *ab initio* quantum mechanics models (HOSHINO and NISHIOKA, 1999; KANG and MUSGRAVE, 2002; TRUCKS et al., 1990).

The first step toward developing a model of the reaction mechanism is to understand constraints imposed by the empirical rate laws obtained from the experimental results. Reaction mechanisms proposed by some of the previous studies are based on empirical rate laws. JUDGE (1971), based on his experimental results of dissolution of thin films of thermally oxidized silicon wafers concluded that the dissolution rate of silica in dilute acidic fluoride solutions (< 1 M) depends on the HF and HF_2^- concentrations in solution but not on the free fluoride (F^-) concentration. Judge (JUDGE, 1971) also suggested that HF_2^- is nearly four to five times more reactive than HF,

based on the correlation of aqueous speciation and the etch rates. He also suggested that at higher total fluoride concentrations, the polymeric HF species of the form $H_nF_{n+1}^-$ may be involved in the dissolution reaction. KIKUYAMA et al. (1992) and PROKSCHE et al. (1992) have suggested similar dissolution mechanisms involving HF and HF_2^-. SPIERINGS (1993) and SPIERINGS and VAN DIJK (1987) concluded that the dissolution of silicate glasses in aqueous hydrofluoric acid solutions is controlled by the adsorption of HF and HF_2^- and the catalytic action of H^+ ions. PROKOPOWICZ-PRIGOGINE (1989) suggested a model along the same lines in which the reaction rate is determined by the adsorption of HF on vicinal silanol groups, HF_2^- ions on surface silanol groups and H^+ ions on the surface bridging oxygens in siloxane units. This adsorption of HF and HF_2^- on the silanol groups makes the bridging oxygen more nucleophilic and as a result increases the adsorption of H^+ ion on the bridging oxygen atoms. This in turn causes the breaking of siloxane bonds. According to this model the rate-determining step is the breakage of the siloxane bond by the combined action of the adsorbed species. They assumed that species sorption, and therefore the rate, follows a Langmuir isotherm. SPIERINGS (1993) also suggests that this model for the dissolution of silicate glasses can be applied to the dissolution of multicomponent glasses and compositionally related crystalline silicates such as feldspars. KLINE and FOGLER (1981) have on the other hand suggested that the reaction mechanism is only dependent of HF molecules along with a catalytic role played by H^+ ions. According to their mechanism, the lattice (terminal oxygens) bonds of the silica surface are protonated by H^+ ions adsorbed at the surface accompanied by a simultaneous nucleophilic attack by HF on the bridging oxygen. The initial adsorption of the HF molecules on the silica surface results in a weakening of the surface bonds by the association of the HF protons with the adjacent lattice (terminal) oxygens. VERHAVERBEKE et al. (1994) suggest that the etching mechanism of silica in hydrofluoric acid involves the dimer H_2F_2 and HF_2^-. They propose that HF_2^- primarily controls the etching at very low concentrations and with increasing total fluoride concentration, the contribution of HF_2^- decreases accompanied with a corresponding increase in the contribution of H_2F_2. At a concentration of 0.1 M, the contribution to etching by both HF_2^- and H_2F_2 is equal. Finally at higher total fluoride concentrations H_2F_2 is primarily

responsible for the etching of silica. They base this reaction mechanism on the best-fit model obtained for their experimental etch rate data at fluoride concentrations above 0.1 M. However, their experimental results could be modeled equally well by using either HF or H_2F_2 because they cannot distinguish between the reaction of two HF molecules and one H_2F_2 molecule due the relationship in Eq. (7). But the authors argue that to model the etching mechanism using HF requires the participation of four HF molecules in the reaction and that is not probable. Hence, the mechanism for etching of silica in dilute fluoride solutions is primarily due to H_2F_2.

KNOTTER (2000) similarly studied the dissolution of vitreous silica and other multicomponent silicate glasses in HF solutions. According to them, the nucleophiles HF_2^- and H_2F_2 react with the silicon atom of a surface silanol (SiOH) group that has lost an H_2O molecule (for pH < 1.5) or OH^- group (for pH > 1.5) and this reaction supplies a F^- ion to the silicon atom. This is the rate-determining step. Knotter (KNOTTER, 2000) also suggests that there is pH dependence because pH influences the protonation and deprotonation of the surface silanol groups and the elimination of a water molecule at low pH is much faster than the elimination of an OH^- at higher pH.

LIANG and READEY (1987), based on results from their experiments on the dissolution of crystalline and amorphous silica in HF-HCl acid mixtures, conclude that the dissolution is a surface reaction-controlled process rather than by diffusion in the liquid. They propose that the dissolution rate depends on the HF concentration and the rate-controlling step is the ligand substitution reaction of HF molecules with a surface complex ion. Their experiments documented a dependence of dissolution rates of quartz on crystallographic direction. They found that fused silica dissolution rates are much faster than the X and Y directions of quartz, but only two times faster than the dissolution rate for the Z directions of quartz. This suggests that some surface bonding geometries react more readily than others and the reaction mechanism is very geometry dependent. This observation partly explains the faster amorphous silica dissolution rates relative to quartz. This is also consistent with the very low etching rates reported for coesite, stishovite and micas in HF solutions (MONK et al., 1993). WOLFF-BOENISCH et al. (2004) performed a dissolution study of multicomponent aluminosilicate glasses in HF solutions and the rates of dissolution observed by them are much faster than the rates of dissolution

of amorphous silica in HF solutions observed in studies compiled in our amorphous silica literature dataset. The faster dissolution rates reported by WOLFF-BOENISCH et al. (2004) could be attributed to bonding geometries of the glasses used in their experiments being more favorable to attack by fluoride species. In our study, and all of those that used quartz grains, the grain surfaces displayed an ensemble of bonding geometries so that the measured rate is an average of the crystallographically different rates.

OSSEO-ASARE (1996) proposed a surface complexation model that is based on his analysis of JUDGE (1971) rate data. He suggests that the surface silanol groups (Si-OH) protonate and deprotonate depending on the pH to give positively charged ($Si-OH_2^+$) and negatively charged ($Si-O^-$) sites respectively. According to him, the fluoride ion adsorbs to the surface by the surface ligand exchange reaction

$$Si-OH + HF = SiF + H_2O \qquad (2.25)$$

and this results in the polarization of the underlying Si-O bonds. The surface Si-F groups then detaches constituting the effective dissolution event. He also suggests "the effects of the aqueous phase variables (e.g. pH) on the dissolution rate are correlated with the effects of these same variables on the surface concentration of adsorbed fluoride". He attributes the decrease in etch rates with increasing pH to the competition between OH^- and F^- ions for adsorption on surface sites.

As discussed earlier, the dissolution rate data from our experiments and the analysis of the literature datasets for quartz and amorphous silica reveals that their dissolution rate can be expressed equally well by any rate law that combines an a_{H^+} term with a a_{HF}, $a_{HF_2^-}$ or a_{F^-} term. This is because the activities of the fluoride species are correlated with each other by the reactions in Eqs. (2.1) and (2.3), as illustrated in Figs. 2.1 and 2.2. As a result all the different empirical rate laws describe the dissolution kinetics equally well. Hence, the approach of using the empirical rate law alone to identify the reacting fluoride species is problematic, although the empirical rate law requires that H^+ is involved in the reaction mechanism.

A few studies have used *ab initio* quantum mechanics models to test a possible reaction mechanism for the dissolution of silica on HF solutions. KANG and MUSGRAVE (2002) developed a quantum chemical model for the etching of silica by HF and H_2O

which involves four sequential bond-breaking steps of one of the three Si-O bonds of the surface silicon atom. This eventually forms a fluorine-terminated silicon surface that HF attacks resulting in a hydrogen-passivated silicon surface and a single SiF_4 molecule that is released from the surface. Water plays a catalytic role in the reaction by simultaneously donating one hydrogen atom to the surface OH group while accepting one hydrogen atom from the attacking HF molecule.

HOSHINO and NISHIOKA (1999) also used *ab initio* quantum chemical calculations to model an etching mechanism that consists of four steps with each step consisting of an attack on the Si-O bonds by a HF molecule. They describe this mechanism as a "switching process involving the dissociation of an Si-O bond and the generation of an Si-F bond".

How can we envision a reaction mechanism for dissolution of silica that is consistent with the empirical rate laws that were developed in this chapter? In order for Si in a Q_3 site to be released into solution three Si-O bonds must be broken. It is unlikely that multiple bonds will break simultaneously so we expect this process to consist of a series of sequential elementary reaction steps. The slowest of these sequential bond-breaking steps is the rate-determining step and the rate of that step is reflected in the empirical rate law. This suggests that the empirical rate law reflects the stoichiometry of the rate-determining step.

A simple "bond breaking" elementary step in silica dissolution would produce a 3-coordinated Si atom ($^{[3]}Si$) and a 1-coordinated O atom ($^{[1]}O$). Although such species are theoretically possible they would be very unstable and thus a great deal of energy would be needed to form them. A more likely reaction scenario involves an activated complex consisting of overcoordinated Si and O atoms that breaks down to reaction products with normal coordination numbers, $^{[4]}Si$ and $^{[2]}O$. See LASAGA and GIBBS (1990) for an example of how hydrolysis of a Si-O bond involves $^{[5]}Si$ and $^{[3]}O$ in the activated complex. The hydrolysis reaction that "breaks" a Si-O bond thus involves the simultaneous electrophilic attack by H from the water molecule on a bridging oxygen atom and a nucleophilic attack on the Si atom by the O atom in the water molecule. When the H atom, acting as a Lewis acid, overcoordinates the bridging oxygen and the O atom, acting as a Lewis base, overcoordinates the Si atom, electrons can move from the Si-O

bridging bond to form a OH bond and a bond between Si and OH from the water molecule. By analogy we propose that the dissolution of silica in reactions involving fluoride species should involve the simultaneous overcoordination of a Si atom by a fluoride species, acting as a Lewis base, and an adjacent bridging oxygen atom by a Lewis acid (H^+ in the experiments reported here, but possibly by other cations). Use of the term "bond-breaking" is a potentially serious source of confusion in discussion of reaction mechanisms. The elementary reaction steps are unlikely to be true bond-breaking processes that result in under coordinated atoms for the reasons described above. Therefore, the reaction appears to involve transfer of electrons from the bond between adjacent over coordinated Si and O atom to form new bonds between the Si and F atoms and the O and H atoms.

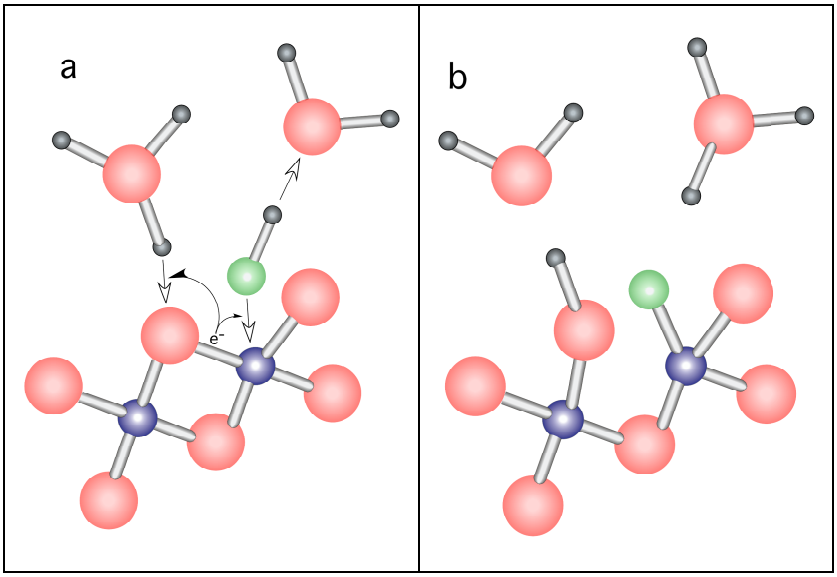

Figure 2.12. Schematic illustration of a proposed Si-O bond breaking mechanism involving H^+ from a hydronium ion and F^- from HF(aq). (a) The activated complex consists of an adsorbed hydronium ion approaching a bridging oxygen atom and an adsorbed HF molecule approaching an adjacent silicon atom. (b) When the oxygen and silicon atoms become over coordinated, electrons move from the Si-O bond to form O-H and Si-F bonds. This lowers the O coordination to 2 and the silicon coordination to 4 and breaks the Si-O bond.

Although we cannot infer the entire reaction mechanism using the empirical rate law, we can learn quite a lot about a possible mechanism for the rate-determining step for silica dissolution. An examination of the empirical rate laws that express the rates as a combination of a a_{H^+} term with a a_{HF}, $a_{HF_2^-}$ or a_{F^-} term derived for quartz and amorphous silica in Tables 2.1 and 2.2 shows that only the first table entries will produce rate laws (Eqs. (2.20) and (2.22)) that have positive reaction orders for a_{HF} and a_{H^+}. Now if the empirical rate law reflects the stoichiometry of the rate-determining step then we expect the reaction orders to be positive numbers. Even though the rate laws with negative reaction orders are mathematically correct, they are not interpretable in a mechanistic fashion. So we prefer to interpret the rate law that expresses the rate as a function of a_{HF}, a_{H^+} and $1/T$ (Eqs. (2.20) and (2.22)). These empirical rate laws imply that the rate-determining step in the reaction mechanism involves a coordinated attack of HF and H^+ on the Si-O bond where the H^+ ion, acting as a Lewis acid, attacks the bridging O atom, while the F end of a HF molecule, acting as a Lewis base, attacks the Si atom (Fig. 2.12). This allows a redistribution of electrons from the Si-O bond to form a O-H and a Si-F bond, thus "breaking" the Si-O bond. For a Q_3 silica site, a sequence of three bond breaking steps are needed to liberate the Si-F species into solution, but we do not know which of the three sequential bond breaking steps is the rate-determining step. The reaction orders for the rate laws (Eqs. (2.20) and (2.22)) are fractional, which might be interpreted to mean that a precursor step for the bond breaking is the sorption of H^+ and HF onto the silica surface. LASAGA (1981), pointed out that sorption onto non-uniform surfaces leads to rate laws with fractional reaction orders. Thus, the fractional reaction order suggests a distribution of sorption site energies on the surface of the silica. Fractional reaction orders are commonly seen in oxides and silicate dissolution (WHITE and BRANTLEY, 1995). Our suggested reaction mechanism is very similar to the one suggested by KLINE and FOGLER (1981) discussed earlier. This is also similar to the previously discussed *ab initio* model suggested by KANG and MUSGRAVE (2002), but instead of the etching mechanism by HF and H_2O as suggested by them, our model proposes the involvement of HF and H^+. We recognize that the dissolution of oxides is

complicated and we hope that our proposed reaction mechanism will stimulate future research.

2.7 REFERENCES

Ault, B. S., 1978. Infrared spectra and structure of the argon-matrix isolated hydrogen difluoride(1-) anion. *J. Phys. Chem.* **82**, 844-846.

Barboux, P., Laghzizil, A., Bessoles, Y., Deroulhac, H., and Trouve, G., 2004. Paradoxical crystalline morphology of frosted glass. *Journal of Non-Crystalline Solids* **345-346**, 137-141.

Baumann, E. W., 1969. Determination of stability constants of hydrogen and aluminum fluorides with a fluoride-selective electrode. *Journal of Inorganic and Nuclear Chemistry* **31**, 3155-3162.

Bell, R. P., Bascombe, K. N., and McCoubrey, J. C., 1956. Kinetics of the depolymerisation of trioxan in aqueous acids, and the acidic properties of aqueous hydrogen fluoride. *Journal of the Chemical Society*, 1286-1291.

Broene, H. H. and Vries, T. d., 1947. The Thermodynamics of Aqueous Hydrofluoric Acid Solutions. *J. Am. Chem. Soc.* **69**, 1644-1646.

Busey, R. H., Schwartz, E., and Mesmer, R. E., 1980. Fluorosilicate equilibriums in sodium chloride solutions from 0 to 60.degree.C. *Inorg. Chem.* **19**, 758-761.

Ciavatta, L., Iuliano, M., and Porto, R., 1988. Fluorosilicate equilibria in acid solution. *Polyhedron* **7**, 1773-1779.

Clark, H. C., Corfield, P. W. R., Dixon, K. R., and Ibers, J. A., 1967. An unexpected product in the reaction of $PtHCl[P\text{-}(C_2H_5)_3]_2$ with tetrafluoroethylene. Structure of the $PtCl(CO)P(C_2H5)_3]_2^+$ cation and evidence or the existence of the SiF_5-ion. *J. Am. Chem. Soc.* **89**, 3360-3361.

Coyle, B. A., Schroeder, L. W., and Ibers, J. A., 1970. The structure of potassium tetrahydrogen pentafluoride. *Journal of Solid State Chemistry* **1**, 386-393.

Crowe, C., Masmonteil, J., and Thomas, R., 1992. Trends in Matrix Acidizing. *Oilfield Review* **4**, 24-40.

Davies, C. W. and Hudleston, L. J., 1924. Transference numbers and ionic complexity of hydrofluoric acid solutions. *Journal of the Chemical Society, Transactions* **125**, 260-268.

Dean, P. A. W. and Evans, D. F., 1967. Spectroscopic studies of inorganic fluoro-complexes. Part I. The 19F nuclear magnetic resonance and vibrational spectra of hexafluorometallates of Groups IVA and IVB. *Journal of the Chemical Society A*, 698-701.

Dyke, T. R., Howard, B. J., and Klemperer, W., 1972. Radiofrequency and Microwave Spectrum of the Hydrogen Fluoride Dimer; a Nonrigid Molecule. *The Journal of Chemical Physics* **56**, 2442-2454.

Edmunds, M. and Smedley, P., 2005. *Essentials of medical geology : impacts of the natural environment on public health*. Elsevier, Amsterdam ; Boston :.

Ellis, A. J., 1963. The effect of temperature on the ionization of hydrofluoric acid. *Journal of the Chemical Society*, 4300-4304.

Ellis, A. J., 1973. Chemical Processes in Hydrothermal Systems - A Review. In: Ingerson, E. (Ed.), *Proceedings of a Symposium on Hydrogeochemistry and Biogeochemistry*. Clarke Co., Washington, D.C.

Ellis, A. J. and Mahon, W. A. J., 1977. *Chemistry and Geothermal Systems*. Academic Press, San Diego, CA.

Farrer, H. N. and Rossotti, F. J. C., 1964. Proton-fluoride association in sodium perchlorate media. *Journal of Inorganic and Nuclear Chemistry* **26**, 1959-1965.

Forrester, J. D., Senko, M. E., Zalkin, A., and Templeton, D., 1963. Crystal structure of KH_2F_3 and geometry of the H_2F_3 ion. *Acta Crystallographica* **16**, 58-62.

Forsans, T., Zundel, J.-P., and Lichanot, A., 1993. Composition of acidification effluents of sandstones through geochemical calculation: validation of fluorosilicate equilibria by potentiometric assay of F. *Applied Geochemistry* **8**, 383-389.

Gaciri, S. J. and Davies, T. C., 1993. The occurrence and geochemistry of fluoride in some natural waters of Kenya. *Journal of Hydrology* **143**, 395-412.

Gennick, I., Harmon, K. M., and Potvin, M. M., 1977. Hydrogen bonding. 8. Preparation, properties, and low-temperature infrared structural analysis of ammonium and alkylammonium trihydrogen tetrafluorides and tetramethylammonium dihydrogen trifluoride. *Inorg. Chem.* **16**, 2033-2040.

Govett, G. J. S., 1961. Critical factors in the colorimetric determination of silica. *Analytica Chimica Acta* **25**, 69-80.

Harouiya, N. and Oelkers, E. H., 2004. An experimental study of the effect of aqueous fluoride on quartz and alkali-feldspar dissolution rates. *Chemical Geology* **205**, 155-167.

Hefter, G. T., 1984. Acidity constant of hydrofluoric acid. *Journal of Solution Chemistry* **13**, 457-470.

Heicklen, J. and Knight, V., 1964. The infrared spectrum of SiF_4. *Spectrochimica Acta* **20**, 295-298.

Hoshino, T. and Nishioka, Y., 1999. Etching process of SiO_2 by HF molecules. *The Journal of Chemical Physics* **111**, 2109-2114.

Ibers, J. A., 1964. Refinement of Peterson and Levy's Neutron Diffraction Data on KHF_2. *The Journal of Chemical Physics* **40**, 402-404.

IUPAC, 1979-1982. *Stability Constants of Metal-ion Complexes*. Pergamon Press, New York.

Judge, J. S., 1971. A Study of the Dissolution of SiO_2 in Acidic Fluoride Solutions. *Journal of the Electrochemical Society* **118**, 1772-1775.

Kang, J. K. and Musgrave, C. B., 2002. The mechanism of HF/H_2O chemical etching of SiO_2. *The Journal of Chemical Physics* **116**, 275-280.

Kikuyama, H., Waki, M., Kawanabe, I., Miyashita, M., Yabune, T., Miki, N., Takano, J., and Ohmi, T., 1992. Etching Rate and Mechanism of Doped Oxide in Buffered Hydrogen Fluoride Solution. *Journal of the Electrochemical Society* **139**, 2239-2243.

Klanberg, F. and Muetterties, E. L., 1968. Nuclear magnetic resonance studies on pentacoordinate silicon fluorides. *Inorg. Chem.* **7**, 155-160.

Kleboth, K., 1969. Zur Theorie der "Fluorokieselsäuredestillation". *Monatshefte für Chemie / Chemical Monthly* **100**, 1494-1498.

Kleboth, K., 1970. Die Bildungskonstanten der Wasserstoff—Fluor-Komplexe in konzentrierten Salzlösungen. *Monatshefte für Chemie / Chemical Monthly* **101**, 767-775.

Kline, W. E. and Fogler, H. S., 1981. Dissolution of silicate minerals by hydrofluoric acid. *Ind. Eng. Chem. Fund.* **20**, 155-161.

Knotter, D. M., 2000. Etching Mechanism of Vitreous Silicon Dioxide in HF-Based Solutions. *J. Am. Chem. Soc.* **122**, 4345-4351.

Kresge, A. J. and Chiang, Y., 1973. Solvent isotope effects on the ionization of hydrofluoric acid. *J. Phys. Chem.* **77**, 822-825.

Lahermo, P., Sandstrom, H., and Malisa, E., 1991. The occurrence and geochemistry of fluorides in natural waters in Finland and East Africa with reference to their geomedical implications. *Journal of Geochemical Exploration* **41**, 65-79.

Lasaga, A. C., 1981. Rate Laws of Chemical Reactions. In: Lasaga, A. C. and Kirkpatrick, R. J. Eds.), *Kinetics of Geochemical Processes*. Mineralogical Society of America, Washington, D.C.

Lasaga, A. C. and Gibbs, G., 1990. Ab-initio quantum mechanical calulations of water-rock interactions: adsorption and hydrolysis reactions. *American Journal of Science* **290**, 263-295.

Liang, D. T. and Readey, D. W., 1987. Dissolution kinetics of crystalline and amorphous silica in hydrofluoric-hydrochloric acid mixtures. *Journal of the American Ceramic Society* **70**, 570-577.

Mahon, W. A. J., 1964. Fluorine in the Natural Thermal Waters of New Zealand. *New Zealand Journal of Science* **7**, 3-28.

Mason, B. H., 1966. *Principles of geochemistry*. Wiley, New York.

McTigue, P., Odonnell, T. A., and Verity, B., 1985. The Determination of Fluoride-Ion Activities in Moderately Concentrated Aqueous Hydrogen-Fluoride. *Australian Journal of Chemistry* **38**, 1797-1807.

Mitra, A., 2008. Silica dissolution at low pH in the presence and absence of fluoride, Virginia Polytechnic Institute and State University.

Monk, D. J., Soane, D. S., and Howe, R. T., 1993. A review of the chemical reaction mechanism and kinetics for hydrofluoric acid etching of silicon dioxide for surface micromachining applications. *Thin Solid Films* **232**, 1-12.

Montgomery, D. C., Peck, E. A., and Vining, G. G., 2001. *Introduction to linear regression analysis*. Wiley-Interscience, New York.

Olsen, A. A. and Rimstidt, J. D., 2008. Oxalate-promoted forsterite dissolution at low pH. *Geochimica et Cosmochimica Acta* **In Press, Accepted Manuscript**.

Osseo-Asare, K., 1996. Etching Kinetics of Silicon Dioxide in Aqueous Fluoride Solutions: A Surface Complexation Model. *Journal of The Electrochemical Society* **143**, 1339-1347.

Ott, R. L. and Longnecker, M., 2001. *An Introduction to Statistical Methods and Data Analysis*. Duxbury, Pacific Grove, California.

Patel, P. R., Moreno, E. C., and Patel, J. M., 1971. Ionization of hydrofluoric acid at 25°C. *Journal of Research of the National Bureau of Standards* **A75**, 205-211.

Perrin, D. D., 1982. *Ionisation constants of inorganic acids and bases in aqueous solution*. Pergamon Press, Oxford [Oxfordshire] ; New York : Pergamon Press, 1982.

Prokopowicz-Prigogine, M., 1989. Reactivity of a silica network of glass: molecular mechanism of the dissolution of a silica network in aqueous HF-HCl solutions. *Glastechnische Berichte (Glastech. Ber.)* **62**, 249-255.

Proksche, H., Nagorsen, G., and Ross, D., 1992. The Influence of NH_4F on the Etch Rates of Undoped SiO_2 in Buffered Oxide Etch. *Journal of the Electrochemical Society* **139**, 521-524.

Reimann, C., Bjorvatn, K., Frengstad, B., Melaku, Z., Tekle-Haimanot, R., and Siewers, U., 2003. Drinking water quality in the Ethiopian section of the East African Rift Valley I--data and health aspects. *The Science of The Total Environment* **311**, 65-80.

Rimstidt, J. D., 1997. Quartz solubility at low temperatures. *Geochimica et Cosmochimica Acta* **61**, 2553-2558.

Rimstidt, J. D. and Barnes, H. L., 1980. The kinetics of silica-water reactions. *Geochimica et Cosmochimica Acta* **44**, 1683-1699.

Rimstidt, J. D. and Newcomb, W. D., 1993. Measurement and analysis of rate data: The rate of reaction of ferric iron with pyrite. *Geochimica et Cosmochimica Acta* **57**, 1919-1934.

Roth, W. A., 1939. Die Gleichgewichte in Flufls‰urelˆsungen. *Justus Liebig's Annalen der Chemie* **542**, 35-43.

Schomburg, D. and Krebs, R., 1984. Structural chemistry of pentacoordinated silicon. Molecular structures of the pentafluorosilicate anion and the diphenyltrifluorosilicate anion. *Inorg. Chem.* **23**, 1378-1381.

Spierings, G. A. C. M., 1993. Wet chemical etching of silicate glasses in hydrofluoric acid based solutions. *Journal of Materials Science* **28**, 6261-6273.

Spierings, G. A. C. M. and van Dijk, J., 1987. The dissolution of Na_2O-MgO-CaO-SiO_2 glass in aqueous HF solutions. *Journal of Materials Science* **22**, 1869-1874.

Sudakova, T. N., Krasnoshchekov, V. V., and Frolov, Y. G., 1978. Determination of the Ionisation Constants of Hydrogen Hexafluoro-silicate in Aqueous and Organic Media. *Russian Journal of Inorganic Chemistry* **23**, 1150-1152.

Trucks, G. W., Raghavachari, K., Higashi, G. S., and Chabal, Y. J., 1990. Mechanism of HF etching of silicon surfaces: A theoretical understanding of hydrogen passivation. *Physical Review Letters* **65**, 504.

Urbansky, E. T., 2002. Fate of Fluorosilicate Drinking Water Additives. *Chem. Rev.* **102**, 2837-2854.

Vanderborgh, N. E., 1968. Evaluation of the lanthanum fluoride membrane electrode response in acidic solutions : The determination of the pK_a of hydrofluoric acid. *Talanta* **15**, 1009-1013.

Verhaverbeke, S., Teerlinck, I., Vinckier, C., Stevens, G., Cartuyvels, R., and Heyns, M. M., 1994. The Etching Mechanisms of SiO_2 in Hydrofluoric Acid. *Journal of the Electrochemical Society* **141**, 2852-2857.

Warren, L. J., 1971. The measurement of pH in acid fluoride solutions and evidence for the existence of $(HF)_2$. *Analytica Chimica Acta* **53**, 199-202.

White, A. F. and Brantley, S. L., 1995. *Chemical weathering rates of silicate minerals*. Mineralogical Society of America, Washington, D.C.

Wolff-Boenisch, D., Gislason, S. R., and Oelkers, E. H., 2004. The effect of fluoride on the dissolution rates of natural glasses at pH 4 and 25°C. *Geochimica et Cosmochimica Acta* **68**, 4571-4582.

Wooster, C. B., 1938. Unilateral Triple Ion Formation in Aqueous Hydrofluoric Acid. *J. Am. Chem. Soc.* **60**, 1609-1613.

Wynne-Jones, W. F. K. and Hudleston, L. J., 1924. The activity of hydrogen-ion in aqueous solutions of hydrogen fluoride. *Journal of the Chemical Society, Transactions* **125**, 1031-1035.

APPENDIX 2.1

Quartz dissolution rates from our experiments in mol/m^{2}sec. The rates have been standardized to a surface area of 0.0902 m^2/g. Values for *pH*, log a_{HF}, log $a_{HF_2^-}$ and log a_{F^-} were calculated using Visual MINTEQ.

Expt. No.	Fluoride Solution Used	Initial m_{NaF} or m_{HF}, molal	Initial m_{HNO_3}, molal	*T*, °C	*pH*	log a_{HF}	log $a_{HF_2^-}$	log a_{F^-}	log *r*, mol/m^{2}sec
2F-III	NaF	0.20	1.00E-03	25	5.54	-3.23	-3.50	-0.87	-9.17
4F-I	NaF	1.00	1.00E-01	25	4.34	-1.51	-1.25	-0.35	-8.24
7F-I	NaF	0.10	1.00E-01	25	2.04	-1.06	-2.65	-2.19	-8.36
8F-III	NaF	0.10	1.00E-03	25	5.18	-3.13	-3.67	-1.14	-9.31
9F-V	NaF	0.10	1.00E-05	25	7.18	-5.13	-5.66	-1.13	-9.98
10F-I	NaF	0.01	1.00E-01	25	1.15	-2.00	-5.42	-4.02	-8.90
11F-III	NaF	0.01	1.00E-03	25	4.14	-3.05	-4.54	-2.09	-9.27
13F-I	NaF	1.00	1.00E-01	25	4.34	-1.51	-1.25	-0.35	-7.98
16F-I	NaF	1.00	1.00E-01	25	4.34	-1.51	-1.25	-0.35	-8.16
17F-III	NaF	1.00	1.00E-03	25	6.50	-3.57	-3.23	-0.26	-9.12
19F-0	NaF	1.00	1.00E+00	25	1.20	0.03	-1.32	-1.95	-7.63
20F-II	NaF	1.00	1.00E-02	25	5.48	-2.57	-2.24	-0.27	-8.95
22F-0	NaF	0.10	1.00E+00	25	0.15	-0.90	-4.24	-3.93	-8.08
23F-I	NaF	0.10	1.00E-01	25	2.04	-1.06	-2.65	-2.19	-8.16
24F-II	NaF	0.10	1.00E-02	25	4.11	-2.12	-2.71	-1.19	-9.03
25F-III	NaF	0.10	1.00E-03	25	5.18	-3.13	-3.67	-1.14	-9.48
26F-IV	NaF	0.10	1.00E-04	25	6.18	-4.14	-4.67	-1.13	-9.86
29F-I	NaF	0.30	1.00E-01	25	3.38	-1.18	-1.56	-0.98	-8.69
30F-II	NaF	0.30	1.00E-02	25	4.73	-2.29	-2.42	-0.74	-9.18
31F-III	NaF	0.30	1.00E-03	25	5.76	-3.30	-3.41	-0.72	-9.51
32F-IV	NaF	0.30	1.00E-04	25	6.77	-4.30	-4.41	-0.71	-9.86
34F-0	HF	3.00	1.00E+00	25	0.07	0.57	-1.37	-2.54	-6.90
35F-I	HF	3.00	1.00E-01	25	0.71	0.46	-0.96	-2.01	-7.06
36F-II	HF	3.00	1.00E-02	25	0.82	0.44	-0.88	-1.92	-7.02
37F-III	HF	3.00	1.00E-03	25	0.83	0.44	-0.87	-1.91	-7.10
38F-IV	HF	3.00	1.00E-04	25	0.83	0.44	-0.87	-1.91	-6.84
39F-V	HF	3.00	1.00E-05	25	0.83	0.44	-0.87	-1.91	-6.88
40F-0	HF	0.30	1.00E+00	25	0.10	-0.43	-3.33	-3.50	-8.15

41F-I	HF	0.30	1.00E-01	25	1.08	-0.53	-2.55	-2.63	-8.41
42F-II	HF	0.30	1.00E-02	25	1.62	-0.56	-2.09	-2.13	-8.18
43F-III	HF	0.30	1.00E-03	25	1.71	-0.57	-2.01	-2.04	-8.32
44F-IV	HF	0.30	1.00E-04	25	1.72	-0.57	-2.01	-2.04	-7.84
45F-V	HF	0.30	1.00E-05	25	1.72	-0.57	-2.01	-2.03	-8.35
46F-0	HF	3.00	1.00E+00	25	0.07	0.57	-1.37	-2.54	-7.01
47F-I	HF	3.00	1.00E-01	25	0.71	0.46	-0.96	-2.01	-7.43
48F-II	HF	3.00	1.00E-02	25	0.82	0.44	-0.88	-1.92	-7.75
49F-III	HF	3.00	1.00E-03	25	0.83	0.44	-0.87	-1.91	-7.54
50F-IV	HF	3.00	1.00E-04	25	0.83	0.44	-0.87	-1.91	-7.27
51F-V	HF	3.00	1.00E-05	25	0.83	0.44	-0.87	-1.91	-7.39
52F-0	HF	1.00	1.00E+00	25	0.10	0.10	-2.29	-2.99	-7.86
53F-I	HF	1.00	1.00E-01	25	0.98	-0.02	-1.64	-2.22	-8.04
54F-II	HF	1.00	1.00E-02	25	1.25	-0.04	-1.42	-1.98	-7.98
55F-III	HF	1.00	1.00E-03	25	1.28	-0.05	-1.39	-1.95	-7.74
56F-IV	HF	1.00	1.00E-04	25	1.28	-0.05	-1.39	-1.94	-7.73
57F-V	HF	1.00	1.00E-05	25	1.28	-0.05	-1.39	-1.94	-7.19
58F-0	HF	0.03	1.00E+00	25	0.10	-1.42	-5.33	-4.50	-8.89
59F-I	HF	0.03	1.00E-01	25	1.11	-1.52	-4.51	-3.59	-8.76
60F-II	HF	0.03	1.00E-02	25	1.97	-1.56	-3.73	-2.77	-8.86
61F-III	HF	0.03	1.00E-03	25	2.32	-1.59	-3.45	-2.46	-8.95
62F-IV	HF	0.03	1.00E-04	25	2.37	-1.60	-3.42	-2.42	-8.55
63F-V	HF	0.03	1.00E-05	25	2.37	-1.60	-3.41	-2.41	-8.47
64F-0	HF	0.03	1.00E+00	55	0.11	-1.42	-5.47	-4.71	-8.36
65F-II	HF	1.00	1.00E-02	55	1.31	-0.04	-1.48	-2.11	-7.21
66F-IV	HF	0.30	1.00E-04	55	1.80	-0.56	-2.06	-2.16	-7.51
67F-0	HF	1.00	1.00E+00	35	0.10	0.10	-2.34	-3.06	-7.81
68-F-I	HF	0.30	1.00E-01	35	1.09	-0.53	-2.60	-2.70	-7.58
69-F-III	HF	0.03	1.00E-03	35	2.35	-1.59	-3.46	-2.50	-7.93

APPENDIX 2.2

Quartz dissolution rates compiled from the literature. All dissolution rates were converted to the units of mol/m^{2}sec. Values for *pH*, log a_{HF}, log $a_{HF_2^-}$ and log a_{F^-} were calculated using Visual MINTEQ.

T, °C	*pH*	log a_{HF}	log $a_{HF_2^-}$	log a_{F^-}	log *r*, mol/m^{2}sec
(HAROUIYA and OELKERS, 2004)					
50	2.00	-4.02	-8.70	-5.33	-11.96
50	2.00	-3.32	-7.29	-4.62	-11.58
50	2.00	-3.03	-6.66	-4.30	-11.45
100	2.00	-4.01	-8.87	-5.60	-10.72
100	2.00	-3.31	-7.46	-4.89	-10.61
100	2.00	-3.01	-6.83	-4.56	-10.47
100	2.00	-2.31	-5.22	-3.64	-10.04
(LIANG and READEY, 1987)					
35	0.62	0.69	-0.64	-1.95	-4.44

50	0.65	0.69	-0.67	-2.02	-4.20
60	0.67	0.69	-0.69	-2.06	-3.99
70	0.69	0.70	-0.71	-2.10	-3.82
100	0.75	0.70	-0.76	-2.20	-3.61
35	0.15	1.17	-0.15	-1.94	-3.83
50	0.18	1.17	-0.19	-2.01	-3.54
60	0.21	1.16	-0.21	-2.05	-3.40
70	0.23	1.16	-0.24	-2.09	-3.29
100	0.29	1.16	-0.29	-2.20	-3.04
35	-0.28	1.60	0.28	-1.94	-3.34
50	-0.24	1.59	0.24	-2.01	-3.21
60	-0.21	1.59	0.21	-2.05	-3.12
70	-0.19	1.58	0.18	-2.09	-3.05
100	-0.12	1.57	0.12	-2.20	-2.91
35	-0.28	1.60	0.28	-1.94	-5.44
50	-0.24	1.59	0.24	-2.01	-5.12
60	-0.21	1.59	0.21	-2.05	-4.92
70	-0.19	1.58	0.18	-2.09	-4.80
35	-0.28	1.60	0.28	-1.94	-5.86
50	-0.24	1.59	0.24	-2.01	-5.56
60	-0.21	1.59	0.21	-2.05	-5.31
70	-0.19	1.58	0.18	-2.09	-5.09
35	-0.28	1.60	0.28	-1.94	-6.38
50	-0.24	1.59	0.24	-2.01	-6.06
70	-0.19	1.58	0.18	-2.09	-5.61

APPENDIX 2.3

Amorphous silica dissolution rates compiled from the literature. All dissolution rates were converted to the units of mol/m^{2}sec. Data from (SPIERINGS, 1993) includes a compilation of published rates from ten different studies and are reported here as a single data set as in the original source. Values for *pH*, log a_{HF}, log $a_{HF_2^-}$ and log a_{F^-} were calculated using Visual MINTEQ.

T, °C	*pH*	log a_{HF}	log $a_{HF_2^-}$	log a_{F^-}	log *r*, mol/m^{2}sec
			(JUDGE, 1971)		
25	4.46	-1.55	-1.21	-0.27	-5.57
25	3.81	-1.10	-0.97	-0.47	-5.27
25	3.36	-0.85	-0.91	-0.66	-5.16
25	3.16	-0.74	-0.91	-0.77	-5.12
25	2.80	-0.59	-0.95	-0.97	-5.09
25	2.39	-0.44	-1.07	-1.23	-5.14
25	0.76	-0.33	-2.48	-2.75	-5.55
25	0.32	-0.62	-3.50	-3.48	-6.01

25	0.20	-0.92	-4.22	-3.90	-6.49
25	0.77	-0.53	-2.86	-2.94	-5.78
25	2.94	-0.89	-1.43	-1.14	-5.48
25	2.58	-0.64	-1.29	-1.25	-5.31
60	4.76	-1.61	-1.20	-0.27	-4.96
60	4.09	-1.15	-0.95	-0.48	-4.57
60	3.62	-0.88	-0.89	-0.68	-4.42
60	3.41	-0.77	-0.89	-0.79	-4.41
60	3.02	-0.60	-0.93	-1.01	-4.39
60	2.59	-0.45	-1.06	-1.29	-4.41
60	0.77	-0.32	-2.63	-2.98	-4.96
60	0.33	-0.62	-3.66	-3.72	-5.52
60	0.20	-0.92	-4.38	-4.14	-6.06
60	0.78	-0.53	-3.02	-3.17	-5.24
60	3.17	-0.91	-1.40	-1.17	-4.78
60	2.79	-0.65	-1.26	-1.29	-4.63
			(KNOTTER, 2000)		
25	0.62	-2.37	-6.69	-4.93	-8.60
25	0.62	-2.07	-6.09	-4.62	-8.60
25	0.62	-1.89	-5.74	-4.45	-8.44
25	0.62	-1.77	-5.49	-4.32	-7.96
25	0.62	-1.61	-5.17	-4.17	-7.66
25	0.62	-1.48	-4.91	-4.04	-7.39
25	0.62	-1.39	-4.74	-3.95	-7.23
25	0.62	-1.30	-4.55	-3.86	-7.09
25	0.62	-1.18	-4.31	-3.74	-6.87
25	0.62	-1.08	-4.13	-3.64	-6.74
			(LIANG and READEY, 1987)		
35	0.62	0.69	-0.64	-1.95	-4.18
40	0.63	0.69	-0.65	-1.97	-4.09
50	0.65	0.69	-0.67	-2.02	-3.94
60	0.67	0.69	-0.69	-2.06	-3.74
70	0.69	0.70	-0.71	-2.10	-3.62
35	0.15	1.17	-0.15	-1.94	-3.58
40	0.16	1.17	-0.17	-1.97	-3.52
50	0.18	1.17	-0.19	-2.01	-3.36
60	0.21	1.16	-0.21	-2.05	-3.21
70	0.23	1.16	-0.24	-2.09	-3.06
24	-0.32	1.61	0.32	-1.89	-3.08
35	-0.28	1.60	0.28	-1.94	-2.88
40	-0.27	1.60	0.27	-1.96	-2.85
50	-0.24	1.59	0.24	-2.01	-2.69
60	-0.21	1.59	0.21	-2.05	-2.60
			(SPIERINGS, 1993)		
23	1.71	-0.57	-2.00	-2.02	-5.78
23	1.52	-0.33	-1.71	-1.97	-5.52
23	1.52	-0.33	-1.71	-1.97	-5.48
23	1.35	-0.13	-1.47	-1.94	-5.22
23	1.30	-0.08	-1.42	-1.94	-5.24

23	1.26	-0.03	-1.37	-1.93	-5.27
23	1.27	-0.04	-1.38	-1.93	-5.24
23	1.26	-0.03	-1.37	-1.93	-5.23
23	1.26	-0.03	-1.37	-1.93	-5.18
23	1.26	-0.03	-1.36	-1.93	-5.14
23	1.17	0.07	-1.26	-1.92	-5.09
23	1.09	0.16	-1.16	-1.92	-4.90
23	0.98	0.28	-1.03	-1.91	-4.89
23	0.97	0.29	-1.02	-1.91	-4.85
23	0.98	0.28	-1.03	-1.91	-4.82
23	0.88	0.38	-0.93	-1.90	-4.74
23	0.87	0.39	-0.91	-1.90	-4.72
23	0.79	0.48	-0.82	-1.90	-4.74
23	0.81	0.46	-0.85	-1.90	-4.72
23	0.80	0.47	-0.84	-1.90	-4.70
23	0.70	0.57	-0.73	-1.89	-4.59
23	0.68	0.60	-0.70	-1.89	-4.57
23	0.64	0.64	-0.66	-1.89	-4.49
23	0.64	0.64	-0.66	-1.89	-4.45
23	0.58	0.70	-0.60	-1.89	-4.48
23	0.58	0.70	-0.60	-1.89	-4.44
23	0.57	0.70	-0.60	-1.89	-4.30
23	0.48	0.79	-0.50	-1.89	-4.21
23	0.47	0.81	-0.49	-1.89	-4.18
23	0.43	0.85	-0.45	-1.89	-4.16
23	0.35	0.93	-0.36	-1.89	-4.01
23	0.25	1.03	-0.26	-1.89	-4.02
23	0.14	1.14	-0.15	-1.88	-3.86
23	0.22	1.06	-0.23	-1.89	-3.77
23	0.11	1.17	-0.12	-1.88	-3.72
23	0.11	1.17	-0.12	-1.88	-3.68
23	0.05	1.23	-0.06	-1.88	-3.70
23	-0.06	1.34	0.06	-1.88	-3.52
23	-0.06	1.34	0.06	-1.88	-3.45
23	-0.11	1.39	0.10	-1.88	-3.38
23	-0.09	1.38	0.09	-1.88	-3.37
23	-0.11	1.39	0.10	-1.88	-3.29
23	-0.14	1.42	0.14	-1.88	-3.27
23	-0.19	1.47	0.19	-1.88	-3.27
23	-0.17	1.46	0.17	-1.88	-3.18
23	-0.23	1.51	0.22	-1.88	-3.06
23	-0.24	1.53	0.24	-1.88	-3.03
23	-0.26	1.54	0.26	-1.88	-3.00

CHAPTER 3. SILICA DISSOLUTION KINETICS AT LOW pH

3.1 ABSTRACT

I performed a series of 81 quartz dissolution and 20 amorphous silica dissolution experiments in batch reactors over a pH range of 0 to 7 to investigate the effect of H^+ on silica dissolution rates. Between pH 3.5 and 7 silica dissolution rates are independent of pH, but they increase significantly below pH 3.5, so that the dissolution rate of both quartz and amorphous silica at pH 0 is more than an order magnitude faster than the dissolution rate at pH 3.5. We found that the empirical rate law for the dissolution of the "disturbed surface" of quartz in the pH range of 0 to 3.5 is

$$r_{qz,pH} = 10^{-0.23}\left(e^{\frac{-59392}{RT}}\right)a_{H^+}^{0.28}$$

where 0 < pH < 3.5 and 25 < T < 55°C. The empirical rate law for amorphous silica dissolution in the pH range 0 to 3.5 is

$$r_{as,pH} = 10^{0.56}\left(e^{\frac{-64754}{RT}}\right)a_{H^+}^{0.40}$$

where 0 < pH < 3.5 and 25 < T < 55°C.

Based on the empirical rate laws I suggest that the rate-determining step in the reaction mechanism involves a coordinated attack of H_3O^+, acting as a Lewis acid reacts, on a bridging O atom and the O end of a H_2O, acting as a Lewis base, on the Si atom. This results in a redistribution of electrons from the Si-O bridging bond to form two Si-OH surface species.

3.2 INTRODUCTION

SiO_2 is the most abundant oxide in the earth and silicate minerals make up approximately 88 weight percent of the earth's crust. Silica exists as a number of different polymorphs but quartz is by far the most abundant and accounts for about 12% of the mineralogy of the earth's crust. This makes silica, its properties, behaviors and

interactions of immense scientific and technological importance. Of particular importance are the interactions of silica with aqueous fluids because these fluids are present in nearly every natural setting. Silica dissolves in water by the reaction: $SiO_2(s) + 2H_2O = H_4SiO_4(aq)$. The mechanism for this reaction involves the negative (oxygen) end of a water molecule mounting a nucleophilic attack on the silicon atom to produce a five-coordinated silicon atom in the activated complex and the dissociation of the bond to a bridging oxygen to form two silanol groups (LASAGA and GIBBS, 1990; XIAO and LASAGA, 1994).

The effect of pH on the dissolution of quartz at high pH has been widely investigated. At high pH, the dissolution rate appears to be controlled by the nucleophilic attack of an OH^- ligand on a Si atom so that silica dissolution rates increase with increasing pH. On the other hand, the dissolution behavior and reaction mechanism of quartz at low pH is not well understood. There are a limited number of studies of quartz dissolution rates at low pH. These studies report inconsistent results and are illustrated in Figs. 3.1a and 3.1b. For example, BRADY and WALTHER (1990); KNAUSS and WOLERY (1988) and WOLLAST and CHOU (1988) report that the dissolution rates of quartz are independent of pH below pH 8. HOUSE and HICKINBOTHAM (1992) and HOUSE and ORR (1992) report that dissolution rate increases from low to high pH. KAMIYA et al. (1974); KNAUSS and WOLERY (1988); MAZER and WALTHER (1994); POKROVSKY et al. (2006); WOLLAST and CHOU (1988) and WORLEY et al. (1996), all report increasing dissolution rates with decreasing pH for pH < 3 at temperatures ranging from 25°C to 200°C. MAZER and WALTHER (1994) and POKROVSKY et al. (2006) also report increasing dissolution rates with decreasing pH below pH 3 for amorphous silica and their results are illustrated in Fig. 3.2. Of these studies only POKROVSKY et al. (2006) recognize and discuss a faster dissolution rate at low pH.

The purpose of this chapter is to investigate the effect of H^+ on the dissolution rate of silica at low pH and to establish a rate law for silica dissolution at these conditions. Additionally, our goal is to explain the rate versus pH trends in terms of a reaction mechanism.

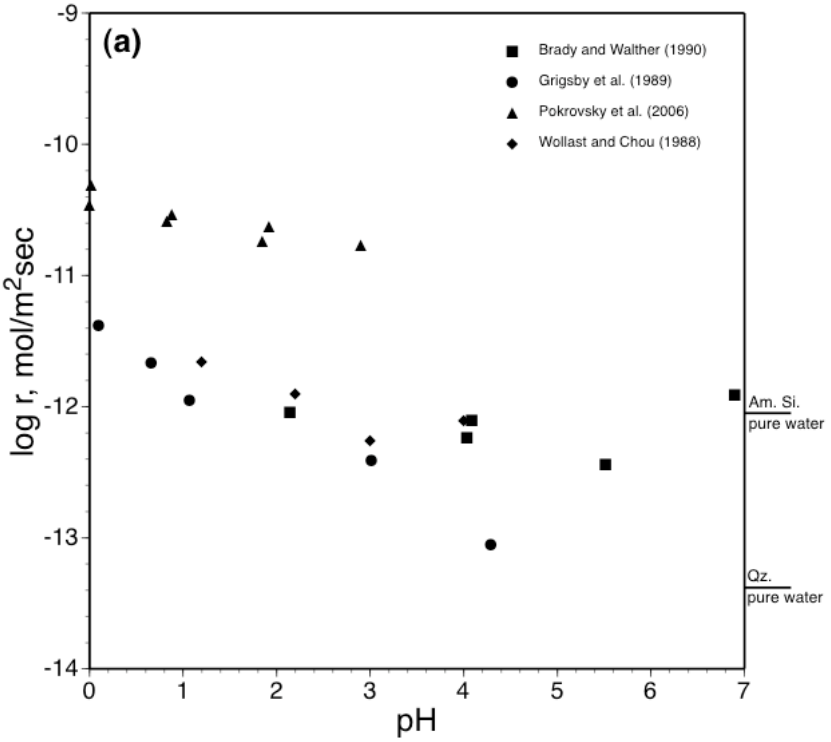
(a)
Brady and Walther (1990)
Grigsby et al. (1989)
Pokrovsky et al. (2006)
Wollast and Chou (1988)
Am. Si.
pure water
Qz.
pure water
log r, mol/m2sec
pH
-9
-10
-11
-12
-13
-14
0
1
2
3
4
5
6
7

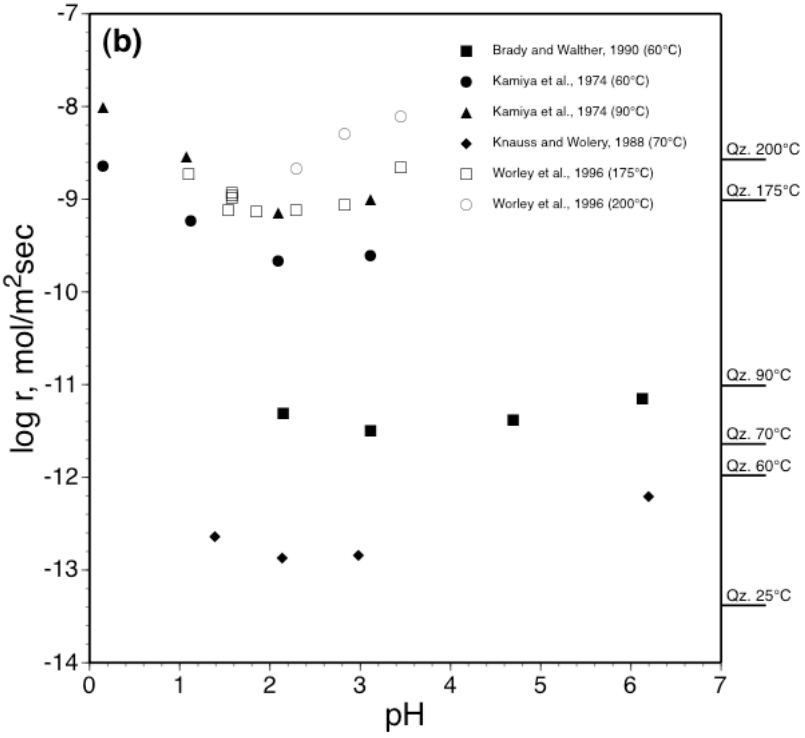
(b)
Brady and Walther, 1990 (60°C)
Kamiya et al., 1974 (60°C)
Kamiya et al., 1974 (90°C)
Knauss and Wolery, 1988 (70°C)
Worley et al., 1996 (175°C)
Worley et al., 1996 (200°C)
Qz. 200°C
Qz. 175°C
Qz. 90°C
Qz. 70°C
Qz. 60°C
Qz. 25°C
log r, mol/m2sec
pH
-7
-8
-9
-10
-11
-12
-13
-14
0
1
2
3
4
5
6
7

Figure 3.1. (a) Reported quartz dissolution rates at 25°C. (b) Reported quartz dissolution rates at 60 to 200°C. Dissolution rates in pure water predicted by RIMSTIDT and BARNES (1980) are shown by the tic marks on the right axis. Note that most studies show a trend toward a faster dissolution rate for pH below 3.5.

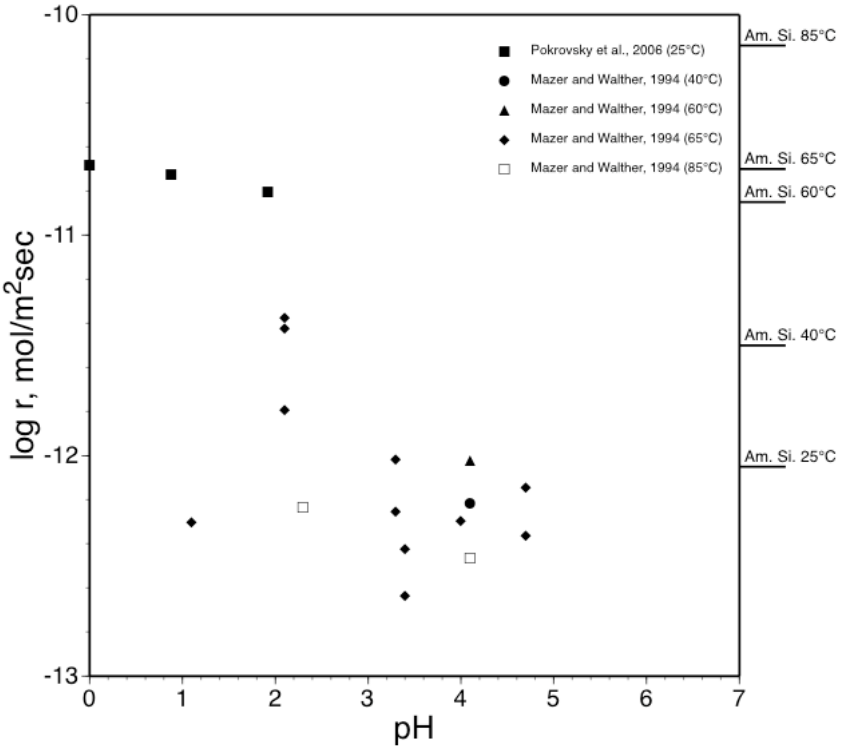

Figure 3.2. Reported amorphous silica dissolution rates. Dissolution rates in pure water predicted by RIMSTIDT and BARNES (1980) are shown by the tic marks on the right axis.

3.3 MATERIALS AND METHODS

3.3.1 Materials

Pure ground crystalline quartz (SIL-CO-SIL 250) obtained from the U.S. Silica Company, Berkeley Springs, West Virginia (grain size < 212 μm) and quartz sand obtained from Corning Glass Works, State College, Pennsylvania (grain size 125-1000 μm) was used for the quartz dissolution part of the study. Prior to the experiments the SIL-CO-SIL quartz grains were leached in boiling distilled water for 14 days using a Soxhlet extraction apparatus in an attempt to remove the "disturbed surface layer". This leached sample was then dried overnight and used for the experiments. The SIL-CO-SIL

leached quartz sample had a BET specific surface area of 0.77 m^2 gm^{-1} as determined by N_2-BET on a Quantachrome Nova 1200 BET Surface Area Analyzer and the Corning quartz sample had a BET specific surface area of 0.092 m^2 gm^{-1} (RIMSTIDT and BARNES, 1980).

Fused quartz (99% pure) obtained from Quartz Scientific, Inc., Sunnyvale, California was used for the amorphous silica dissolution part of the study. The amorphous silica sample was prepared by first soaking the fused quartz material in an ethanol-bath for 24 hours, then treated with 32% (vol.) H_2O_2 for two days and finally with 10% (vol.) HNO_3 for three days to remove any surficial impurities. The sample was rinsed thoroughly with deionized water before and after each chemical/cleaning treatment. This clean material was then powdered/ground in a ceramic shatter box. The amorphous silica sample had a N_2-BET specific surface area of 1.54 m^2/gm.

3.3.2 Experimental Design and Analytical Methods

Stock solutions of hydrochloric acid (HCl), sulfuric acid (H_2SO_4), nitric acid (HNO_3), and perchloric acid ($HClO_4$) solutions were made by diluting reagent grade acids to 1 molal concentration. Each stock solution, with a pH of approximately zero, was diluted to prepare working solutions with pH ranging from 0 to 6 by titrating into deionized water.

Eighty-one batch reactor quartz dissolution experiments and twenty batch reactor amorphous silica experiments were performed. The reactors were either Teflon bottles or polyethylene bottles (30-60 mL). A silica sample ranging in mass from 5 to 35 grams was used for each experiment. To this sample, a known mass of an acid solution (25-35 grams) was added. The pH of the run solution was measured using a Ag/AgCl pH electrode at the beginning and at the end of each experiment. The reactors were sealed and immersed in a constant temperature water bath set at 25 (±1) °C, 35 (±1) °C or 55 (±1) °C for 2-10 days for the rate experiments. The experimental conditions are tabulated in Appendix 1.

A sample (approximately 1 mL) of solution was periodically withdrawn over the duration of each experiment. Each sample was filtered through a 0.22 μm nylon filter to remove any suspended silica particles and then weighed and stored in a polyethylene

bottle. The dissolved silica concentration in each sample was determined by the silicomolybdate blue colorimetric method (GOVETT, 1961) using standards prepared by diluting 1000 ppm commercial silica standard solution.

3.3.3 Correction for sample withdrawal

Because each experiment was sampled multiple times, a correction for the changing surface area to mass ratio was performed in order to be able to analyze the data as an ideal batch reactor experiment. This was done by first summing the change in concentration over each time interval and multiplying by the mass of solution present at the time of sampling. This product was divided by the mass of solution present at the beginning of the experiment to obtain the corrected concentration, m_c (molal).

$$m_c = \frac{\sum_{1}^{n} \Delta m \cdot M}{M_0} \qquad (3.1)$$

where Δm is the change in Si concentration (molal), M is the mass (g) of the solution at sample time and M_0 is the initial mass (g) of the solution. This adjusted the sample concentration downward by 2 to 25 percent. This correction method is discussed in detail by OLSEN and RIMSTIDT (2008) and also used in MITRA (2008).

3.3.4 Calculation of rates by initial rate method

Extracting a rate from concentration versus time data is often challenging because the mathematical form of the rate law is unknown, so that the concentration versus time data must be fit to an arbitrary integrated rate law that only approximates the correct function. This problem of fitting the concentration versus time data to obtain a rate is a potential source of uncertainty in reported rates. The problem worsens when the experiments are run to a greater extent of reaction because the concentration versus time data usually shows an initial steep slope that eventually shallows out over the duration of the experiment.

The initial rate method is widely used in chemical kinetics because it provides a simple way to obtain a rate from batch reactor data for well-constrained conditions. At zero time there is no extent of reaction and the derived rate applies to the initial set of

conditions (initial solution concentrations, initial mineral surface reactivity, initial temperature, etc.), which have been set by the experimenter.

The quartz dissolution experiments in our study were run for an average of 10 days and were sampled multiple times. We chose to fit the concentration versus time data to the integrated form of a first order rate law modified from equation (52) in RIMSTIDT and BARNES (1980))

$$m = \mathrm{a}\left(1 - e^{-\mathrm{b}t}\right) \qquad (3.2)$$

In Eq. (3.2), *a* is the concentration at equilibrium and *b* is the precipitation rate constant.

Differentiating Eq. (3.2) gives,

$$\frac{dm}{dt} = \mathrm{ab}e^{-\mathrm{b}t} \qquad (3.3)$$

and when t = 0, $e^{-\mathrm{b}t} = 1$, hence

$$r = \left(\frac{dm}{dt}\right)_{t=0} = \mathrm{ab} \qquad (3.4)$$

At time = 0, the product of the *a* term and *b* term estimate from this fit gives the rate of quartz dissolution in mol/m^{2}sec. Before fitting the data the concentration values for each experiment were divided by the surface area of the sample to obtain a reduced concentration in mol/m^2. Those data were then fit to the Eq. (3.2) by nonlinear regression using the JMP statistical software version 7.0 and the *a* and *b* term estimates from each fit was used to calculate the rates for each experiment.

The amorphous silica experiments were reacted over a comparatively shorter duration (2 to 3 days) so the data fit the function $m = \mathrm{a} + \mathrm{b}t + \mathrm{c}t^2$ quite well (RIMSTIDT and NEWCOMB, 1993). The derivative of this fit is $\frac{dm}{dt} = \mathrm{b} + 2\mathrm{c}t^2$ and at $t = 0$ (RIMSTIDT and NEWCOMB, 1993), $r = \left(\frac{dm}{dt}\right)_{t=0} = \mathrm{b}$. This apparent rate was converted to the rate of quartz dissolution (r, mol/m^{2}sec) using the relationship:

$$r = \frac{r' M}{A} \qquad (3.5)$$

where M is the mass (g) of the solution at sample time and A is surface area (m^2) of the quartz sample.

The rate data obtained from these experiments were analyzed using the JMP statistical software version 7.0. A *p*-value of less than 0.05 was chosen as the cut off for deciding that a regression coefficient is not statistically significant (OTT and LONGNECKER, 2001). JMP uses partial regression plots to illustrate the results of the multiple linear regression models. Partial regression plots provide a better representation of the effect of each individual independent variable on the dependent variable as opposed to using scatter plots of the dependent variables versus the independent variable (e.g., log *r* versus *pH*), which do not account for the other independent variables used in the regression model. See MONTGOMERY et al. (2001) for a discussion of partial regression plots.

3.4 RESULTS

3.4.1 Empirical rate law for quartz

The results of all the quartz dissolution experiments are tabulated in Appendix 3.1 and the log *r* values from these experiments are plotted versus pH in Figure 3.4. Figure 3.4 shows that the log *r* values from the experiments at different temperatures appear to be grouped into two distinct trends with different slopes. The break point between the two trends appears to lie between pH 3 and 4. Hence, we analyzed the data between pH 0 and 3.5 and between pH 3.5 and 7.0, separately.

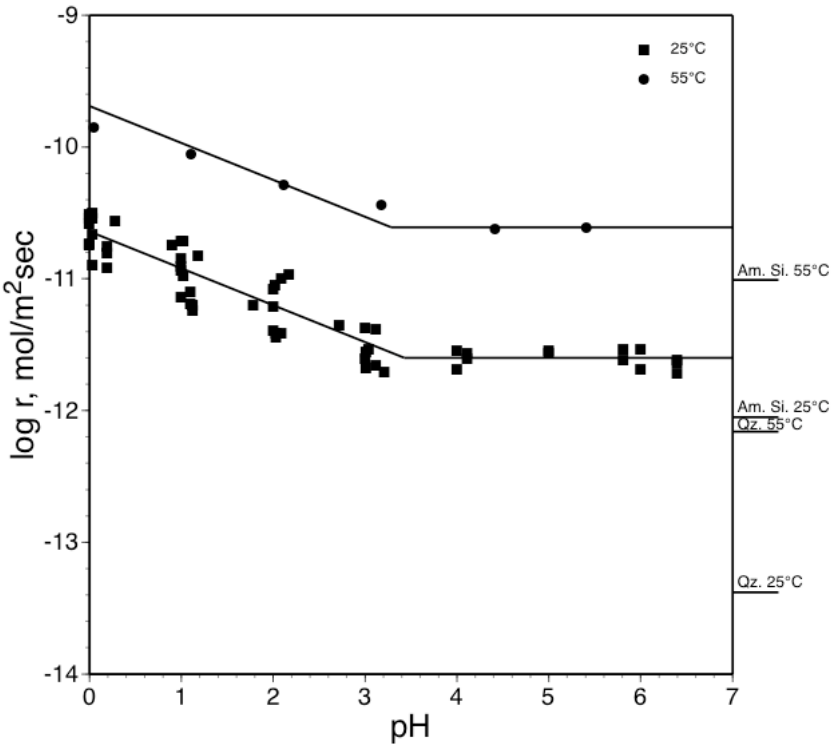

Figure 3.4. Log *r* versus *pH* for all quartz dissolution experiments. The lines are the results of the regression analysis. Dissolution rates in pure water predicted by RIMSTIDT and BARNES (1980) are shown by the tic marks on the right axis. Our experiments using different acids demonstrated that the fast rates are not due to an anion effect because the dissolution rates are comparable for all acids (Appendix 3.1).

A preliminary regression model produced by fitting the 25°C rate data between pH 3.5 and 7.0 produced

$$\log r_{qz,i} = -11.51(0.10) - 0.02(0.02)pH \qquad (3.6)$$

where the numbers in the parenthesis are one standard error of the regression coefficient (R^2 = 0.07) and log $r_{qz,i}$ is the pH-independent rate. Because the slope of the regression line is nearly zero and the R^2 of the regression model is so low (0.07; Prob>t = 0.39), the most parsimonious model is that the regression line has a slope of zero. Therefore, we used the mean of response to find that

$$\log r_{qz,i} = -11.60(0.017) \qquad (3.7)$$

where the number in the parenthesis represents one standard error. Similarly, the mean of the response of the 55°C rates predicts that

$$\log r_{qz,i} = -10.61(0.006) \qquad (3.8)$$

Eqs. (3.7) and (3.8) can be transformed to the rate laws

$$r_{qz,i} = 10^{-11.60} \qquad (3.9)$$

$$r_{qz,i} = 10^{-10.61} \qquad (3.10)$$

Thus, we see that the quartz dissolution rates between pH 3.5 and 7.0 are independent of pH.

All of the data between pH 0 and 3.5, were regressed against pH and $1/T$ to get

$$\log r_{qz,pH} = -0.23(0.89) - 0.28(0.02)pH - 3101.85(266.31)/T \qquad (3.11)$$

where the numbers in the parenthesis are one standard error of the regression coefficients (R^2 = 0.87; n = 49). Figure 3.5 shows the partial regression plots for this regression model. Eq. (3.11) can be transformed to the empirical rate law

$$r_{qz,pH} = 10^{-0.23}\left(e^{\frac{-59392}{RT}}\right)a_{H^+}^{0.28} \qquad (3.12)$$

where 0 < pH < 3.5 and 25 < T < 55°C.

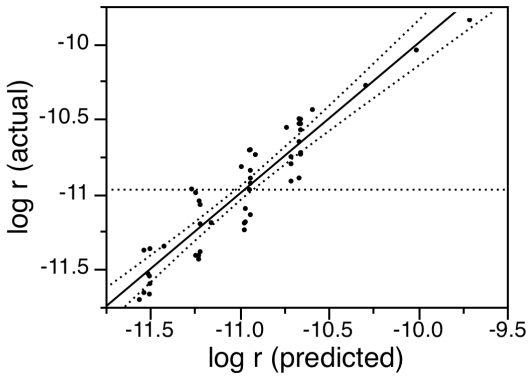

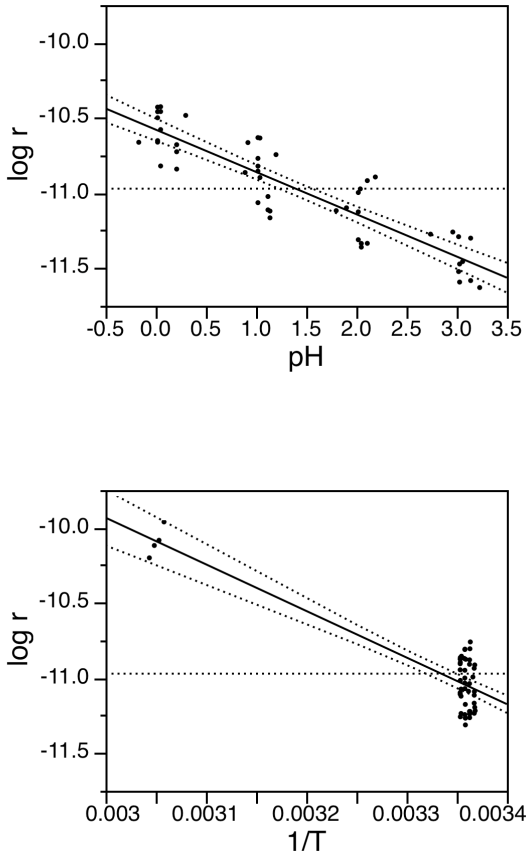

Figure 3.5. Partial regression plots for the multiple linear regression model of quartz dissolution rates for pH between 0 and 3.5 as a function of *pH* and 1/*T*. The first graph shows predicted log *r* versus observed log *r*. The next two graphs show the effect of *pH* and 1/*T* respectively on log *r*.

3.4.2 Empirical rate law for amorphous silica

The results of all the amorphous silica dissolution experiments are tabulated in Appendix 3.2 and the log *r* values from these experiments are plotted versus pH in Figure 3.6. Figure 3.6 shows that the log *r* values from our amorphous silica experiments at different temperatures appear to be grouped into two distinct trends with different slopes similar to the quartz dissolution rates with the break point between the two trends of results between pH 3 and 4. But because there are insufficient data in the pH range of 3.5

to 7.0 to allow for a statistical analysis, we only analyzed the results from the amorphous silica dissolution experiments in the pH range of 0 to 3.5.

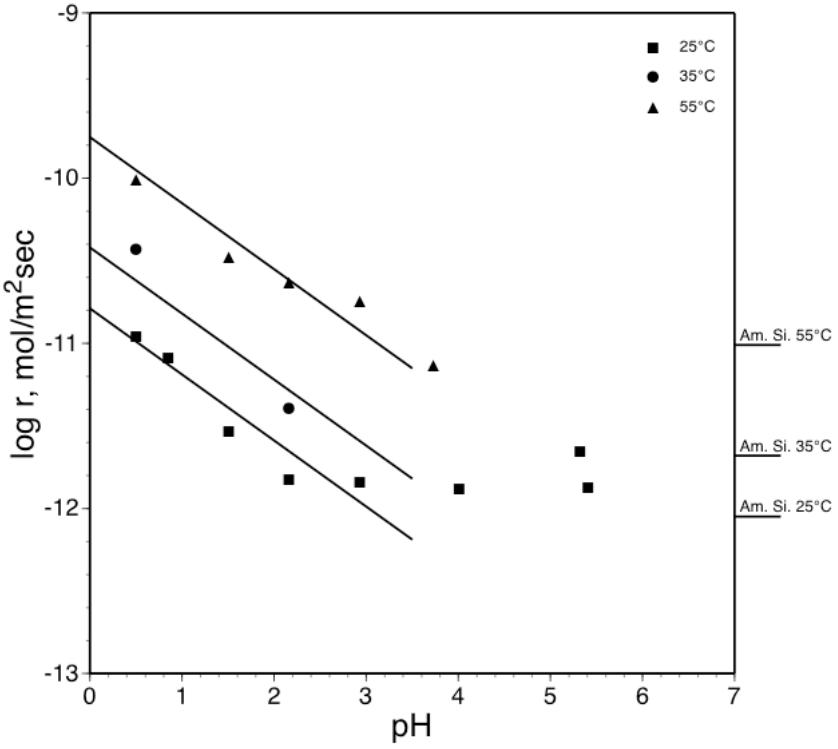

Figure 3.6. Log *r* versus pH for all the amorphous silica dissolution experiments. The lines are the results of the regression analysis. Dissolution rates in pure water predicted by RIMSTIDT and BARNES (1980) are shown by the tic marks on the right axis.

We analyzed the rate data between pH 0 and 3.5 from all our experiments for all temperatures and the model fit shows that the dissolution rates are a function of *pH* and $1/T$

$$\log r_{as,pH} = 0.56(1.02) - 0.40(0.05)pH - 3381.94(311.55)/T \qquad (3.13)$$

where the numbers in the parenthesis are one standard error of the regression coefficients (R^2 = 0.95; n = 11). Figure 3.7 shows the partial regression plots for this regression model. Eq. (3.13) can be transformed to the empirical rate law

$$r_{as,pH} = 10^{0.56}\left(e^{\frac{-64754}{RT}}\right)a_{H^+}^{0.40} \qquad (3.14)$$

where 0 < pH < 3.5 and 25 < T < 55°C.

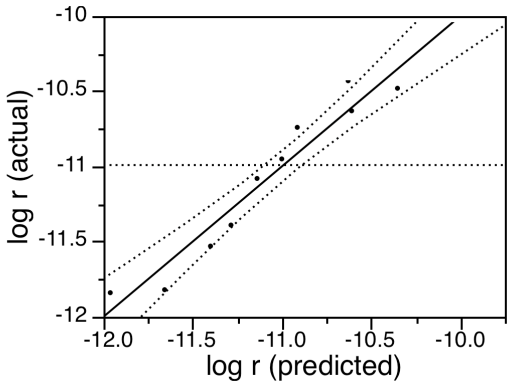

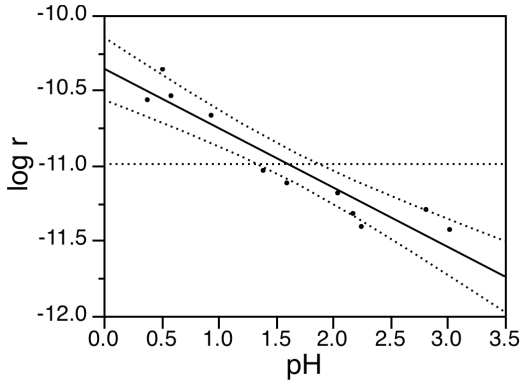

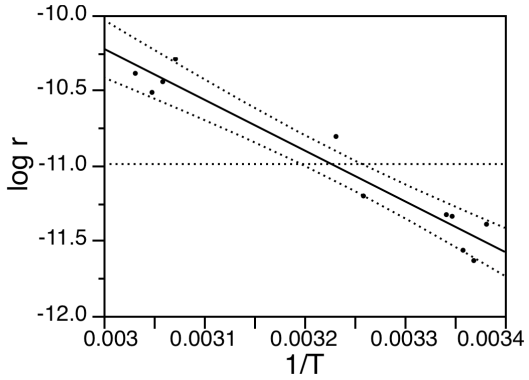

Figure 3.7. Partial regression plots for the multiple linear regression model of amorphous silica dissolution rates for pH between 0 and 3 as a function of pH and $1/T$. The first graph shows predicted log r versus observed log r. The next two graphs show the effect of pH and $1/T$ respectively on log r.

3.5 DISCUSSION

3.5.1 Comparison with past studies

Fig. 3.8 (b) compares the quartz dissolution rates (-11.60 mol/m^{2}sec at 25°C and -10.61 mol/m^{2}sec at 55°C) for pH > 3.5 from this study with the quartz dissolution rates predicted by RIMSTIDT and BARNES (1980) (-13.38 mol/m^{2}sec at 25°C and -12.16 mol/m^{2}sec at 55°C). The dissolution rates found in our experiments are > 1.5 orders of magnitude higher. On the other hand, our pH > 3.5 amorphous silica dissolution rates (-11.80 mol/m^{2}sec at 25°C) are consistent with the rates predicted by RIMSTIDT and BARNES (1980) (-12.05 mol/m^{2}sec at 25°C) (Fig. 3.8c). In fact, for pH > 3.5, the rates from our quartz dissolution experiments are similar to the amorphous silica dissolution rates (Fig. 3.8a). These faster dissolution rates for quartz appear to be the result of a "disturbed surface layer" on the quartz surface. This "disturbed surface layer" effect is well known and has been discussed in detail (ASTA et al., 2008; BALL et al., 1997; D'EUSTACHIO, 1946; HENDERSON et al., 1970; KOOPMANS and RIECK, 1965; LIER et al., 1960; TALBOT and KEMPIS, 1960; TALBOT and KEMPIS, 1963).

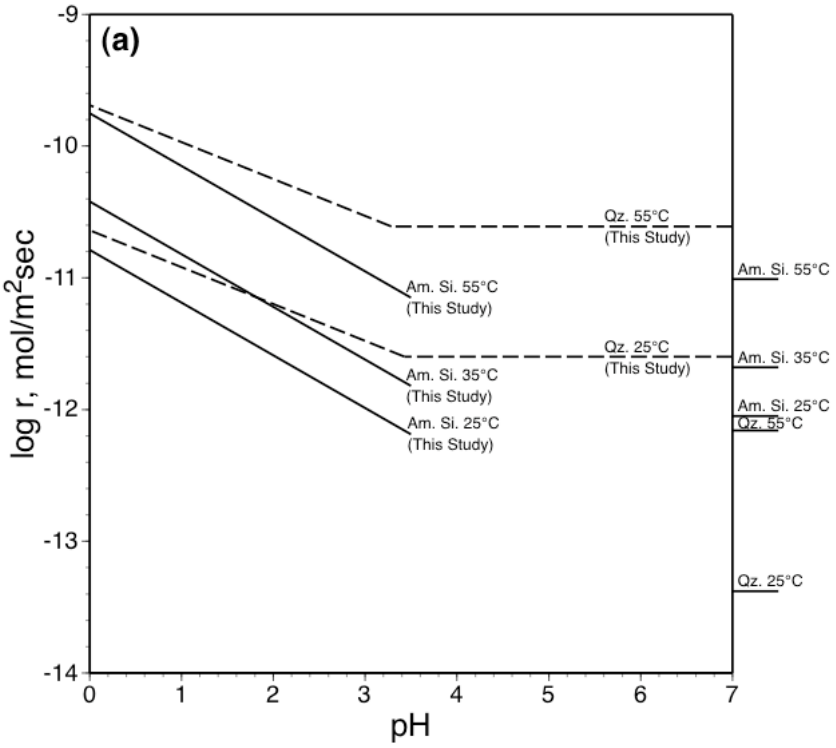

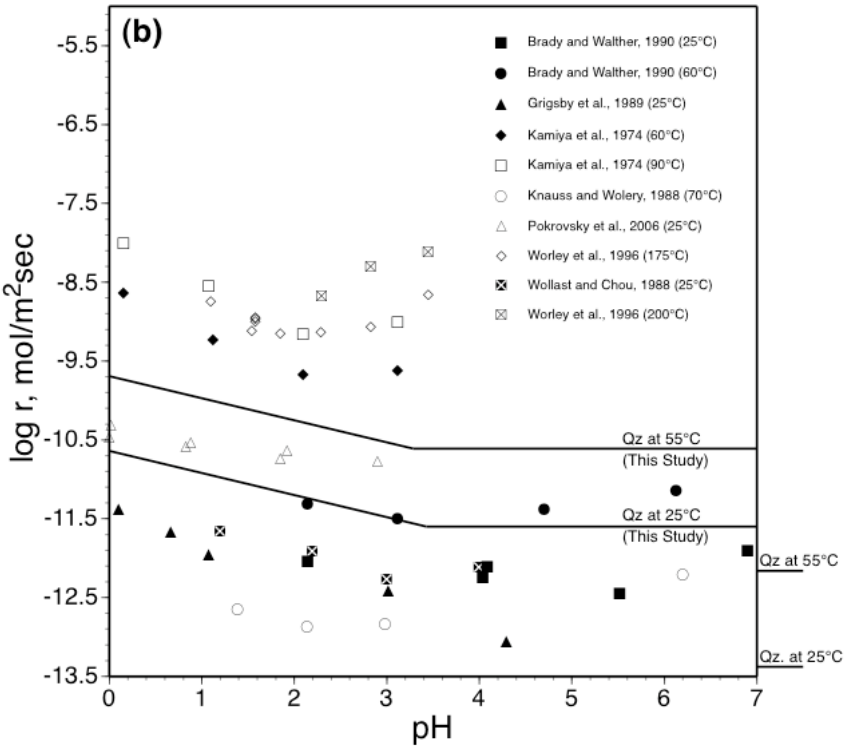
(b)
Brady and Walther, 1990 (25°C)
Brady and Walther, 1990 (60°C)
Grigsby et al., 1989 (25°C)
Kamiya et al., 1974 (60°C)
Kamiya et al., 1974 (90°C)
Knauss and Wolery, 1988 (70°C)
Pokrovsky et al., 2006 (25°C)
Worley et al., 1996 (175°C)
Wollast and Chou, 1988 (25°C)
Worley et al., 1996 (200°C)
Qz at 55°C (This Study)
Qz at 25°C (This Study)
Qz at 55°C
Qz. at 25°C
log r, mol/m2sec
pH

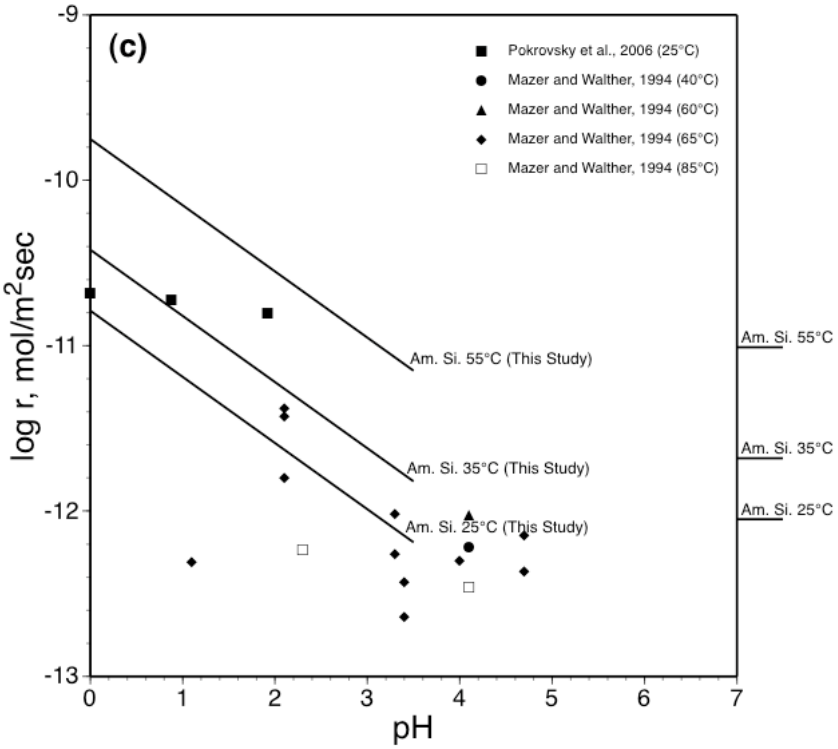
(c)
Pokrovsky et al., 2006 (25°C)
Mazer and Walther, 1994 (40°C)
Mazer and Walther, 1994 (60°C)
Mazer and Walther, 1994 (65°C)
Mazer and Walther, 1994 (85°C)
Am. Si. 55°C (This Study)
Am. Si. 35°C (This Study)
Am. Si. 25°C (This Study)
Am. Si. 55°C
Am. Si. 35°C
Am. Si. 25°C
log r, mol/m2sec
pH

Figure 3.8. Comparison of (a) the quartz and amorphous silica dissolution rates from our experiments, (b) our quartz dissolution rates with rates from the literature, and (c) our amorphous silica dissolution rates with rates from the literature. Dissolution rates in pure water predicted by RIMSTIDT and BARNES (1980) are shown by the tic marks on the right axis.

Both quartz and amorphous silica show an increase in dissolution rates by more than an order of magnitude as pH decreases from 3 to 0 (Figs. 3.4 and 3.6). This behavior is consistent with that observed by other studies (Figs. 3.1 and 3.2). As can be seen from Fig. 3.8 (a), rates reported by BRADY and WALTHER, 1990; GRIGSBY et al., 1989 and WOLLAST and CHOU (1988) are about half a order of magnitude lower than our rates at 25°C, although they exhibit a similar slope. On the other hand, rates from POKROVSKY et al. (2006) are similar to our rates at pH = 0, but their rates at pH = 3 (-10.77 mol/m^2sec) are about one half an order of magnitude higher than our rates at pH 3 (~ -11.53 mol/m^2sec). At higher temperatures, there exists a similar discrepancy between our dissolution rates and the published dissolution rates, even though the slopes are similar. Dissolution rates measured at 70°C reported by KNAUSS and WOLERY (1988) are actually one and half orders of magnitude slower than our quartz dissolution rates at 25°C. But their rates increase with pH, above pH 3, which is not consistent with our results and other published rates in this pH range. On the other hand, KAMIYA et al. (1974) report quartz dissolution rates at 60°C that are an order of magnitude higher than our rates at 55°C. Fig. 3.8 (b) shows that our amorphous silica dissolution rates at 25°C for pH 0 are similar to rates reported by POKROVSKY et al. (2006) at pH 0. But their reported rates at pH 3 are nearly an order of magnitude higher than our rates at pH 3.

Although, there is a large amount of scatter in these rate data and some outright disagreements between studies, most studies show a distinct trend for faster silica dissolution rates at pH < 3.5. Evaluation of all of these studies to identify the source(s) of scatter and disagreement is beyond the scope of this project but we can suggest that the likely problem is that the reaction rate is strongly influenced by the reactivity of the silica surfaces. This problem is often dismissed as a "reactive surface layer" on quartz, but the cause of this extra reactivity is not understood. The very slow reaction rates for silica

phases at low temperatures means that extremely long reaction times are needed to remove excessively reactive sites from grain surfaces. This makes low temperature rate measurements difficult and time consuming. Thus, although we are confident that silica dissolution rates become faster with decreasing pH below 3.5, well constrained dataset, especially for quartz, awaits an improved experimental design.

3.5.2 Reaction Mechanism

Although several studies have shown faster quartz dissolution rates at pH < 3, only a few have actually discussed this phenomenon. WOLLAST and CHOU (1988) suggested that the observed faster quartz dissolution rates below pH 3 may be proportional to the concentration of the positively charged surface species $>SiOH_2^+$, which increases in concentration with decreasing pH. HIEMSTRA and VAN RIEMSDIJK (1990) proposed a multiple activated complexes model for quartz, which predicts an increase in dissolution rates of nearly three orders of magnitude corresponding to a decrease in pH from two to zero. POKROVSKY et al. (2006) explained their results using a model based on faster dissolution of protonated surface silanol groups ($>SiOH_2^+$) caused by the polarization of Si-O bonds. According to POKROVSKY et al. (2006), near pH = 0, $>SiOH_2^+$ is present on up to 30-50% of surface sites and the observed dissolution rates have a reaction order of one with respect to the surface concentration of $>SiOH_2^+$.

Based on the empirical rate laws found here, we suggest an alternative explanation for faster dissolution rates at low pH. Although we cannot infer the entire reaction mechanism using the empirical rate laws, they do inform us about the mechanism for the rate-determining step and we speculate that other elementary steps are similar. In order for Si in a Q_3 site to be released into solution three Si-O bonds must be broken. It is unlikely that multiple bonds will break simultaneously so we suggest that this process consists of a series of sequential elementary reaction steps. The slowest of these sequential bond-breaking steps is the rate-determining step and the empirical rate law reflects the rate of that step. Furthermore, the empirical rate law reflects the stoichiometry of the rate-determining step. A simple "bond breaking" elementary step in silica dissolution would produce a 3-coordinated Si atom ($^{[3]}Si$) and a 1-coordinated O

atom ($^{[1]}$O). Although such species are theoretically possible they would be very unstable and a great deal of energy would be needed to form them. The use of the term "bond breaking" is a potentially serious source of confusion in discussions of reaction mechanisms because the elementary reaction steps for silicate minerals are unlikely to result in under-coordinated atoms for the reasons described above. A more likely reaction scenario involves an activated complex consisting of overcoordinated $^{[5]}$Si and $^{[3]}$O atoms that break down to reaction products with normal coordination numbers, $^{[4]}$Si and $^{[2]}$O. See LASAGA and GIBBS (1990) for an example of how hydrolysis of a Si-O bond involves $^{[5]}$Si and $^{[3]}$O in the activated complex. The hydrolysis reaction that "breaks" a Si-O bond in their model involves the simultaneous electrophilic attack by H from the water molecule on a bridging oxygen atom and a nucleophilic attack on the Si atom by the O atom in that water molecule. When the H atom, acting as a Lewis acid, overcoordinates the bridging oxygen and the O atom, acting as a Lewis base, overcoordinates the Si atom, electrons move from the Si-O bridging bond to form a O-H bond at the bridging oxygen and a bond between Si and the OH from the water molecule. Therefore, the reaction appears to involve transfer of electrons from existing bonds to form new bonds.

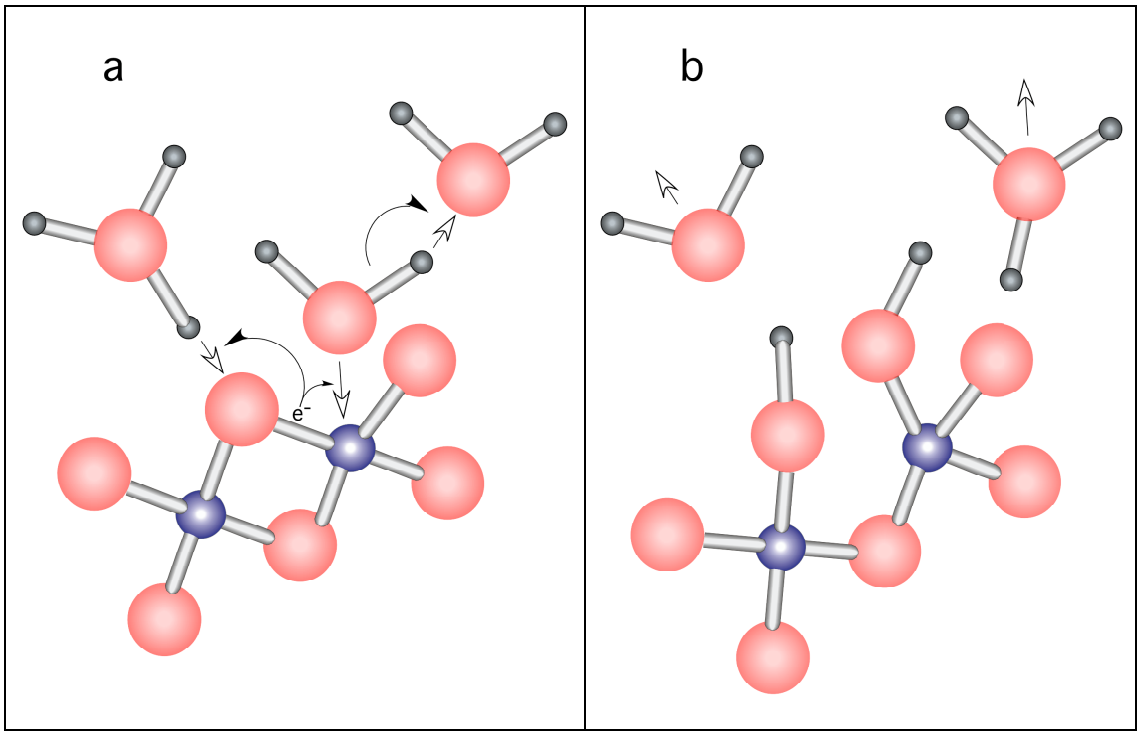

Figure 3.9. Schematic illustration of a possible elementary bond-breaking step for the dissolution of silica in acidic solutions. (a) The activated complex consists of a hydronium ion (Lewis acid) adsorbed to a bridging oxygen atom and a water molecule (Lewis base) adsorbed at a Si site. As the hydronium ion mounts an electrophilic attack on the bridging oxygen and the water molecule mounts a nucleophilic attack on the Si atom, electrons shift from the Si-O bridging bond to create two Si-OH surface species (b) This reaction consumes one water molecule and regenerates a hydronium ion.

Our results suggest that the rate-determining step for silica dissolution at low pH involves a coordinated attack of H_3O^+ and H_2O on a Si-O bond. The H_3O^+ ion, acting as a Lewis acid approaches the bridging O atom, while the O end of the H_2O, acting as a Lewis base, attacks the Si atom (Fig. 3.9). This allows a redistribution of electrons from the Si-O bond to form a O-H and a Si-O bond, thus "breaking" the Si-O bond. The reaction orders for the rate laws (Eqs. (3.12) and (3.14)) are fractional, which could be interpreted to mean that a precursor step for the bond breaking is the adsorption of H_3O^+ and H_2O onto the silica surface. LASAGA (1981), pointed out that adsorption onto non-uniform surfaces leads to rate laws with fractional reaction orders. Thus, the fractional

reaction order suggests a distribution of sorption site energies on the surface of the silica. Fractional reaction orders are commonly seen in oxides and silicate dissolution (WHITE and BRANTLEY, 1995).

3.5.3 Applications

Although the faster quartz dissolution rates at low pH have not been recognized in natural environments because such low pH conditions are uncommon, this effect could be of importance in oxidizing vapor dominated geothermal systems, acid crater lakes, and acid mine drainage settings. Low pH, high fluorine environments can produce dramatic geological features. A good example is Steamboat Springs, Nevada (SCHOEN et al., 1974) where the intensive leaching has removed most of the alkali and alkaline earth elements from the rock leaving behind a mass of aluminosilicate and silica phases. COCHRANE (1986) and OWENS and PASEK (2007) have argued convincingly that the kyanite and pyrophyllite deposits of Virginia and North Carolina are the metamorphosed ancient equivalents of these modern acid hot springs.

3.6 REFERENCES

Asta, M. P., Cama, J., Soler, J. M., Arvidson, R. S., and Luttge, A., 2008. Interferometric study of pyrite surface reactivity in acidic conditions. *American Mineralogist* **93**, 508-519.

Ball, M. C., Brown, D. S., and Perkins, L. J., 1997. Diffuse layers on the surface of mineral quartz. *Journal of Materials Chemistry* **7**, 365-368.

Brady, P. V. and Walther, J. V., 1990. Kinetics of quartz dissolution at low temperatures. *Chemical Geology* **82**, 253-264.

Cochrane, J. C., 1986. Petrogenesis of the Willis Mountain and East Ridge Kyanite Quartzite, Buckingham County, Virginia. Master of Science, Virginia Polytechnic Institute and State University.

D'Eustachio, D., 1946. Surface Layers on Quartz and Topaz. *Physical Review* **70**, 522-532.

Govett, G. J. S., 1961. Critical factors in the colorimetric determination of silica. *Analytica Chimica Acta* **25**, 69-80.

Grigsby, C. O., Tester, J. W., Trujillo, P. E., and Counce, D. A., 1989. Rock-water interactions in the Fenton Hill, new Mexico, hot dry rock geothermal systems I. fluid mixing and chemical geothermometry. *Geothermics* **18**, 629-656.

Henderson, J. H., Syers, J. K., and Jackson, M. L., 1970. Quartz disolution as influenced by pH and the presence of a disturbed surface layer. *Israel Jour. Chem.* **8**, 357-372.

Hiemstra, T. and van Riemsdijk, W. H., 1990. Multiple activated complex dissolution of metal (hydr) oxides: A thermodynamic approach applied to quartz. *Journal of Colloid and Interface Science* **136**, 132-150.

House, W. A. and Hickinbotham, L. A., 1992. Dissolution kinetics of silica between 5 and 30°C. Application of a titrimetric method. *Jounal of the Chemical Society, Faraday Transactions* **88**, 2021-2026.

House, W. A. and Orr, D. R., 1992. Investigation of the pH dependence of the kinetics of Quartz dissolution at 25°C. *Jounal of the Chemical Society, Faraday Transactions* **88**, 233-241.

Kamiya, H., Ozaki, A., and Imahashi, M., 1974. Dissolution rate of powdered quartz in acid solution. *Geochemical Journal* **8**, 21-26.

Knauss, K. G. and Wolery, T. J., 1988. The dissolution kinetics of quartz as a function of pH and time at 70°C. *Geochimica et Cosmochimica Acta* **52**, 43-53.

Koopmans, K. and Rieck, G. D., 1965. On the thickness of the disturbed layer on ground quartz powder with particle size of 1.5 μm. *British Journal of Applied Physics* **16**, 1913-1914.

Lasaga, A. C., 1981. Rate Laws of Chemical Reactions. In: Lasaga, A. C. and Kirkpatrick, R. J. Eds.), *Kinetics of Geochemical Processes*. Mineralogical Society of America, Washington, D.C.

Lasaga, A. C. and Gibbs, G., 1990. Ab-initio quantum mechanical calulations of water-rock interactions: adsorption and hydrolysis reactions. *American Journal of Science* **290**, 263-295.

Lier, J. A. V., Bruyn, P. L. D., and Overbeek, J. T. G., 1960. The Solubility of Quartz. *J. Phys. Chem.* **64**, 1675-1682.

Mazer, J. J. and Walther, J. V., 1994. Dissolution kinetics of silica glass as a function of pH between 40 and 85°C. *Journal of Non-Crystalline Solids* **170**, 32-45.

Mitra, A., 2008. Silica dissolution at low pH in the presence and absence of fluoride, Virginia Polytechnic Institute and State University.

Montgomery, D. C., Peck, E. A., and Vining, G. G., 2001. *Introduction to linear regression analysis*. Wiley-Interscience, New York.

Olsen, A. A. and Rimstidt, J. D., 2008. Oxalate-promoted forsterite dissolution at low pH. *Geochimica et Cosmochimica Acta* **In Press, Accepted Manuscript**.

Ott, R. L. and Longnecker, M., 2001. *An Introduction to Statistical Methods and Data Analysis*. Duxbury, Pacific Grove, California.

Owens, B. E. and Pasek, M. A., 2007. Kyanite Quartzites in the Piedmont Province of Virginia: Evidence for a Possible High-Sulfidation System. *Economic Geology* **102**, 495-509.

Pokrovsky, O. S., Golubev, S. V., and Mielczarski, J. A., 2006. Kinetic evidences of the existence of positively charged species at the quartz-aqueous solution interface. *Journal of Colloid and Interface Science* **296**, 189-194.

Rimstidt, J. D. and Barnes, H. L., 1980. The kinetics of silica-water reactions. *Geochimica et Cosmochimica Acta* **44**, 1683-1699.

Rimstidt, J. D. and Newcomb, W. D., 1993. Measurement and analysis of rate data: The rate of reaction of ferric iron with pyrite. *Geochimica et Cosmochimica Acta* **57**, 1919-1934.

Schoen, R., White, D. E., and Hemley, J. J., 1974. Argillization by Descending Acid at Steamboat Springs, Nevada. *Clays and Clay Minerals* **22**, 1-22.

Talbot, J. H. and Kempis, E. B., 1960. Finely Ground Quartz : Evidence against a `Disturbed' Layer. *Nature* **188**, 927-929.

Talbot, J. H. and Kempis, E. B., 1963. Effect of Grinding on Quartz Particles. *Nature* **197**, 66-66.

White, A. F. and Brantley, S. L., 1995. *Chemical weathering rates of silicate minerals*. Mineralogical Society of America, Washington, D.C.

Wollast, R. and Chou, L., 1988. Rate control of weathering of silicate minerals at room temperature and pressure. In: Lerman, A. and Meybeck, M. Eds.), *Physical and Chemical Weathering in Geochemical Cycles*. Kluwer Academic Publishers.

Worley, W. G., Tester, J. W., and Grigsby, C. O., 1996. Quartz dissolution kinetics from 100-200°C as a function of pH and ionic strength. *AIChE Journal* **42**, 3442-3457.

Xiao, Y. and Lasaga, A. C., 1994. Ab initio quantum mechanical studies of the kinetics and mechanisms of silicate dissolution: H+(H3O+) catalysis. *Geochimica et Cosmochimica Acta* **58**, 5379-5400.

APPENDIX 3.1

Quartz dissolution rates from our experiments in mol/m^{2}sec and the experimental conditions.

Expt No.	Solid	Solid Mass (g)	Solution Mass (g)	Duration (hrs)	*A/M* (m^2/g)	Solution	*T* °C	*pH*	log *r* (mol/m^{2}s)
02A-0	SIL-CO-SIL	5.01	25.222	216.2	151.9	HCl	25	0.00	-10.73
12A-0	SIL-CO-SIL	5.003	25.789	217	148.4	HNO_3	25	0.00	-10.72
19A-0	SIL-CO-SIL	5.004	24.98	38.8	153.2	HCl	25	0.00	-10.50
21A-0	SIL-CO-SIL	2.506	24.701	47.7	77.6	HCl	25	0.00	-10.53
23A-0	SIL-CO-SIL	2.504	25.309	52.3	75.7	HCl	25	0.00	-10.57
26B-0	SIL-CO-SIL	2.504	25.668	51.7	74.6	HNO_3	25	0.00	-10.53
28B-0	SIL-CO-SIL	2.513	26.138	47.2	73.5	$HClO_4$	25	0.03	-10.50
36C-0	Corning	10.015	20.234	1056	45.5	HCl	25	0.03	-10.65
40B-0	SIL-CO-SIL	10.001	20.313	7104	376.5	HCl	25	0.03	-10.89
44C-0	Corning	35.029	35.799	219	90	HNO_3	25	0.19	-10.75
50A-0	SIL-CO-SIL	8.004	20.617	222.5	296.9	HNO_3	25	0.19	-10.91
56C-0	Corning	12.333	20.492	144.5	55.4	HCl	25	0.19	-10.80
32B-0	SIL-CO-SIL	2.503	26.502	47	72.2	H_2SO_4	25	0.28	-10.56
33B-I	SIL-CO-SIL	2.509	24.714	46.9	77.6	H_2SO_4	25	0.90	-10.74
03A-I	SIL-CO-SIL	5.004	24.9	216.2	153.7	HCl	25	1.00	-10.84
13A-I	SIL-CO-SIL	5.004	24.929	217.3	153.5	HNO_3	25	1.00	-11.14
20A-I	SIL-CO-SIL	5.008	25.083	38.7	152.7	HCl	25	1.00	-10.70
22A-I	SIL-CO-SIL	2.507	24.925	47.7	76.9	HCl	25	1.00	-10.93
24A-I	SIL-CO-SIL	2.503	25.009	52.3	76.5	HCl	25	1.00	-10.89
27B-I	SIL-CO-SIL	2.503	24.7	51.6	77.5	HNO_3	25	1.00	-10.71

29B-I	SIL-CO-SIL	2.502	24.953	47.2	76.7	$HClO_4$	25	1.02	-10.97
37C-I	Corning	10.013	19.909	1056	46.3	HCl	25	1.10	-11.10
41B-I	SIL-CO-SIL	10.01	19.918	1056	384.4	HCl	25	1.10	-11.19
45C-I	Corning	35.042	34.748	219	92.8	HNO_3	25	1.12	-11.19
51A-I	SIL-CO-SIL	8.005	20.064	222.5	305.1	HNO_3	25	1.12	-11.24
57C-I	Corning	12.193	19.928	144.5	56.3	HCl	25	1.18	-10.82
34B-II	SIL-CO-SIL	5.006	24.947	46.8	153.5	H_2SO_4	25	1.78	-11.19
04A-II	SIL-CO-SIL	5.008	24.761	216.1	154.7	HCl	25	2.00	-11.07
14A-II	SIL-CO-SIL	5.004	24.921	217.3	153.6	HNO_3	25	2.00	-11.38
25A-II	SIL-CO-SIL	2.503	24.924	52.3	76.8	HCl	25	2.00	-11.20
30B-II	SIL-CO-SIL	5.009	24.96	47.1	153.5	$HClO_4$	25	2.02	-11.05
46C-II	Corning	35.049	34.678	219	93	HNO_3	25	2.03	-11.41
52A-II	SIL-CO-SIL	10.006	19.932	222.5	383.9	HNO_3	25	2.03	-11.43
38C-II	Corning	10.007	19.925	1056	46.2	HCl	25	2.09	-10.99
42B-II	SIL-CO-SIL	10.019	19.885	7104	385.3	HCl	25	2.09	-11.41
58C-II	Corning	12.109	19.941	144.5	55.9	HCl	25	2.17	-10.97
35B-III	SIL-CO-SIL	5.006	24.947	46.8	153.5	H_2SO_4	25	2.72	-11.35
05A-III	SIL-CO-SIL	5.004	24.728	216	154.8	HCl	25	3.00	-11.36
15A-III	SIL-CO-SIL	5.002	24.76	217.2	154.5	HNO_3	25	3.00	-11.60
47C-III	Corning	35.042	34.607	219	93.2	HNO_3	25	3.01	-11.55
53A-III	SIL-CO-SIL	10.007	19.897	222.5	384.7	HNO_3	25	3.01	-11.67
31B-III	SIL-CO-SIL	5.002	25.012	47.1	152.9	$HClO_4$	25	3.04	-11.53
39C-III	Corning	10.029	19.909	1056	46.4	HCl	25	3.12	-11.37
43B-III	SIL-CO-SIL	10.014	19.973	7104	383.5	HCl	25	3.12	-11.66
59C-III	Corning	12.154	19.799	144.5	56.5	HCl	25	3.21	-11.70
06A-IV	SIL-CO-SIL	5.004	24.769	216	154.6	HCl	25	4.00	-11.54
16A-IV	SIL-CO-SIL	5.007	24.752	217.1	154.7	HNO_3	25	4.00	-11.68
48C-IV	Corning	35.033	34.619	219	93.1	HNO_3	25	4.11	-11.56
54A-IV	SIL-CO-SIL	10.002	19.913	222.5	384.1	HNO_3	25	4.11	-11.60
07A-V	SIL-CO-SIL	5.004	24.154	215.9	158.4	HCl	25	5.00	-11.54
17A-V	SIL-CO-SIL	5.007	24.736	217.1	154.8	HNO_3	25	5.00	-11.56
49C-V	Corning	35.057	34.622	219	93.2	HNO_3	25	5.81	-11.53
55A-V	SIL-CO-SIL	10.001	19.86	222.5	385.1	HNO_3	25	5.81	-11.61
08A-VI	SIL-CO-SIL	5.007	24.835	215.8	154.2	HCl	25	6.00	-11.53
18A-VI	SIL-CO-SIL	5.008	24.897	217	153.8	HNO_3	25	6.00	-11.68
01A-VII	SIL-CO-SIL	5.008	25.061	215.8	152.8	DI Water	25	7.00	-11.62
09A-VII	SIL-CO-SIL	5.003	24.951	215.3	153.4	DI Water	25	7.00	-11.61
10A-VII	SIL-CO-SIL	5.002	24.928	215.3	153.5	DI Water	25	7.00	-11.71
64C-0	Corning	30.013	30.739	1061.5	89.8	HNO_3	55	0.05	-9.84
65C-I	Corning	30.021	29.903	1061	92.4	HNO_3	55	1.11	-10.04
66C-II	Corning	30.031	29.858	1061	92.5	HNO_3	55	2.12	-10.28
67C-III	Corning	30.023	29.726	1060.8	92.9	HNO_3	55	3.18	-10.44
68C-IV	Corning	30.011	29.661	1060.8	93.1	HNO_3	55	4.42	-11.71
69C-V	Corning	30.037	29.668	1061	93.1	HNO_3	55	5.41	-11.71

APPENDIX 3.2

Amorphous silica dissolution rates from our experiments in mol/m^2sec and the experimental conditions.

Expt No.	Solid Mass (g)	Solution Mass (g)	Duration (hrs)	*A/M* (m^2/g)	Solution	*T* °C	*pH*	log *r* (mol/m^2s)
1a-VII	2.008	25.109	168.0	122.7	DI Water	25	5.41	-11.87
2a-0	2.009	25.910	168.0	119.0	HNO_3	25	0.85	-11.08
3a-0	1.001	20.577	72.0	74.7	HNO_3	25	0.50	-10.95
4a-I	1.011	20.028	72.0	77.5	HNO_3	25	1.51	-11.53
5a-II	1.010	19.998	72.0	77.5	HNO_3	25	2.16	-11.82
6a-III	1.009	19.974	72.0	77.5	HNO_3	25	2.93	-11.84
7a-IV	1.017	20.008	72.0	78.0	HNO_3	25	4.01	-11.88
8aV	1.009	19.939	72.0	77.7	HNO_3	25	5.32	-11.65
9a-0	1.013	20.615	73.0	75.4	HNO_3	35	0.50	-10.43
11a-II	1.015	19.970	73.0	78.0	HNO_3	35	2.16	-11.39
15a-0	1.083	20.544	73.0	80.9	HNO_3	55	0.50	-10.01
16a-I	1.041	20.082	73.0	79.6	HNO_3	55	1.51	-10.48
17a-II	1.043	20.000	73.0	80.1	HNO_3	55	2.16	-10.63
18a-III	1.024	20.028	73.0	78.5	HNO_3	55	2.93	-10.74
19a-IV	1.017	20.000	73.0	78.1	HNO_3	55	3.73	-11.13